NASA Contractor Report 2978

Rocket Exhaust Ground Cloud/ Atmospheric Interactions

BaoChuan Hwang and Robert K. Gould

CONTRACT NAS1-14504
JULY 1978

NASA

NASA Contractor Report 2978

Rocket Exhaust Ground Cloud/ Atmospheric Interactions

BaoChuan Hwang and Robert K. Gould
AeroChem Research Laboratories, Inc.
Princeton, New Jersey

Prepared for
Langley Research Center
under Contract NAS1-14504

National Aeronautics
and Space Administration

**Scientific and Technical
Information Office**

1978

TABLE OF CONTENTS

LIST OF TABLES

LIST OF ILLUSTRATIONS

SUMMARY

This study comprises two separate tasks: (1) an attempt to identify and minimize the uncertainties and potential inaccuracies of the NASA Multilayer Diffusion Model (MDM) using data from selected Titan III launches, and (2) a systematic analysis of the physical/chemical processes which take place during the buoyant rise of a rocket exhaust ground cloud and formation of a realistic time-dependent model. The former study is based on detailed parametric calculations using the MDM code and a comparative study of several other diffusion models, the NASA measurements, and the MDM.

The comparative studies and parametric calculations show that: (1) The MDM consistently overpredicts the ground level concentrations in the cases examined if the appropriate input standard deviation of the wind azimuth angle is chosen. (2) The current lack of micrometeorological information at KSC causes wide uncertainties in the results calculated from the model. (3) Environmental hazard analyses which require, as input, pollutant concentrations throughout the entire planetary boundary layer (PBL) must employ MDM with caution. (4) In a shallow PBL condition, the uncertainties in the entrainment constant used in the MDM cloud rise formula can cause a factor of three ($\overset{\times}{\div}$ 3) error in the ground level predictions. For such conditions, the center of the exhaust cloud should be placed below the PBL height for the model calculations in order to give a conservatively high pollutant level prediction at the ground. (5) The other models included in the study contribute to an understanding of the relative merits of the diffusion modeling technique. The strengths of these models can be used as guidelines for developing a new and advanced diffusion model in the future.

The results of the second task can be summarized as: (1) The value 2500 cal g^{-1} used in the MDM for the heat release from the Shuttle (or Titan III) solid fuel is reasonable. (2) Deluge water injected into the exhaust plume has little effect on the subsequent concentration predictions. (3) An average loading of about 1 g m^{-2} of alumina (about 15% of the alumina initially in the cloud) will be deposited on the ground in a worst case example, as for the Titan III launch of 20 May 1975.

I. INTRODUCTION

A. STATEMENT OF THE PROBLEM

Concerns over the environmental impact of the toxic exhaust ground clouds generated by Space Shuttle launches have stimulated the development of mathematical models which can predict the dispersion of the exhaust effluents in the planetary boundary layer (PBL) under various meteorological conditions. One of these models (developed by NASA to provide real-time predicting capability) is the Multilayer Diffusion Model (MDM) described in Ref. 1. Some calculated results of ground cloud rise, cloud path, and HCl downwind concentration using this model for a number of Titan III launches have already been reported and analyzed (see e.g., Ref. 2). However, the assumptions incorporated into the MDM have led to concern that there might be large uncertainties associated with the predicted results. Critical analyses of the MDM model and its potential deficiencies can be found in Refs. 3-6. Since it is anticipated that the MDM will be used as the basis for assessing the environmental hazards of NASA launch vehicles, particularly the Space Shuttle, it was deemed necessary to: (1) evaluate the magnitude of the errors in calculations of concentrations and dosage fields using the NASA/MSFC MDM under various meteorological conditions and (2) provide a method by which the present model can be improved so that realistic launch constraints can be developed based on the improved model. In order to answer these questions, the chemical and physical processes occurring during the early period before diffusion becomes dominant must be considered because they may seriously alter the initial input required for a diffusion calculation and may cause environmental problems in the near field of the launch pad due to the dry and wet deposition of particles from the cloud.

B. BACKGROUND

The transport, evolution and atmospheric interaction processes of the exhaust cloud formed during rocket launches are most conveniently treated when separated into two stages: first, the buoyant force-dominated cloud rise phase and second, the atmospheric turbulence and ambient wind-dominated

diffusion process. When the cloud is initially formed at the launching pad, large quantities of debris from the ambient environment are entrained in it. The large size debris particles from the pad surroundings coagulate with the smaller aerosols of Al_2O_3, formed from the solid rocket propellant, and carry much of the Al_2O_3 to the ground during the earlier periods of cloud rise. This phenomenon is known as dry deposition. As the cloud continues to rise and cool, condensation of HCl and H_2O onto the remaining Al_2O_3 and H_2O aerosol particles may occur. Therefore, when the acid aerosol particle grows due to coagulation and condensation and finally falls out, part of the HCl will be removed from the exhaust cloud (wet deposition). This dry and wet deposition, in addition to causing a possible environmental problem in the near field of the launch pad ($\leq$ 5 km), also affects estimations of the HCl inventory and the size and number of particles present at cloud stabilization. Errors in these composition estimates are particularly important since the data are used as input to diffusion models (e.g., NASA MDM) by which downwind ground level pollutant concentration is computed. In addition, a copious quantity of water is injected into the exhaust plume in the first few seconds in order to protect the launch pad structures from heat and to dampen and reduce acoustical energy feedback to the Shuttle. This deluge water may affect the chemical and physical processes during the cloud rise and may be especially significant in the prediction of the cloud stabilization height.

Diffusion modeling of the rocket ground cloud in the PBL is further complicated by the lack of an adequate means to describe the microstructure of the PBL, as well as by the obvious existence of irregularities in initial cloud shape, uncertainties in pollutant concentration distributions, and nonuniformities in wind field and boundary conditions. In general, mathematical modeling of the diffusion transport takes either of two approaches, i.e., one obtains either an analytical or a numerical solution to the diffusion equation; in either case, for a practical problem, the turbulent terms are closed by the use of gradient transport theory. Analytical solutions to the diffusion equation can be obtained only for very limited conditions; for example, if the flow field is stationary and homogeneous, and the mean wind profile is uniform, the off-diagonal diffusivities may be ignored and the

mean concentration distribution for the instantaneous point source in the free flow field can be expressed by the well-known Gaussian distribution obtained by solving the diffusion equation. Although numerical approaches provide the capability of fitting more complex conditions, their applicability and accuracy are often limited by the large computer core storage on run time required. However, the ultimate accuracy of either approach still relies on the parameters chosen to describe the turbulence mechanism and the information on the advective wind in the flow field. Reviews of turbulent diffusion studies can be found in Refs. 7 to 9. More detailed descriptions of several advanced diffusion modeling techniques for practical calculations are given in Section IV.A.

The currently used NASA MDM program is based on the classic Gaussian model coupled with diffusion parameters from Cramer.[10] Two primary techniques are employed in the MDM, viz., the unlayered first-order technique or the layered technique, each of which has two models. The two unlayered models are: (i) the cylindrical distribution, "model 1", employed when describing the complete exhaust plume in the mixing layer and (ii) the ellipsoidal distribution, "model 3", employed for the ground cloud when meteorological conditions allow use of the assumption of a quasi-homogeneous mixing layer. The two layered models are: (i) the static-plume, "model 2", and the multilayered distribution, "model 4". Model 2 is used for diffusive transport at altitudes of 3000 to 8000 m where the turbulent transport mechanism can be ignored. In model 4, the surface mixing layer is divided into homogeneous (in a statistical sense) layers with a well distributed source. Models 3 and 4 assume that the top of the mixing layer totally reflects the effluents and that the ground surface has a specified absorption coefficient. As mentioned above, the Gaussian model results from a very ideal fluid field which rarely occurs in the PBL of the real world. Its applicability thus fully depends on empirical validation for each practical problem. In addition, the Cramer diffusion coefficients used in the MDM to model the physics of atmospheric turbulent transport are derived from a series of experiments which were carried out in the lower portion of the PBL. Therefore they need to be validated for the diffusion study of a rocket generated cloud which is distributed throughout the entire PBL.

To provide a data base for refinement and verification of transport models, an extensive monitoring program was performed after a number of Titan III launches (e.g., Ref. 11). During the diffusion process, data were taken with both airborne and ground-based sampling. Since the results calculated from MDM do not provide a time history of the pollutant concentration at a given position, a direct and systematic comparison between the available data, (especially the airborne data) by which refinements or verifications could be made, has never been conducted.

C. BRIEF DESCRIPTION OF APPROACH

This research program has comprised an effort to ascertain the aforementioned uncertainties and potential inaccuracies of the MDM, as well as a systematic attempt to model the physical/chemical processes occurring during the cloud rise period. The exhaust and early cloud properties such as the post-afterburning chemical composition, effective heat release, deluge water effects, and overall physical properties during cloud rise are discussed in Section II. This phase of the study is needed for predicting specific concentration distributions in the stabilized cloud as well as for modeling the coagulation, sedimentation, and condensation processes which take place during cloud rise itself.

Parametric calculations using the MDM code to identify and/or minimize error limits due to uncertainties in the input data have been partially discussed in previous studies.[3,6] In this report, the sensitive input quantities identified in those studies have been used parametrically in calculations for different meteorological conditions. Our emphasis, however, is on the problems associated with the lack of information on turbulence in the PBL at KSC, which has not been discussed previously; Section III summarizes the results.

With respect to the accuracy of predictions of cloud diffusion, this program has included a comparative study of five different diffusion modeling techniques including the MDM and comparisons with available measurement data. The objective of this phase of the study has been to address the following questions: (1) Do the measurements conducted by NASA provide a useful data base for the verification of diffusion models? (2) What would be the predicted results if other models were used in making an assessment, i.e., can they yield better results than MDM? How? and Why? (3) Can guidelines be developed for

improving the performance of MDM without substantially altering its present condition? (4) What kind of approach for modeling the atmospheric diffusion of a rocket generated cloud in the PBL is indicated, if a better assessment is required in the future?

The modeling techniques examined in this study, in addition to the MDM are:

(1) The Air Force/Vandenberg METS[12] model which is a Gaussian model with Turner-Pasquill stability classes for the determination of power law type dispersion parameters.

(2) The NUS TREATS[13] model which uses a Gaussian assumption for horizontal distribution and an integrated moment scheme for determining dispersion parameters.

(3) The Lawrence Livermore ADPIC[14] code which is based on a particle-in-cell/pseudovelocity transport scheme in which only diagonal eddy diffusivities are used.

(4) The AeroChem DISF[15] code which is a diffusion model for shear flow obtained by solving the diffusion equation via a second-order eddy diffusivity closure scheme and the Lagrangian approach for statistical quantities.

This study concentrates on the clouds produced by Titan III rocket launches at Kennedy Space Center on 10 December 1974, 20 August 1975, and 14 March 1976. The comparative results and the interpretation of meteorological information are given in Section IV. The reasons for selecting these three launches are: (1) more complete experimental data are available on these launches than for others; (2) the Titan III rocket uses the same propellant as the Shuttle SRM (and is about 1/2 the mass flow), and (3) these launches cover a broad range of interesting meteorological conditions. To elaborate on the latter point, it should be noted that the December launch was a night launch in the winter time with the presence of a shallow stable stratified PBL; the August launch took place in a daytime sea-breeze condition at KSC in which a high inversion layer was present; and the March launch was accompanied by strong humidity, variable wind direction and a moderately weak inversion layer (see Section IV.B for more detailed discussion).

A model for the coagulation of Al_2O_3 and debris particles has been developed to provide particle size distribution, particle densities, the mass fraction of alumina and the mass of sedimentation in each particle size class prior to the onset of condensation. Section V is devoted to the formulation of this model, its validation and the results of calculations.

The authors are indebted to Scott Wagner, Joseph Mathis, Richard Bendura, Richard Gomberg, Gerald Gregory, and Gerald Pellett of NASA/Langley (Environmental Field Measurement Branch, Marine and Applications Technology Division) for their constructive discussions and advice during this study. The authors also wish to thank the people who ran their diffusion models for this comparative study, in particular Christine Sherman and Rolf Lange at Lawrence Livermore Laboratory, Martin Chandler at NUS Corporation, and Darryl Dargitz at Vandenberg Air Force Base. The helpful comments and assistance on the report from Dr. William Miller at AeroChem are gratefully acknowledged. We also thank James Mills who coded the CRAM program and ran the computer programs for us at AeroChem.

II. EXHAUST AND CLOUD RISE PROPERTIES

In our overall approach to modeling the physical chemical processes in the cloud rise regime, the exhaust and early cloud properties have been calculated through the following rather complex but straightforward procedure.

A. EXHAUST COMPOSITION

The post-afterburning exhaust composition is calculated based on the assumption of complete combustion. An extensive study[16] using exact values for nozzle exit plane compositions and conditions and a low altitude afterburning/mixing plume program (LAPP[17] code) has shown that this assumption is very closely approached. This is especially true for the major species which are the only ones that need be considered since the chemistry of the minor species is not important in the determination of overall cloud characteristics.

The post-afterburning plume composition is shown in Table I. The values given include added air but only that required for combustion. This amounts to about 149% (by weight) of the rocket propellant for the solid engine (SRM) and 137% of the propellant weight for the liquid engine (orbitor). In addition, Table II gives comparative values for the masses of three major post-afterburning exhaust products that result from calculations invoking the above assumption and those produced by extensive calculations using the LAPP code for Titan and Shuttle SRMs. The values given are all based on the products of 100 g propellant. It should be noted that the value cited by Gomberg and Stewart[16] for this comparison has been derived by using the amount of alumina (Al_2O_3) in the plume as a normalization factor with which to obtain the amounts of other gases not specified in their calculations. They show a very good agreement if we account for the error and uncertainty induced from the thermal-kinetic data, in the numerical scheme, of the exit plane conditions, etc.

B. HEAT CONTENT AND EFFECTS OF DELUGE WATER

With the complete burning assumption, the heat release from the propellant is found to be 2847 cal g^{-1} for the solid engine SRM and 3117 cal g^{-1}

for the liquid orbitor engine. These values do not include the effect of the deluge water. The effective fuel heat content for the solid engine is essentially the same as the value calculated by Stewart and Grose[3] and is slightly higher than the value of 2500 cal g^{-1} currently used in the NASA/MSFC MDM.[1] The value for the liquid engine is about a factor of 6 higher than the value used in the NASA/MSFC MDM (version 5).[1]

The principal potential effects of the deluge water on the chemical/physical process during cloud rise are: (i) changes in chemical composition due to possible quenching of some of the high temperature afterburning reactions and (ii) reduction of the effective heat content in the cloud due to the vaporization of the deluge water. A study[18] of the former problem was recently conducted at NASA/Langley and concludes that changes in the concentrations of major species are negligible. In other words, the complete burning assumption used in the present study is still applicable even during the first few seconds of firing in which the deluge water is injected. In considering the effect of the deluge water on the effective heat content and subsequently on the prediction of the cloud stabilization height using the present cloud rise model, we have included all of the water to be used in the Acoustic Water Suppression System (AWSS) for the launching of the Space Shuttle in order to determine its maximum effect. In the present plans for the AWSS, water will be poured under the firing pad and into the plume trench at a rate of 6500 gallons per sec over about 8 sec after rocket ignition. This represents a mass flow rate of about 2.46×10^7 g sec^{-1}. If the stabilized cloud is assumed to contain 17 sec of exhaust, which is a reasonable value based on Titan ground cloud data (a detailed discussion of this point is given below), then the total amount of effective available heat, Q_h will be

$$Q_h = \dot{M}_S \times h_S \times t_f + \dot{M}_L \times h_L \times t_f - h_w \times \dot{M}_w \times 8 = 4.27 \times 10^{11} \text{ (cal)} \qquad (1)$$

where $\dot{M}_S$, $\dot{M}_L$ and $\dot{M}_w$ are the mass flow rates (g sec^{-1}) of the solid engine, liquid engine, and poured water, respectively, h_S and h_L are the effective heat release (cal) per gram of propellant, h_w is the latent heat of water vaporization at room temperature, and t_f is the firing time during which the cloud is formed (now $\equiv$ 17 sec).

This value for the total heat content equals about 80% of the total heat content excluding the effect of deluge water. Since the predicted stabilization height, Z_m, is proportional to the 1/4 power of the total heat content (i.e., $Z_m \propto Q_h^{1/4}$) in the presently used Briggs[19] formula in MDM, the effect of deluge water on the prediction of the stabilization height is less than 5% in the worst case. It can certainly be ignored. For the Titan III rocket, the mass flow rate of trench water (which is the only deluge water in use) is about 1.4×10^6 g sec^{-1} but it is employed over only a 5 sec period at most after firing. Therefore, the average heat available for the first 10 sec of launch of Titan III is about 2750 cal g^{-1} if the trench water is considered. This value is slightly higher than that used in the NASA/MFSC MDM; the differences, however, are apparently negligible for the reason mentioned above.

C. PHYSICAL PROPERTIES IN THE CLOUD RISE REGIME

Since the net effect on buoyant cloud rise of atmospheric entrainment due to turbulence is not well known, an exact calculation of the cloud shape, its concentration distribution, and other physical properties during cloud rise would require an expensive and time-consuming direct numerical simulation process. Such a calculation is presently impractical. Therefore, we have continued to use the Briggs formula, as in the NASA/MSFC MDM, for the estimation of cloud rise speed when observations are not available. The cloud shape is assumed spherical; the rest of the physical properties, especially those required in calculations of coagulation and condensation (or heterogeneous chemistry) during the cloud rise, are obtained from a model based on an energy balance, combined with the above assumptions for cloud volume and cloud rise speed (Briggs formula). The primary physical properties required, in addition to the volume and cloud rise speed, are the temperature and mass of air entrained.

The following diagram illustrates the formulation of the energy balance during the cloud rise:

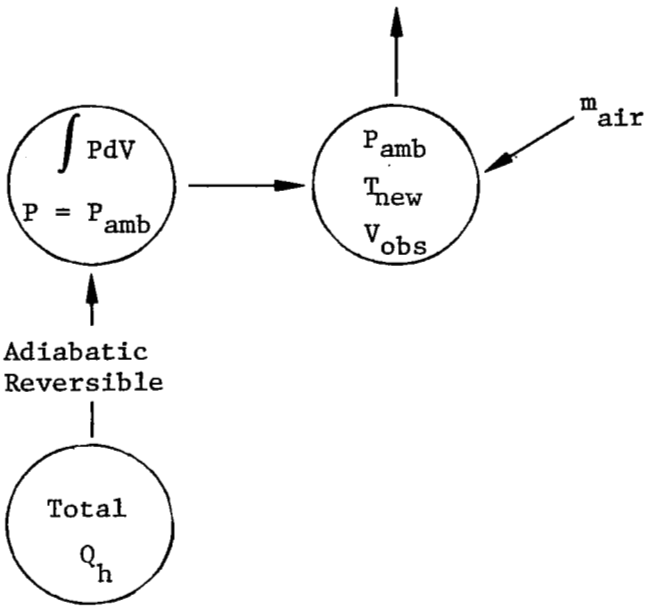

where Q_h is the total effective heat content in the cloud, P, P_{amb} are the instantaneous pressure in the cloud and ambient environment where the cloud locates, m_{air} is the mass of air entrained due to turbulent mixing and V_{obs} is the observed cloud volume at the following stage.

When the buoyant cloud rises, it will cool mainly due to expansion and entrained cool air. An instantaneous pressure balance between the cloud and the ambient environment can be reasonably assumed. With this assumption, the temperature and the mass of air entrained can be calculated, using the perfect gas law, if the real cloud volume is known. The mathematical form for this formal process can be written

$$Q_h - \int_{t_o}^{t} PdV = \sum_{i \in P} \left(m_i \int_{298}^{T} C_{p_i} \, dT' \right)$$

$$+ \int_{t_o}^{t} C_{p_{air}} \, m_{air} \, (T(t') - T_{amb}(t'))dt' + 1/2 \; M \; W^2(t) \quad (2)$$

and

$$M(t) = \int_{t_o}^{t} m_{air}(t')dt' + \sum_{i \varepsilon P} m_i \qquad (3)$$

where P is the set of post-afterburning chemical species, in which the elements are identified by means of a sub-index "i", W is the cloud rise speed, and m, T, t, and C_p represent the mass, temperature, time, and specific heat constant, respectively. The subscript "air" refers to entrained ambient air, "amb" to ambient, and "obs" to observed.

The terms on the left hand side of Eq. (2) give the total heat content, and the work done by adiabatic reversible expansion due to the cloud rising from higher to lower ambient pressure. The terms on the right hand side consist of the internal energy of each species in the cloud, the energy required to heat up the entrained cool ambient air and the kinetic energy of the cloud. The potential energy is negligible. The total mass M(t) at time t in the second equation can be obtained from the observed volume, temperature and pressure by using the perfect gas law; i.e.,

$$M/V_{obs(t)} \cdot T(t) \cdot K_{gas} = P_{amb}(t) \qquad (4)$$

where K_{gas} is a gas constant, i.e., $K_{gas} = n \times R$,
where $R = 8.2 \times 10^{-5}$ (atm•m^3/mole•K) and n is the number of moles in a unit mass which equals

$$n = \left\{ \sum \frac{C_i}{MW_i} \right\}$$

where MW_i is the molecular weight and C_i is the mass fraction of species i in the cloud.

The total heat content, Q_h, used in Eq. (2) is calculated from Eq. (1) for the Shuttle. If the observation data for the cloud rise history are not available, the cloud rise speed W is obtained from Briggs' formula which gives

$$W = 1/4\ A^{1/4}\ S^{1/2}\ [\sin(t\ s^{1/2})][1 - \cos(ts^{1/2})]^{-3/4} \qquad (5)$$

where $s = \frac{g}{T_R} \frac{\partial \phi}{\partial Z}$, the Brunt Vaisala frequency

and $$A = \frac{3Q_h}{\rho_{air} C_{p_{air}} \pi(\gamma)^3 \frac{\partial\phi}{\partial z}}$$

where ρ_{air} and T_R are the density and temperature, respectively, of ambient air near the ground, γ is the entrainment constant and $\frac{\partial\phi}{\partial z}$ is the vertical gradient of ambient virtual potential temperature. Also if an observed volume is not available, the spherical-cloud shape assumption gives the volume as follows:

$$V_{obs}(t) = (\gamma \cdot Z(t))^3 \cdot \pi \cdot \frac{4}{3} \tag{6}$$

and

$$Z(t) = \int_{t_I}^{t} W(t)dt + Z_o \tag{7}$$

where $Z(t)$ is the cloud altitude at time t and Z_o is the initial cloud center location. t_I in Eq. (7) represents the time which will give the initial cloud rise speed from Eq. (5).

The second term in the left hand side of Eq. (2) can be written in algebraic form, i.e.,

$$\int PdV = -\frac{1}{\gamma'} V_o P_o^{1/\gamma'} P^{1-1/\gamma'} + \frac{1}{\gamma'} V_o P_o \tag{8}$$

where γ' is the specific heat ratio, i.e.

$$\gamma' = \frac{C_p}{C_v}$$

Substituting Eqs. (3) to (8) into Eq. (2) closes the energy balance equation. Then the historical temperature variation during the cloud rise as well as the mass of entrained air can be solved implicitly. A numerical program following the above procedure is given in Appendices A and B as a subroutine, CLDRISE, of the cloud rise aerosol model (CRAM) program.

A set of results using this model for volume, temperature rise, speed and entrained air mass for three Titan III launches at KSC is shown in Fig. 1. There is insufficient observation information at present to make meaningful comparisons. However, these can be made whenever data become available.

III. PARAMETRIC STUDIES USING THE MDM CODE

A parametric study of version 5 of the MDM program was carried out to (1) place bounds on the uncertainties in MDM predictions of exhaust effluent concentrations and (2) establish guidelines for the use of the MDM and/or provide directions for its modifications. Such a study also provides good background for comparative studies using the various diffusion models employed in this program.

The present work concentrates on the MDM model 4 because it is the model presumed capable of accounting for the inequalities of the source cloud (at stabilization) and the inhomogeneous nature of the real world. Since each species in the cloud is treated as an inert gas in MDM, it is sufficient to consider only one species, namely HCl. The meteorological conditions examined were those occurring during the two Titan III launches, viz., 10 December 1974 and 20 August 1975. Figures 2 and 3 show the temperature, wind speed, wind direction, and humidity for these two launches. The meteorological data are adapted from the most recent rawinsonde measurement taken before the launch and are used as the reference basis for the calculations.

The original parametric studies with MDM were made by Stewart and Grose.[3] Their work mainly covered two specific meteorological conditions, viz., low level sea-breeze conditions and the fall fair weather regime. Table III, adapted from their report, summarizes the kinds of parameters and the range of their variations in this work. Their reasons for selecting these parameters and this range of variations are not given here. Briefly, they concluded that the ground level concentration predictions using MDM are strongly dependent on the cloud geometry assumed at stabilization, the concentration distribution, the depth of the PBL, and the layer transition time. It should be noted that (1) their study was based on version 2 of the MDM[20] program, (2) the meteorological conditions they considered are different from ours, and (3) the operational procedure for preparing the input for MDM has been changed since then. It should also be noted that the initial work by Stewart and Grose did not cover all the parametric uncertainties in the MDM. Hence a further discussion, to a sufficient extent to support our later comparative

study, should be given. This report emphasizes parameters which have not been discussed in those previous studies. They are separated into two categories; the first concerns those parameters which are related to the diffusion process and the second comprises those which affect the initial description of the cloud. A brief discussion of the calculational results using the sensitive input parameters found in previous studies is given in Section III.C.

A. PARAMETERS AFFECTING DIFFUSION

The three kinds of parameters in this first category are the diffusion parameters, the boundary absorption factor, and the mean wind speed.

1. Diffusion Parameters

As mentioned above, the MDM program assumes a steady-state Gaussian dispersion. Using the Gaussian distribution form, the only unknown parameters are the standard deviations of the mean concentration dispersions, σ_x, σ_y, and σ_z, in alongwind, crosswind and vertical directions, respectively. The alongwind dispersion parameter σ_x used in MDM is based on the expression for alongwind cloud growth derived by Tyldesley and Wallington,[21] i.e.,

$$\sigma_x = \left\{\left(\frac{L}{4.3}\right)^2 + \sigma_*^2\right\}^{1/2}$$

where σ_* is alongwind standard deviation of initial pollutant distribution

and

$$\begin{cases} L = 0.28 \cdot \dfrac{(\Delta U)}{U} \cdot x & \text{as } U > 0 \text{ or } \dfrac{\Delta\Phi}{\Delta z} < 0 \\ L = 0 & \text{for all other cases,} \end{cases}$$

where ΔU is the wind speed difference between that at the top and the bottom of the PBL. The problems associated with the use of this expression have been discussed by Stewart and Grose.[3] Since Dumbauld (one of the authors of the MDM) recommends using 0.6 rather than 0.28 in the above expression because in his experience, it yields more realistic results, we have used 0.6 in all calculations in the present study. The resulting peak in the concentration maxima obtained with 0.28 is about 80% higher than that obtained with 0.6.

The expressions for crosswind and vertical dispersion parameters, σ_y and σ_z, in MDM are based on Cramer's formula,[10] in which they are related to the standard deviation of the wind azimuth angle $\sigma_A(z,\tau)$ and elevation angle $\sigma_E(z,\tau)$, where z is the height of source location and τ is the so-called source release time. At present, τ is taken as the time required for the cloud to rise to the stabilization height and z is the height of the center of each subcloud.

In the preprocessor program, $\sigma_A(z,\tau)$ and $\sigma_E(z,\tau)$ in the entire PBL are determined by a very simple expression, i.e.,

$$\sigma_A(z,\tau) = \sigma_E(z,\tau) = \sigma_{A_o}/2 \tag{9}$$

where σ_{A_o} is the standard deviation of azimuth angle measured over 10 minutes at a reference height (usually at 4 m above the ground).

Expression (9) implicitly incorporates the assumptions (1) that the atmospheric flow is isotropic, i.e., $\sigma_A = \sigma_E$ and (2) that σ_A and σ_E are independent of height. These assumptions are inadequate because the atmospheric flow field is nonisotropic and σ_A and σ_E are only independent of height near ground level (the altitude is unlikely to be more than 15% of the PBL thickness, see Section IV.B.1); in general, σ_A and σ_E decrease monotonically at upper portions of the convection layer. It should also be noted that the assumption, $\sigma_A = \sigma_{A_o}/2$ in (9) has not been proven theoretically or empirically. In addition, while direct measurements of σ_{A_o} have been made at each tower at KSC, the values of σ_{A_o} vary considerably for different towers at different times. Therefore, the effects due to the inadequate assumptions and the uncertainties of the value of σ_{A_o} should be determined.

Two approaches are utilized to determine the effects caused by the above problems.

(i) Assume

$$\sigma_A(z,\tau) = \frac{\sigma_{A_o}}{2} \quad \text{and} \quad \sigma_E(z,\tau) = \frac{\sigma_{E_o}}{2}$$

where σ_{E_o} is the standard deviation of wind elevation angle measured over 10 minutes at a reference height a few meters from the ground. The values of σ_{A_o} and σ_{E_o} are obtained from four sources: (1) the average value of the tower measurements, (2) the interpolation method

suggested by Record et al,[22] (3) similarity theory, see Section IV.B.1, and (4) the value given by Susko and Stephens.[23] Table IV lists the values of σ_{A_o} and σ_{E_o} obtained from these four sources. Since only σ_{A_o} is available for tower measurement, a simple assumption that $\sigma_{A_o} = \sigma_{E_o}$ is used in the calculation for source (1).

(ii) By definition, $\sigma_A(z,\tau) \simeq \sigma_v(z,\tau)/U(z,\tau)$ and $\sigma_E(z,\tau) \simeq \sigma_w(z,\tau)/U(z,\tau)$, where σ_v and σ_w are the standard deviations of the turbulent wind fluctuation components in the crosswind and vertical directions, respectively. Values of σ_v and σ_w are obtained from the method discussed in Section IV.B.1. Since the values of σ_A and σ_E used in the MDM are dependent on the release time, we have used the expression given by Cramer et al,[24] i.e.,

$$\sigma_A(z,\tau) = \sigma_A(z,\tau_o)\left(\frac{\tau}{\tau_o}\right)^{1/5}$$

The predicted maximum ground concentrations from the five different sets of σ_A and σ_E described in (i) and (ii) above for the December launch are shown in Fig. 4. As shown, they differ significantly in the near field (2 km $\leq x \leq$ 10 km) of the launch pad. In particular, the values obtained using either the measurement data (i.1 curve) or the theoretically more exact interpolation method for the σ_A and σ_E (ii curve) are much lower than the values obtained using other adopted methods. It should be mentioned that the predicted results from MDM could be even lower than the lowest value shown in Fig. 4 if one used the measurement data for σ_A and σ_E from the lower portion of the PBL and the monotonic decay profile for the upper portion. This is because (1) a vertically uniform profile for σ_A and σ_E is implicit in the calculation using measurement data, and (2) the σ_A and σ_E for the lower portion (calculation (ii) above) were about 7° and 4°, respectively, which are higher than the 2° measured value (see Table IV). However, it is clear that the present lack of turbulence information can lead to a wide uncertainty in the MDM predicted results.

2. Earth Absorption Factor

The MDM program (models 3 and 4) utilizes the simple mirror reflection method to treat boundary effects. An absorption factor, γ_p is used to determine the strength of the absorption of the earth surface. For instance, water surfaces may absorb all HCl reaching them, but some land surfaces, like highways, may reflect most or all of the HCl. Therefore, we cannot classify the earth surface in the KSC area as being uniform. Since γ_p is assumed uniform, it is of interest to see the effect of varying the value of γ_p on the ground concentration prediction. The results obtained from the two launches are almost identical, as shown in Fig. 5. It can be expected that a greater effect would be observed in the far field, but even there the variation is less than a factor of two. Since the greatest variation in the peak of maximum concentration predictions (or 10 minute time-mean-concentration) is less than 50%, we can conclude that the surface absorption parameter is not an important factor in predicting ground pollutant level. For reference, comparisons of the results of varying γ_p and σ_{A_o} and σ_{E_o} in MDM for the December launch are shown in Fig. 6; it is obvious that the diffusion parameter dominates.

3. Wind Speed

The wind profiles used in the diffusion calculation at KSC can be obtained from one of three measurements, viz., rawindsonde, windsonde or jimsphere. The rawindsonde measurements are used more widely probably because they provide more complete mesoscale meteorological information, (i.e., temperature, pressure, wind speed, wind direction, humidity, etc.,). However, all the measurements are taken at different locations and at different times, often not at the time of launch. Furthermore, even the wind profiles adopted from these three different measurements at very close intervals show considerable differences (see Fig. 7). In other words, the wind profile used in the diffusion predictions may not represent the real situation and the effect caused by the uncertainty of wind speed must be determined. In the present study, calculations were made by changing the magnitude of wind speed but not the wind profile. It was found that in both the December and August cases no more than $\pm$ 85% change in the time-mean-concentration was produced by $\mp$ 100% change in average wind speed, but there were no changes in the maximum concentrations. This is because the

formulation for the maximum concentration in the MDM program is independent of the magnitude of wind speed and the turbulence parameters, σ_{A_o} and σ_{E_o}, in the calculations were invariant. Theoretically, the σ_{A_o} and σ_{E_o} are dependent on wind speed; because $\sigma_A \simeq \frac{\sigma_v}{U}$, $\sigma_A \simeq \frac{\sigma_w}{U}$, and σ_v and σ_w are not dependent on the magnitude of U, σ_A and σ_E will vary with U. Since, in our calculations the σ_{A_o} or σ_{E_o} are based on the tower data, there is no reason to change them when we vary the wind speed obtained from soundings.

B. PARAMETERS AFFECTING INITIAL CLOUD DESCRIPTION

The second category of parameter studied includes the vertical mean gradient of ambient virtual potential temperature, $\Delta\phi/\Delta z$, the entrainment constant, γ, and the standard deviations σ_{x_o}, σ_{y_o} and σ_{z_o} for the source distribution in the stabilized cloud. The effects of varying σ_{z_o} are covered in the discussion on rearranging the vertical source strength, Section III.C.; the remaining parameters will now be addressed.

1. The Gradient of Virtual Potential Temperature $\Delta\phi/\Delta z$

If $\Delta\phi/\Delta z$ has a factor of two uncertainty, then a 20% variation for the stabilization height, Z_m, can be induced, because $Z_m \propto \left(\frac{\Delta\phi}{\Delta z}\right)^{-1/4}$. For the present MDM program, a 20% change in stabilization height can cause "at most" a 230% increase (or decrease) in the total amount of pollutant considered in the dispersion. Since the MDM program is an inert diffusion model, an increase (or decrease) of 230% in the initial source strength would cause a 230% increase (or decrease) in the predicted ground level concentration as well. Therefore a factor of two variation in $\Delta\phi/\Delta z$ implies "at most" a 230% variation in the prediction of the ground level concentrations. However, since a big change in $\Delta\phi/\Delta z$ would mean significant change in the atmospheric structure and thus question the validity of MDM, it is logical to assume that $\Delta\phi/\Delta z$ is approximately constant over time and space. Also, the three factors for determining $\Delta\phi/\Delta z$, namely temperature, pressure, and humidity, are fairly reliable measurements and it is unlikely that $\Delta\phi/\Delta z$ would have a factor of two variation.

2. The Entrainment Constant γ

For the rocket generated cloud, the entrainment constant used in the Briggs formula in the MDM model has not been fully validated. However a previous study by Hart,[25] using a one-dimensional cloud rise model* showed that the proper entrainment constant is about one on the basis of comparisons with the limited observed data of Titan III clouds. This entrainment constant value is different from the recommended value of 0.64 in the MDM model. It should also be noted that Hart's study showed very limited success in comparisons with the Titan III clouds in stable conditions. Therefore the effects due to the uncertainty of the entrainment constant should be investigated. Since, for stack plumes, the value taken is usually between 0.5 and 1.3,[26] we have made a series of calculations varying γ from 0.5 to 1.3 for the December and August launches. The resulting ratio of source strength is given in Fig. 8. As shown, γ has an insignificant effect on the diffusion prediction in the August case which is a daytime launch and we can generalize that the sensitivity of MDM to the entrainment constant in a deep PBL condition is fairly low. By contrast, the entrainment constant can cause a factor of three ($\overset{\times}{\div}$ 3) variation in predicted ground level results for a shallow PBL.

3. The Standard Deviations, σ_{x_o} and σ_{y_o}, of Initial Pollutant Distribution

The σ_{x_o} and σ_{y_o} now in MDM are chosen arbitrarily. In order to determine their sensitivity in the diffusion calculation, they have been varied consistently for all sublayers, by ± 10%, ± 30%, and ± 50%; such consistent variation keeps the elliptical cloud shape assumption, which is incorporated in MDM, intact. The resulting peak of maximum concentrations for the December launch is shown in Table V as an example. It is found that there are insignificant changes in the predictions resulting from the above variations in these two parameters for the December launch. However, there is about an 85% increase for the August launch when one makes a 30% decrease in

---

* The main difference between this model and the Briggs cloud rise formula is that this model introduces an additional equation of state to more accurately account for the buoyancy force; this equation of state is basically similar to the one described in Section II.B.

the σ_{x_o} and σ_{y_o}; in contrast there is only a 35% decrease for a 30% increase of σ_{x_o} and σ_{y_o}. It should be kept in mind that the sensitivity of the standard deviations of the initial pollutant distribution to MDM is higher for the case of a deep PBL than for a shallow PBL.

C. SENSITIVE PARAMETERS IN PREVIOUS STUDIES

Calculations using the sensitive parameters found in previous studies for the August and December launch cases have been performed. The resulting conclusion is similar to that of previous studies except that varying the source strength distribution in each layer would not have a significant effect on the ground level concentration if a notable amount of the exhaust were not mandatorily placed in the lower portion of the PBL. In addition, it should be mentioned that over a realistic range of variations in the depth of the PBL the change in the results is within a factor of two. As a precise example, although the depth of the PBL for the August launch cannot be determined exactly, it should range between 1000 and 2000 m. (Further discussion is given in Section IV.B.2.) Under such consideration, the calculations showed that the variation of the predicted peak of maximum ground level concentration is less that a factor of two. Nevertheless, since other studies[27] have shown that the peak in mass concentration at the ground level can reach 4 ppm while 8 ppm is the short term acceptable limit, the error of a factor of two caused by the uncertainty of the depth of the PBL cannot be neglected. A model which is capable of determining the depth of the PBL is apparently desired.

IV. COMPARATIVE STUDY OF GROUND CLOUD DIFFUSION MODELS

A. A BRIEF REVIEW OF SELECTED DIFFUSION MODELS

Basically every model of atmospheric diffusion processes starts with the diffusion equation (formulated from the mass conservation equation) and then uses some technique to close the turbulent fluctuation terms in the equation. The usual technique, called K theory or gradient transport assumptions, employs eddy diffusivities to relate the gradient of mean quantities to the turbulent flux, e.g., $\overline{u_i'c'} = K_{ij} \frac{\partial \bar{C}}{\partial x_j}$. Here, u_i' is the fluctuating velocity component in the i direction, c' is the fluctuating concentration and the overbar denotes an average quantity. K_{ij} is the eddy diffusivity tensor which is obtained by utilizing either one or another of many possible assumptions or empirical results. Since the K theory has been virtually the only kind used to date for practical calculations of atmospheric diffusion processes, all modeling techniques selected for this comparison are limited to this category. Table VI lists these selected models, each of which is briefly described below.

1. NASA/MSFC Multilayer Diffusion Models (MDM)

The MDM[1] program is based on the classic Gaussian distribution assumption (see Section I.B). The standard deviations of the mean concentration dispersions, σ_x, σ_y, σ_z, (usually called dispersion parameters) are obtained from Cramer's formula for vertical and crosswind terms and from Tyldesley and Wallington's[21] for the alongwind term. The treatment of vertical wind shear, turbulent nonhomogeneity and source irregularity involves dividing the flow field (the PBL) into sublayers and having the source in each sublayer disperse in a Gaussian form which depends on its initial local properties. A more detailed discussion of this model can be found in Ref. 5.

2. Meteorological Effluent Transport Simulation Model (METS)

Using an approach similar to the MDM program, the METS model[12] employs the Gaussian distribution assumption for the gaseous and liquid constituents and the layered structure. The vertical and the crosswind dispersion

parameters are given by power law expressions and the alongwind parameters by Tyldesley and Wallington's equations, i.e.,

$$\sigma_y = \sigma_{y_o} \left(\frac{x}{x_o}\right)^{p_y}$$

$$\sigma_z = \sigma_{z_o} \left(\frac{x}{x_o}\right)^{p_z}$$

$$\sigma_x = L_x^{P_x} + \sigma_{x_o}$$

where σ_{z_o}, σ_{y_o} are the initial standard deviations, and x is the downwind distance from the center of the source at x_o. The exponents p_y, p_z are determined by fitting the empirical Turner-Pasquill[28] curves for different stability classes. The stability class for each sublayer is dependent on the calculated local gradient Richardson number (see Section IV.B).

Two additional models have been incorporated into the METS model to account for the diffusion of particulates (e.g., Al_2O_3) and the hydrochemisorption of HCl. These additions are beyond the scope of the present study of inert pollutant diffusion and no discussion is given here. However, these two submodels are based on very intuitive assumptions coupled with different empirical formulations for different physical/chemical processes (e.g., descriptions of the aerosol growth and sedimentation velocity are both derived from the empirical studies of water droplets in natural clouds).

3. TREATS Model

An integrated moment scheme (over the entire horizontal plane at each altitude) is used in the TREATS[13] model to determine the dispersion parameters σ_x,σ_y (related to second moments). A Gaussian distribution assumption is then adopted to describe the concentration distribution on a horizontal plane for each altitude. This model starts with the mean concentration diffusion equation which is closed by using the diagonal eddy diffusivities, i.e.,

$$\left(\frac{\partial}{\partial t} + u\frac{\partial}{\partial x} + v\frac{\partial}{\partial y} + w\frac{\partial}{\partial z}\right)\overline{C} = \left(\frac{\partial}{\partial x} K_x \frac{\partial}{\partial x} + \frac{\partial}{\partial y} K_y \frac{\partial}{\partial y} + \frac{\partial}{\partial z} K_z \frac{\partial}{\partial z}\right)\overline{C} + \lambda \overline{C} \tag{10}$$

where $\bar{C}$ is the mean concentration of contaminant, u, v, w are the x, y, z components of the mean velocity, K_x, K_y, K_z are the eddy diffusivities and λ is a decay constant (which is set to zero in this study). A four-step procedure is followed: (1) both sides of Eq. (10) are multiplied by $x^n y^m$, where $0 \leq n + m \leq 2$; (2) the equation is then integrated over the horizontal plane at a fixed height; (3) the boundary assumptions $\iint \bar{C}(x, y, z, t)\, dxdy = 0$ or $\substack{x \to \infty \\ y \to \infty}$ and incompressibility assumption $\partial u/\partial x + \partial v/\partial y = 0$ are applied to the integral equations from (2); and (4) the diffusivities are assumed independent of the horizontal coordinates. The following set of equations is obtained;

$$\frac{\partial \sigma_x^2}{\partial t} = 2K_x + \left(w + 2K_z \frac{\partial \ln \theta_{oo}}{\partial z}\right) \frac{\partial \sigma_x^2}{\partial z} + \frac{\partial}{\partial x} K_z \frac{\partial \sigma_x^2}{\partial z} + 2K_z \left(\frac{\partial \bar{x}}{\partial z}\right)^2 \tag{11}$$

$$\frac{\partial \sigma_{xy}}{\partial t} = w \frac{\partial \sigma_{xy}}{\partial z} + 2.0\, K_z \frac{\partial (\ln \theta_{oo})}{\partial z} \frac{\partial \sigma_{xy}}{\partial z} + 2 \frac{\partial \bar{x}}{\partial z} \frac{\partial \bar{y}}{\partial z} K_z + \frac{\partial}{\partial z} \left(K_z \frac{\partial \sigma_{xy}}{\partial z} \right) \tag{12}$$

$$\frac{\partial \bar{x}}{\partial t} = u + \frac{\partial \bar{x}}{\partial z} \left(w + 2K_z \frac{\partial \ln \theta_{oo}}{\partial z} \right) + \frac{\partial}{\partial z} \left(K_z \frac{\partial \bar{x}}{\partial z} \right) \tag{13}$$

$$\frac{\partial \theta_{oo}}{\partial t} = \frac{\partial}{\partial z} \left(K_z \frac{\partial \theta_{oo}}{\partial z} \right) + w \frac{\partial \theta_{oo}}{\partial xz} + \lambda \theta_{oo} \tag{14}$$

All the quantities in the above equations depend only on the vertical coordinate z and time t. $\bar{x}(z,t)$ is the maximum center location of instantaneous concentration, i.e.,

$$\bar{x}(z,t) = \frac{\theta_{1o}}{\theta_{oo}}$$

where

$$\theta_{nm} = \iint x^n y^m \bar{C}(x,y,z,t)\, dxdy$$

θ_{oo} is the total mass of pollutant at altitude z and time t.

If the eddy diffusivities K_x, K_y, K_z are somehow known, Eqs. (11) to (14) form an initial value problem of a set of differential equations

which can be solved numerically. A standard finite difference scheme is used in the TREATS model. Evaluation of the eddy diffusivities K_x, K_y and K_z, which are not known in general, proceeds as follows:

a. Horizontal Eddy Diffusivity K_x and K_y - The method incorporated to determine the eddy diffusivity K_y is based on the assumption that

$$K_y = \frac{d}{dt} \sigma_y^2$$

The standard deviation σ_y of the crosswind concentration distribution is given by a functional expression which depends on the local stability. The functional expression is derived by fitting the Pasquill-Gifford[29] curves for the corresponding stability class. The local stability class at each altitude is assigned on the basis of the local temperature gradient. The alongwind eddy diffusivity K_x is assumed to be equivalent to K_y in the present study.

b. Vertical Eddy Diffusivity K_z - Two different methods of evaluating K_z are used in this study for TREATS. One follows the same procedure as that for K_y; the Pasquill-Gifford curves for the vertical dispersion parameters σ_z are utilized. The other alternative approach adopts Blackadar's formulation[30] for the eddy viscosity. If the turbulent Schmidt number is assumed to be one, the eddy diffusivity K_z will be

$$K_z = \ell^2 \left\{ \left(\frac{\partial u}{\partial z} \right)^2 + \left(\frac{\partial v}{\partial z} \right)^2 \right\}^{1/2} \phi^{-2}$$

where ϕ is the non-dimensional wind shear and ℓ is a mixing length. (Blackadar's formulation is based only on mixing length theory.) The non-dimensional wind shear ϕ can be derived from similarity theory. In this study, expressions for ϕ have been based on the studies of the surface layer for unstable, stable and neutral atmospheres (see Section IV.B). Two kinds of mixing length expressions are incorporated. They are

$$\ell = \frac{k(z+z_o)}{1 + \frac{k(z+z_o)}{\lambda}} \qquad (15)$$

where $$\lambda = \frac{2.7 \times 10^{-4} V_g}{f}$$

and $$\ell = 0.0063 \frac{u_{*o}}{f} \tanh \frac{kzf}{0.0063\ u_{*o}} \qquad (16)$$

In these equations V_g is the geostrophic wind speed, k is the Von Karman constant, f is the Coriolis parameter, and u and v are, respectively, the east and north components of the wind at the level where K_z is being evaluated.

Expression (16)[31] for mixing length ℓ was obtained by fitting the measurement data collected from towers ranging from 18 to 150 m high at KSC, where similarity theory was used.

4. Atmospheric Diffusion, Particle-in-Cell (ADPIC) Model

The simplified mean concentration diffusion Eq. (10) can be rewritten for an incompressible flow field in the form;

$$\frac{\partial \overline{C}}{\partial t} + \nabla \cdot \left\{ \left(\tilde{U} - \frac{K \nabla \overline{C}}{\overline{C}} \right) \overline{C} \right\} = \frac{\partial \overline{C}}{\partial t} + \nabla \cdot (\tilde{U}_p \overline{C}) = 0 \qquad (17)$$

where '—' denotes the ensemble average, '~' denotes a vector, K is a diagonal 3 x 3 matrix, and $\tilde{U}_p = \tilde{U} - \frac{K \nabla \overline{C}}{\overline{C}}$ is called the pseudo-transport velocity.

Equation (17) represents the conservation of mass of a contaminant material $\overline{C}$ in a fictitious flow field of velocity $\tilde{U}_p$. Imposing a strong assumption that the fictitious flow field is of constant density (or negligible expansion rates), i.e., $\nabla \cdot \tilde{U}_p = 0$, Eq. (17) implies that a contaminant element will travel following the pseudovelocity $\tilde{U}_p$. The ADPIC model[14] is developed on this basis. The numerical procedure can be described as follows:

1. The flow field is divided into a number of cells. Based on the initial concentration distribution and the computer storage used, each cell is given a number of discrete contaminant elements.
2. Using each cell as a unit, the velocity term $\tilde{U}_D = - \frac{K \nabla C}{C}$ due to the turbulent flux (diffusion), which is the second term of pseudo-velocity, $\tilde{U}_p$, is calculated by a finite difference scheme. $\tilde{U}_D$ is then added to the actual wind velocity $\tilde{U}$ at each cell corner to yield a pseudovelocity $\tilde{U}_p$.

3. Each tagged contaminant element in a given cell is transported for one time step Δt with velocity $\tilde{U}_p$ which is interpolated from the pseudovelocity $\tilde{U}_p$ at the corners of the cell. In other words, the tagged element is relocated in a new position $\tilde{x}_{new}$ given by

$$\tilde{x}_{new} = \tilde{x}_{old} + \tilde{U}_p \cdot \Delta t$$

The new concentration distribution after a time step is thus obtained on the basis of the new position of each element.

The eddy diffusivities K_x, K_y, K_z currently incorporated in the ADPIC code for this study take the following forms:

a. Horizontal Diffusivities - Using the Kolmogoroff theory[32] in the inertial subrange of the turbulence eddies and the isotropy assumption in the horizontal plane, the horizontal eddy diffusivity can be written as

$$K_x = K_y \propto \varepsilon^{1/3} \ell^{4/3} \tag{18}$$

The proportional constant in the Obukhov expression (Eq. (18)) is taken as one and the length scale, ℓ, is given by

$$\ell = \sigma_x(t) = (\sigma_o^{2/3} + \frac{2}{3} \varepsilon^{1/3} t)^{3/2} \tag{19}$$

where σ_o is the initial standard deviation. The rate of energy dissipation, ε, is assigned as constant (= 2.0) in the model.

When Eq. (19) for length scale reaches its maximum at long times, a slight modification for K_x, K_y, based on the work of Walton,[33] is used, i.e.,

$$K_{x,y}(t) = \left[\frac{1}{K_{max}} + \frac{1}{K'_{x,y}(t)} \right]^{-1}$$

where the $K'_{x,y}(t)$ on the right hand side is that obtained from Eqs. (19) and (18) and K_{max} is a constant (e.g., $K_{max} = 5 \times 10^9$ cm^2 sec^{-1} for $\sigma_o = 204$ m).

b. Vertical Eddy Diffusivity - Since the turbulent shear stress in the surface layer is approximately constant, the eddy viscosity can be obtained from

$$K_m = u_{*o} \left(1 / \frac{\partial u}{\partial z} \right) \tag{20}$$

From similarity law, the nondimensional wind shear $\phi = \frac{kz}{u_{*_o}} \frac{du}{dz}$ would be a function of nondimensional altitude, z/L, where L is the Monin-Obukhov length scale (see Section IV.B.1). The functional form for ϕ in different stability conditions is well known; hence the eddy viscosity can be put into the form

$$K_m = u_* kz \frac{1}{\phi} = \left(\frac{kz}{\phi}\right)^2 \frac{\partial u}{\partial z} \tag{21}$$

Using the Reynolds analogy gives $K_m = K_z$ from the above expression for the eddy diffusivity.

Above the surface layer ($\geq$ 75 m in the ADPIC model), K_z is taken to be constant at its value at the 75 m calculated from Eq. (21). It should be noted that the widely used assumption that the vertical eddy diffusivity is constant above the surface layer is arbitrary.

5. A Model for Diffusion in Shear Flow (DISF)

The DISF model[15] is obtained by analytically solving the diffusion equations via a second-order eddy diffusivity closure scheme and the Lagrangian approach for statistical quantities. The flow field is assumed to be a uniform shear gradient layer.

Neglecting the molecular diffusion effects allows one to write the governing differential equations in Eulerian form for the concentration field as

$$\frac{\partial C}{\partial t} + u_i \frac{\partial C}{\partial x_i} = 0 \tag{22}$$

The assumption of indelibility of the tagged points enables identification of the instantaneous point source at the origin as the initial condition, i.e.,

$$C(\tilde{x},0) = \delta(\tilde{x}) \tag{23}$$

The appropriate solution to Eq. (22) with the initial condition (23) is

$$C(\tilde{x},t) = \delta(\tilde{x} - \tilde{x}(\tilde{0},t)) \tag{24}$$

where $\tilde{x}(\tilde{0},t)$ is the instantaneous position of the tagged element at time t. This solution is averaged over the whole ensemble space to give the expression for the mean concentration of contaminant,

$$\overline{C}(\tilde{x},t) = P(\tilde{x};\ \tilde{O},t) \tag{25}$$

where $P(\tilde{x};\ \tilde{O},t)$ is the probability density distribution function for $\tilde{x}(\tilde{O},t)$.

The dispersion tensor σ_{ij} (of which the dispersion parameters σ_x, σ_y, σ_z are the diagonal terms) can then be written as

$$\sigma_{ij}(t) = \int_{\tilde{x}} X_i(\tilde{O},t)X_j(\tilde{O},t)\ P(\tilde{x};\ \tilde{O},t)\ d\tilde{X} = \int_{\tilde{x}} \overline{C}(\tilde{x},t)\ x_i(\tilde{O},t)\ x_j(\tilde{O},t)\ d\tilde{x} \tag{26}$$

The differential equation for the mean concentration $\overline{C}(\tilde{x},t)$ can be derived directly from Eq. (22). If the eddy diffusivity tensor is used to close the turbulent flux term, the equation becomes

$$\left[\frac{\partial}{\partial t} + \left(U_i \frac{\partial}{\partial x_i}\right)\right]\overline{C}(\tilde{x},t) = \frac{\partial}{\partial x_i} K_{ij}(\tilde{x},t) \frac{\partial}{\partial x_j} \overline{C}(\tilde{x},t) \tag{27}$$

Equation (27) is the general form of Eq. (10) where only the diagonal terms of the eddy diffusivity tensor are considered.

To obtain an analytical solution of Eq. (27), the eddy diffusivity tensor is assumed to be space-independent. Based on Eqs. (25), (26) and (27), a set of equations relating the diffusivity K_{ij} to the dispersion tensor σ_{ij} can be obtained.[34] That is, for a free flow field with constant shear velocity

$$\frac{d}{dt}\sigma_{11} - 2S\,\sigma_{13} = 2\,K_{11}$$

$$\frac{d}{dt}\sigma_{13} - S\,\sigma_{33} = K_{13} + K_{31}$$

$$\frac{d}{dt}\sigma_{22} = 2\,K_{22}$$

$$\frac{d}{dt}\sigma_{33} = 2\,K_{33}$$

with $$K_{23} = K_{32} = K_{12} = K_{21} = 0 \tag{28}$$

Furthermore, one can obtain the following expressions by applying straightforward Lagrangian methods to the dispersion tensor,

$$K_{11} = \overline{V_1'^2}\int_0^t R_{11}(\tau)\,d\tau + S\,\overline{V_1'V_3'}\int_0^t \tau R_{13}(\tau)\,d\tau$$

$$K_{13} + K_{31} = \overline{V_1'V_3'}\int_0^t \left[R_{31}(\tau) + R_{13}(\tau)\right]d\tau + S\,\overline{V_3'^2}\int_0^t \tau R_{33}(\tau)\,d\tau$$

$$K_{22} = \overline{V_2'^2}\int_0^t R_{22}(\tau)\,d\tau,\quad K_{33} = \overline{V_3'^2}\int_0^t R_{33}(\tau)\,d\tau \tag{29}$$

where R_{ij} is the Lagrangian correlation tensor, V_i' is the mixed Eulerian/Lagrangian fluctuation velocity and S is the constant mean shear gradient. The eddy diffusivity tensor is non-diagonal as can be seen by examining Eq. (29).

Substituting Eq. (29) into (27), the solution to the mean concentration equation can be expressed as a generalized Gaussian distribution

$$C(\tilde{x},t) = \frac{Q}{(2\pi)^{3/2}|A|^{1/2}}\exp\left\{-\frac{1}{2}(\tilde{x} - \tilde{x}_o)^T \cdot A^{-1} \cdot (\tilde{x} - \tilde{x}_o)\right\} \tag{30}$$

where $A = |\sigma_{ij}|$, Q is the source strength, $\tilde{x}_o$ is the source location, and superscript T denotes the transposition of a vector. It should be repeated that (30) is a solution for an instantaneous point source in a free uniform shear flow under an assumption of nonspacially dependent K_{ij}.

Based on Lagrangian expressions of σ_{ij} given by Corrsin,[35] a set of explicit and feasible expressions for the dispersion tensor σ_{ij} "over all the time ranges" is proposed.

$$\begin{aligned}
\sigma_x^2 &= \sigma_{11} = C_1 t^2(A_1 t + \exp(-B_1 t)) \\
\sigma_y^2 &= \sigma_{22} = C_2 t(1 - \exp(-B_2 t)) \\
\sigma_z^2 &= \sigma_{33} = C_3 t(1 - \exp(-B_3 t)) \\
\sigma_{xz} &= \sigma_{13} = C_4 t^2(A_4 + \exp(-B_4 t))
\end{aligned} \tag{31}$$

where the constants are given by

$$A_1 = \frac{2}{3} S^2 T_{33} \frac{\overline{V_3'^2}}{\overline{V_1'^2}}, \quad B_1 = A_1 - \frac{2}{3} S \frac{\overline{V_1'V_3'}}{\overline{V_1'^2}}, \quad C_1 = \overline{V_1'^2}$$

$$B_2 = 1/(2T_{22}) \qquad C_2 = 2T_{22}\,\overline{V_2'^2}$$

$$B_3 = 1/(2T_{33}) \qquad C_3 = 2T_{33}\,\overline{V_3'^2}$$

$$A_4 = ST_{33}\frac{\overline{V_3'^2}}{C_4} \qquad B_4 = -\frac{1}{2} S \frac{\overline{V_3'^2}}{C_4}$$

$$C_4 = \overline{V_1'V_3'} - ST_{33}\,\overline{V_3'^2}$$

In these expressions for constants, T_{22} and T_{33} are the Lagrangian integral time scales in vertical and lateral directions.

The effects of boundaries are accounted for by assuming an instantaneous fictitious concentration whose maximum concentration core is located at a point $\tilde{x}_\infty$ The maximum fictitious core $\tilde{x}_\infty$ is determined through a simple analytical geometry calculation by means of an isopleth of concentration.

A relationship between the fictitious core $\tilde{x}_\infty$ and the actual core $\tilde{x}_o$ is, for the lower boundary

$$\tilde{x}_\infty = (x_\infty, y_\infty, z_\infty)$$

$$x_\infty = x_o - \left| 2 z_o \frac{\sigma_{13}}{\sigma_{33}} \right|$$

$$z_\infty = - z_o$$

$$y_\infty = y_o$$

and for the upper boundary

$$x_\infty = x_o - \frac{2(H - z_o)\sigma_{13}}{\sigma_{33}}$$

$$y_\infty = y_o$$

$$z_\infty = 2H - z_o$$

where H is the thickness of the flow field. When boundaries are appropriately accounted for, as indicated above, the instantaneous concentration distribution can be written as

$$\bar{C}(\tilde{x},t) = \frac{Q}{(2\pi)^{1/2}|A|^{1/2}} \left\{ \exp\left[-\frac{1}{2}(\tilde{x} - \tilde{x}_o)^T \cdot A^{-1} \cdot (\tilde{x} - \tilde{x}_o)\right] \right.$$

$$+ \gamma_g \exp\left[-\frac{1}{2}(\tilde{x} - \tilde{x}_\infty)^T \cdot A^{-1} \cdot (\tilde{x} - \tilde{x}_\infty)\right]$$

$$\left. + \gamma_u \exp\left[-\frac{1}{2}(\tilde{x} - \tilde{x}_{Ho})^T \cdot A^{-1} (\tilde{x} - \tilde{x}_{Ho})\right]\right\} \tag{32}$$

where γ_g and γ_u are the constants accounting for the absorption strength of the ground and upper boundaries, respectively.

The dosage at a position $\tilde{x}$ for a point source, initially at $\tilde{x}_o$, can then be obtained through integration

$$\bar{D}(\tilde{x}) = \lim_{X \to \infty} \frac{1}{U_{\text{¢}}} \int_o^X \bar{C}(\tilde{x},\eta)d\eta$$

where X is the alongwind distance from $\tilde{x}_o$ and $U_{\text{¢}}$ is the mean wind speed at $\tilde{x}_o$. Since this is not feasible analytically, particularly with the proposed specifications of the dispersion tensor (31), a Runge Kutta numerical integration method is employed.

B. INTERPRETATION OF ATMOSPHERIC DATA FOR DIFFUSION STUDY

The meteorological information required for the diffusion calculation is interpreted from the rawinsonde measurements for mean quantities (the meso-scale properties) and data gathered at thirteen towers with heights varying from 18 to 150 m for turbulent quantities. The towers and instrumentation at Cape Kennedy are described in Ref. 36 and will not be described in detail here. The meteorological data for each of the Titan III launches have been summarized in Refs. 37 and 38. The locations and heights of the towers are given in Fig. 9. Mean quantities such as wind speed, wind direction, and temperatures were available from some towers and at some of the following levels: 1.83, 3.66, 16.46, 46.34, 62.20, 89.02, 119.82 and 150.91 m. From each tower the standard deviation of wind azimuth angle is given at the 1.83 m level; the lapse rate, which is the temperature difference between 1.83 and 3.66 m is also available. In this section, emphasis is placed on the quantities required in calculations using the five models described above.

1. Atmospheric Turbulence in the PBL

The planetary boundary layer is a turbulent flow field which generally comprises three physical layers: a surface layer near the ground, a mixing layer at the top, and a free convection layer in between. The surface layer is, by definition, that region in which vertical variation of the transport mechanism characteristics, such as friction velocity and heat flux can be ignored. It is usually considered to be 30 m high. However, a recent study[39] of the turbulent wind field below 150 m in the KSC area indicates that relationships which are valid in the surface layer may apply up to the top of the Kennedy tower (150 m). In addition, a measurement in Minnesota[40] also showed that the relationship at the surface layer can be extended to the bottom of the mixing layer (approximately 15% of the PBL height). Therefore, this study considers the PBL to consist of only two layers, one below and the other above 150 m. Interpretation of the turbulence in each layer individually is discussed below.

a. Turbulent Wind Field Below 150 m - The statistics of atmospheric flow over homogeneous terrain in equilibrium in the surface

layer, and thus up to 150 m are determined by three parameters; the roughness length z_o, the friction velocity, u_* and the Monin-Obukhov length, L.

Based on similarity theory, the diabatic wind profile can be written as

$$U = \frac{u_{*_o}}{k}\left[\ln(ze^{-\psi}) - \ln(z_o)\right] \tag{33}$$

where k is the Von Karman constant and can be assumed to be 0.4.

The function ψ in Eq. (33) is recommended from previous studies[39,41] to be

$$\psi = \begin{cases} \ln\frac{2z}{L_o}\,\frac{1+x}{1-x} - 2\tan^{-1}\frac{z}{L_o} + \pi/2 & \text{unstable} \\ 1 & \text{neutral} \\ -5\ z/L_o & \text{stable} \end{cases} \tag{34}$$

where $x = (1 - 16\ z/L_o)^{1/4}$ and L_o is the Monin-Obukhov length at the lower portion ($\leq$ 30 m) of the layer.

The u_{*_o} and z_o thus can be determined by using Eqs. (33) and (34) if L_o is known, i.e., u_{*_o} is proportional to the slope of the curve plotted from the tower measurement of mean velocity vs. $\ln(ze^{-\psi})$, and z_o is given by the intercept of the curve with the ordinate.

The Monin-Obukhov length L is defined as

$$L = -\frac{u_*^3\ C_p\ \rho\ T}{k\ g\ H} \tag{35}$$

where C_p is specific heat at constant pressure, T absolute temperature, ρ density, g gravity constant and $H = \rho\ C_p\ \overline{w'q'}$ the vertical heat flux. The length L_o is related to the flux Richardson number R_f in the lowest 10 m by

$$L_o = z/R_f \tag{36}$$

Since the measurement of $\overline{w'q'}$ is not provided, the gradient Richardson number is used instead, i.e.,

$$R_f = R_g = \frac{g}{T}(\gamma_d - \gamma_\ell)/\left(\frac{du}{dz}\right)^2 \tag{37}$$

where γ_ℓ is the lapse rate of temperature and γ_d is the adiabatic lapse rate.

Precisely, the ratio of R_f and R_g is given[42] as

$$\frac{R_f}{R_g} = \frac{\gamma_T}{\nu_T} \simeq \frac{1}{\phi}$$

where ν_T is the eddy viscosity, γ_T is the eddy conductivity and ϕ is the non-dimensional wind shear given by,

$$\phi = \begin{cases} (1 - 16\ z/L)^{-1/4} & \text{unstable} \\ 1 & \text{neutral} \\ 1 + 4.7\ z/L & \text{stable} \end{cases} \qquad (38)$$

The length L_o is thus determined by applying Eqs. (36) and (37) to observations of wind and temperature at 1.83 m and 16.46 m; z in Eq. (36) is given as the average value (9.15 m) of these two heights. With the length L_o, u_{*_o} and z_o at each tower have been interpolated using Eqs. (33) and (34) for each of the Titan III launches. The observed mean wind velocity used in the calculation is based on 30 min averages. In the present study the average value of u_{*_o} measured at towers along the path of the cloud and at the highest towers (110 or 313) is used for each launch case.

Based on similarity theory, the standard deviation of wind fluctuations, σ_u, σ_v and σ_w at alongwind, crosswind and vertical directions, respectively, are given as

$$\begin{aligned} \sigma_u &= A_u\ u_* \\ \sigma_v &= A_v\ u_* \\ \sigma_w &= A_w\ u_* \end{aligned} \qquad (39)$$

The constants A_u, A_v, A_w are not known precisely. Table VII lists, as a reference, the values obtained in different experiments. In this study, the values suggested by Yaglom[43] are employed. In fact, the constant expressions for A_u, A_v, and A_w are only true for a near-neutral atmosphere. Experiments at Kansas[44] and Minnesota[40] as well as the numerical simulation[45] of an unstable PBL suggested that the ratio of σ_w/u_{*_o} can be fit by an expression

$$\frac{\sigma_w}{u_{*_o}} = 1.89(-\ z/L)^{1/3} \qquad (40)$$

A more general form has been also proposed in recent literature,[46] i.e.,

$$\frac{\sigma_w}{u_*} = 1.3(\phi - 2.5\ z/L)^{1/3} \tag{41}$$

where ϕ is given in Eq. (38). Although little is known about the ratios σ_u/u_{*_o} and σ_v/u_{*_o}, the ratio σ_v/u_{*_o} is found to be very sensitive to stability. Nevertheless, a constant expression for them seems to be best so far.

In our calculation of σ_w using Eqs. (40) and (41) for the August launch in unstable atmospheric conditions below 150 m, the ratio of σ_w/u_* below 100 m is within 15% of 1.07 from Eq. (40) and 1.37 from Eq. (41). The average value of these two constants is surprisingly close to Yaglom's value for A_w, 1.25.

b. Turbulent Wind Field Above 150 m - In the limited literature dealing with turbulence above 150 m, no consistent results are to be found. In this study the work is based on a simple governing equation of a steady-state, neutral barotropic PBL, i.e.,

$$-\frac{d}{dz} u_*^2 = \frac{d}{dz} \overline{u'w'} = f(V - V_g) \tag{42}$$

where V and V_g are the component of above ground wind and geostrophic wind, respectively, at right angles to the surface wind.

The geostrophic wind is taken as the wind at the top of the PBL. The calculation for u_*^2 using Eq. (93) is started at 10% of the height of the PBL with the initial value $u_{*_o}^2$. Figure 10 shows the relative value $u_*^2/u_{*_o}^2$ vertically for the December and August cases. The constant value for u_* in the lower portion is found to have up to 5% error up to 1/6 of the PBL.

In view of the lack of information regarding σ_u, σ_v, and σ_w it is assumed that the relationship of Eq. (39) is also valid for the layer above 150 m. This seems reasonable for a strongly convective PBL in which the mixing layer is nearly neutral. (The results from the Minnesota experiment support this point.) However, it should be kept in mind that neither of the three selected launch cases is in a strongly convective condition. A determination of these basic quantities should be obtained if the

capability to make confident environmental assessments is desired.

Since the mean wind profile for the August case (Fig. 3) shows a negative wind shear between 500 and 1000 m, the positive vertical momentum flux in this region would imply that the eddy viscosity is negative, and that there is thus a negative eddy diffusivity by the Reynolds analogy. Although negative eddy diffusivities may (and here do) occur occasionally in descriptions of strongly bounded flows, none of the codes employed can handle them. Therefore, a negative value of u_*^2 in the region between 500 and 1000 m as shown by the dashed line in Fig. 10, is used in the DISF calculation because DISF was the only model requiring u_*^2 as input.

2. Mesoscale Meteorological Properties

The required mesoscale meteorological information such as wind speed, wind direction, temperature, pressure, and relative humidity in the PBL is based on the sounding measurements performed by the Air Force Eastern Test Range Weather Group. There are three kinds of measurements (rawinsonde, windsonde and jimsphere) at different times. Since only one measurement is given at a time at KSC, a full-scale description for the atmospheric flow at the KSC area depends on the theoretical model. In this study, all models except ADPIC are based on the assumption of homogeneity in the horizontal plane and stationarity during the period of calculations; a simple meteorological model to simulate the full scale wind field accounting for the spatial and time changes is discussed in Section IV.C.1. The present study uses mainly rawinsonde measurements; windsonde and jimsphere measurements are used only for reference. The wind speed, wind direction, humidity, and virtual potential temperature from rawinsonde measurements for the three Titan III launches, (the set of measurements at nearest time of launch is used), are shown in Figs. 2, 3, and 11.

The virtual potential temperature ϕ_v is calculated using Tabata's expression,[47] i.e.,

$$\phi_v = T \left[\frac{1 + 1.61\ W_m}{1 + W_m}\right] \left[\frac{1000}{P}\right]^{0.288}$$

where T is air temperature (°K), P barometric pressure (mb) and W_m is mixing ratio given by

$$W_m = \frac{0.622 \cdot RH \cdot e_s}{P - RH \cdot e_s}$$

where RH is the relative humidity (%), e_s is saturation vapor pressure = $10^{(c-dx-ex^2)}$, x = 1000/T, and the constants c, d, and e are given by c = 8.42926604, d = 1.82717843, e = 0.07208271. The virtual potential temperature is plotted instead of the air temperature because it is the main parameter for determining the thickness of the PBL, the existence of the inversion layer, the stability of the layer, etc.

As mentioned before, a sensitive and important meteorological parameter in the prediction of the cloud ground concentration is the thickness of the PBL. The PBL in this study is defined as the region in which the turbulence cannot be ignored in the transport process. In a well-mixed PBL capped by a temperature inversion, e.g., in sunny (clear) daytime, it will be approximately neutrally stratified at the upper portion and its mean wind profile will be nearly uniform vertically. Idealized characteristics of the well-mixed PBL are shown in Fig. 12. From the plots in Fig. 12, it is evident that none of the selected launch cases is similar to this ideal condition; in fact, the August case is a sea-breeze condition. At Florida it is shown that the sea breeze usually initiates a storm;[48] thunder during the launch time was indeed heard at the KSC weather station. The March case was a late afternoon launch (at 2027 EDT) and the December case was a night launch (at 0310 EDT). Since the detailed data on turbulence needed to establish the thickness of the PBL is not available in these cases and since an ideal PBL did not exist during these launches, the PBL thickness must be inferred from observations of cloud behavior, as discussed below.

a. August Case - As shown in Fig. 3, the virtual potential temperature increases sharply after 1600 m, the wind speed changes dramatically after 1850 m, and the relative humidity drops significantly between 400 and 700 m. These observations are not consistent; any determination based on these mean quantities would not be very meaningful. Alternately, we can use the simplest balance Eq. (42) and integrate it, and obtain

$$u_*^2(z) - u_{*_o}^2 = f \int_o^z (V_g - V)dz \qquad (43)$$

If the top of the PBL is assumed to be a zero vertical momentum flux, $u_*^2(Z_i) = 0$, where Z_i is the thickness of the PBL, and $V_g = -A\, u_{*_o}$, which is the Kazanski-Monin relationship, Eq. (43) becomes

$$u_{*_o}^2 = -Af\, Z_i u_{*_o} - \int_o^{Z_i} f \cdot V\, dz \qquad (44)$$

Since $u_{*_o}^2$ is known, f is the Coriolis parameter taken to be 5.5×10^{-5} (sec^{-1}), and V is known at each height, we can obtain Z_i by solving Eq. (44) for a given A. It is found that only one Z_i exists for the value of A between 5 and 15†: Z_i is found to be 1800 m. We have found that u_*^2 equals approximately 0 at 1950 m in Fig. 10, where a different approach was used (the geostrophic wind was assumed to be the wind at 2000 m). The close agreement between these two results is not surprising because they are both derived from the same equation and use very similar values for V_g. The prediction of 2000 m for the thickness of the PBL does not agree with the value of 1090 m given in Ref. 23. It is not clear how that value was derived. However, real-time tracking of the cloud by camera shows that the cloud dispersed faster below 2000 m and that an inversion cap existed at about 2000 m. In other words, observation implies that turbulence cannot be ignored up to 2000 m and thus the thickness of the PBL will be no less than that height.

b. December Case - Using the approach of the August case for the December case, the thickness of the PBL is found to be about 510 m. It is slightly different at the 540 m height, where the u_*^2 is zero, shown in Fig. 10. The virtual temperature increases strongly after 620 m and the humidity drops significantly at about the same height as shown in Fig. 2, so again the thickness of the PBL seems to be about 600 m. In fact, the results from airborne measurements[11] at an altitude between 560 m and 610 m demonstrate a very slow dilution of the cloud in this region indicating very low turbulence levels. Since the Titan ground cloud is always stabilized at pretty high levels (with an order of magnitude of 1000 m), most of the exhaust mass will stay above the PBL under a shallow PBL condition. If the PBL is assumed to be thicker, more of the

---

† A = 12 is often used in conditions without data.

exhaust mass will remain in the PBL. Since increase of mass in the PBL will certainly increase the ground level prediction, for conservative purposes we will use the higher value 660 m (the height at which measurements were obtained) for the PBL thickness in the diffusion calculations for the December case.

c. March Case - In this late afternoon case, all the meteorological parameters have a turning point between 700 and 1100 m (see Fig. 11). The IR observation of the cloud showed a separation of the atmospheric flow at about 1100 m. Since at this time of day one expects to be in a period of transition, any estimate will be subject to significant error. For the calculations we simply take the thickness as the sounding measurement height of 1088 m.

It would be interesting to know the actual ratio of the selected thickness Z_i and the widely used length scale u_*/f for the Ekman layer; the ratios $Z_i f/u_*$ used for the August, December, and March cases are 0.18, 0.16, 0.14, respectively. They are all lower than the value 0.28 obtained from a simulation of the idealized neutral atmospheric boundary layer.[49] However, before a more precise micrometeorological model is established to provide the information on the PBL height, we may use 0.16 u_*/f to be a reference height for determining the PBL height from the sounding measurements.

C. CONCENTRATION CALCULATIONS

Although each model selected for the diffusion calculations uses different forms of input data, the basic information required by each is (i) the initial cloud shape and concentration distribution, (ii) the advective wind field and boundary conditions, (iii) the statistical/physical quantities needed (generally different for each model) to describe the turbulent mechanism, and (iv) the type and location of output desired from the calculations.

This basic information for the aforementioned three Titan III launches is given in Appendix C. The cloud shape and concentration distribution at cloud stabilization are calculated using the NASA/MDM preprocessor program[1] for the layered model 4; the meteorological data and the thickness of the PBL are determined as described in the previous section; surface measurement data are taken directly from the tower measurements. All the

statistical parameters required for calculations by TREATS, ADPIC and DISF are interpolated by following the procedure given before. Calculation methods using the MDM program have been covered in the parametric studies of Section III; diffusion calculations using the other four models are described below.

1. The METS Model

Utilizing the input information given in Appendix C, calculations using METS were made employing several options in the program to provide an upper bound of its predictions. The METS calculations that include particles and chemistry give a higher ground prediction of HCl than if they are not included. The particle size distribution in the calculation is chosen randomly.

2. The TREATS Model

In this study, the flow field is divided into 45 sublayers, at each of which moment integrations over the entire horizontal space are calculated. The source strength and input information for each sublayer are obtained by linearly interpolating values provided in Appendix C. The time step for the calculation is set at 30 seconds.

For the August study, three calculations have been made using different eddy diffusivities K_z as given in the review section of the TREATS code. Since the value of K_z calculated from the Blackadar formulation (15)and (16) is about one and is probably too small for $z \leq 100$ m in a convective PBL in general, a more probable value of $K_z = 30$ for $z \leq 100$ m is used in the August calculations. The value 30 is calculated using the expression for K_z based on the similarity theory as given in the review section on ADPIC. There is only one calculation for the March study and two for the December study. The March calculation uses the K_z from Pasquill-Gifford curves and the December calculations use the K_z from Pasquill-Gifford curves and the Blackadar formulation (15) and (16). The parameters required for the calculation in the Blackadar formulation, (e.g., z_o and u_{*_o}) use, for all three launches, the average value of those interpolated from tower data using similarity theory.

3. The ADPIC Model

Because of limits imposed by the availability of computer storage, the total number of grids for each calculation is assigned to be 41 × 41 × 15 = 25215. The grid size is 150 m vertically, 500 m laterally, and 500 m longitudinally in the August study; 80, 500, and 500, respectively, in the March study; and 50, 1000, and 1000, respectively, in the December study. The maximum number of source terms is five. Each may be located at an (x, y, z) with a Gaussian distribution of material in three dimensions. Each dimension has a right and left (or up and down) cutoff distance from x,y,z. Each source may also be a different species with individual particle distribution. The total number of species plus locations must be less than five. Initially, the concentration in each pancake is assumed to be uniform vertically and Gaussian in the horizontal. Each sample point is assigned a weight of 819 g, 444 g and 135 g for August, March and December, respectively. The total source is represented by 20,000 samples in each case. Each cell has many more than one sample particle.

As described in the brief review of the ADPIC program in the previous section, the program can utilize any time averaged advective wind field as input at a given time. Therefore, the ADPIC program can account for the variation of wind field downstream. Since only one mean wind measurement (from rawinsonde) at KSC is given at intervals of two hours or longer, the change of wind field with respect to space as well as time must be estimated if the nonhomogeneity or nonstationarity of the atmospheric wind field is to be considered. A simple three dimensional wind field model[50] is employed; it utilizes the surface tower measurements because they provide the space and time variations. The procedure to create a wind field is as follows: (1) It is assumed that the vertical wind at each tower location has the same profile as the rawinsonde measurement but different wind direction and magnitude of wind speed; the wind direction and the magnitude of the wind speed are determined by fitting the lower portion of the assigned profile to the measured wind data of the tower. (2) The wind field at each grid point is then interpolated from the wind value at the tower locations by allowing a minimal adjustment which relies on the constraint of incompressibility of the flow field (i.e., $\nabla \cdot \tilde{u} = 0$). (3) The simulated wind field is changed whenever the tower measurements change. Each of the sixteen towers shown in Fig. 9

is used in estimating the wind field. Two sets of wind data, separated by 30 minutes each, are used in the August study; ten sets and twelve sets over five minutes each are used in the March and December studies, respectively.

4. The DISF Model

Since this model is formulated for a point source, a diffusion calculation for an irregular non-point source would require an integration of point source calculations over the entire initial cloud, i.e.,

$$\overline{C}(\tilde{x},t) = \iiint \overline{C}(\tilde{x};\ \tilde{x}_o,\ t)\ d\tilde{x}_o \qquad (45)$$

where $\tilde{x}_o$ is a point position in the cloud and $\overline{C}(\tilde{x};\ \tilde{x}_o,\ t)$ is the concentration at $\tilde{x}$ at time t from a source point $\tilde{x}_o$, as given in Eq. (32). This is not practical because it cannot be integrated analytically and numerical integration requires large computer times. An alternative approach is to divide the initial cloud discretely into a number of cell sources, each of which is treated as a point source. The total number of cell sources is assigned to be 40 for each layered pancake in the present study. The number of pancakes is the same as that given in Appendix C. In order to reduce the error induced by the discrete approach, each layer is divided in the following way, which shows a cross section

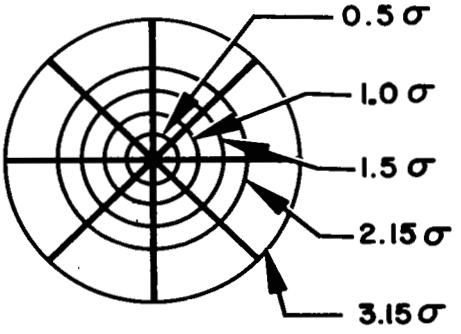

where σ is the standard deviation of concentrations at the time of cloud stabilization. The point source is located at the center of each cell. The physical quantities used (e.g., mean wind field) for a calculation from a point source are determined by the following method:

1. Wind direction is the average value of wind directions in the range of altitude between 1/6 of the PBL thickness downward from the altitude of the point source and 1/6 of the PBL thickness upward. Wind directions outside the boundaries are ignored.
2. The wind shear and wind speed are derived from the best linear fit of the measured wind data in the range cited above.
3. The turbulence intensities and stress are assumed to be constant below the 1/6 depth of the PBL at the value interpolated from tower data using similarity theory (see Section IV.B). Above 1/6 of the PBL, the average value of an assigned turbulence profile within the range given in (1) is used.

D. COMPARISON

1. Model to Model Comparison

The results calculated from all five models for the three Titan launches are shown in Figs. 13 to 19. Three kinds of values from the calculations are plotted for the comparison. They are (1) maximum instantaneous concentration, (2) maximum integrated concentration (dosage), and (3) the path of maximum ground level concentration. Only one species (HCl) is considered. As mentioned before, some of the models used to make calculations employ estimated values for some input parameters which may not have much physical validity. At present, only the plot that gives the highest value for each model (except MDM) is given in each comparison. There are at least two plots from MDM calculations in each figure showing concentration or dosage. The reasons for doing this are: (1) Although it was generally recommended that the MDM calculations should be performed using tower measurements of σ_{A_o}, we used both tower data and the interpolated σ_{A_o} from similarity theory (which are more consistent with the input requirements of the other models). (2) It is of interest to see whether the uncertainties from a basic input parameter, σ_{A_o}, which is used to describe the turbulence mechanism in the MDM will cover the range of predicted results from other models. (3) We hoped to determine the best approach for using MDM (in terms of doing an environmental impact study or determining launch constraints should the MDM be used for these purposes in the future).

Since the use of the TREATS model with the Blackadar mixing length formulation (15) and (16) yields the highest value, the plots in Figs. 13 to 17 represent results using this approach. The dosage plots in Figs. 14 and 17 from the METS model were obtained from calculations which include the chemistry and particles because otherwise near zero values would result.

The figures and comparisons are discussed below for each launch case.

a. 20 August 1975 Case - For this typical afternoon sea breeze weather condition at KSC, ADPIC, TREATS and DISF predict nearly equal maximum instantaneous ground concentrations downstream, especially in the near field of the launch complex, while results from the MDM give a higher level. Specifically, the plotted results in Figs. 13 and 14, from the MDM model 3 and model 4 calculation using the value of σ_{A_o} given in Ref. 23, show a very high maximum concentration in the near field although in the far field they show a better value, nearly equal to those obtained from the other three models. It should be noted that all the predictions will converge far downstream ($\approx$ 100 km) if the wind field is frozen. There is a slight difference between dosage comparisons and the instantaneous concentration comparisons. In Fig. 14, it is clearly seen that DISF gives higher predictions of maximum dosage than ADPIC and TREATS but merges with the MDM results about 30 km from the launch pad. The METS model did not provide enough information for a clear comparison, but apparently predicts values too low in the near field. For a reference, the results from TREATS using two alternatives for the vertical eddy diffusivity (see previous section) are in the bound of the 30% variation for maximum concentration and 50% for dosage from the plotted values in the figures. It should be mentioned that the plots of Figs. 13 and 14 ignore the fact that each model predicts a different transport direction at downwind distances. Figure 15 thus gives ground paths of the maximum concentration downstream from the five models. In this figure, DISF and MDM have the same path 8 km from the launch complex. The TREATS path is the furthest from the MDM and the ADPIC and DISF paths lie between the TREATS and MDM paths. It is interesting that the METS model predicts a path jumping between the paths of MDM and TREATS.

b. 10 December 1974 Case - For this nocturnal case, the comparisons, Figs. 16 and 17, show characteristics similar to the 20 August 1975 runs, except for the following points: (1) All the predictions for the maximum instantaneous concentration converge much faster downstream. (2) There is a big difference in the near field between the MDM predicted results using measured and interpolated σ_{A_o}; the former is much lower than the latter. (3) ADPIC gives very low predictions. (4) ADPIC, DISF, and TREATS predict very different maximum concentrations in the near field. (5) The METS model gives a low dosage prediction, especially downstream.

In Fig. 16 for the comparison of maximum concentrations, two additional results are shown which were calculated using MDM models 3 and 4 with an input provided by a different version of the NASA preprocessor program. Clearly they produce very high predictions which are probably unrealistic (see Section IV.F).

One additional plotted result from MDM is also given in Fig. 17 for the comparison of maximum dosage predictions. This line results from the use of a vertically varied σ_{A_o} for input, as mentioned in Section III.A.1. This predicted result seems to correlate better with the results calculated from the other models. However, its lower prediction in the near field raises some concern that the MDM model may underestimate the ground level concentration in the near field ($\leq$ 10 km) from a rocket launch if better and more accurate turbulence information for the PBL is available and used in the MDM calculation.

c. 14 March 1976 Case - This is a late evening case. Figure 18 shows good agreement for maximum concentration predictions from all models in the near field except the MDM using interpolated σ_{A_o} which gives a slightly higher prediction on the ground. The dosage plot, Fig. 19, demonstrates the much higher prediction from DISF than from all the others after 15 km. This high predicted value from DISF downstream is caused by the assumption of a vertically exponential decay of turbulence intensity above the surface layer, while actually the lower atmosphere at KSC at launch time somehow still maintained some turbulence strength. The existence of strong turbulence above the surface layer is shown by the observation that the south cloud (with which we are concerned here) dissipated 15 minutes (6 km downwind) after launch.

Hence it is reasonable to assume that, after moving 10 km downwind, the cloud is vertically well-mixed and further dilution is controlled by horizontal dispersion. Since the horizontal dispersion rate is increased after 10 minutes, the maximum dosage should decrease downwind. Therefore, the increased profile of the maximum dosage predicted by DISF must result from an insufficient vertical dilution at earlier times (or a slow diffusion). Since turbulence is the only mechanism that controls the dilution it is clear that the turbulence input for the DISF model is too weak. However, the important advantage of the plotted results from DISF for the present study is that they provide a conservative prediction of possible ground level concentration far downstream. Since the DISF predicted values are still lower than the peak value predicted by MDM using interpolated σ_{A_o} (although this peak value is at the near field of the launch pad) the MDM predicted peak of maximum ground level concentration seems to be a conservative input for analysis of the ground level environmental hazard.

It should be mentioned that all the results calculated from DISF using any profile other than exponential decay for turbulence above the surface layer fall in the range below the conservative prediction line drawn in Fig. 19.

2. Model to Measurements Comparison

In order to better evaluate the models, their predicted results and available measurements have been compared. These comparisons utilize both ground-based and in-cloud airborne measurements and emphasize the August and December launches. The flight path of the aircraft in the August study, as shown in Figs. 20 and 21 is plotted from ground-based radar tracking data but in the December study it is based on the airplane crew's visual record of the aircraft location during measurements. The HCl data were obtained from the chemiluminescence monitors; detailed information on the monitors can be found in Ref. 51.

a. August 20 Case - Airborne Measurements - Fifteen aircraft passes were made through the cloud at altitudes from about 1100 m to 1600 m (see Fig. 21). For the sake of simplicity we have chosen six data sets for the comparative analysis, viz., passes 5, 6, 9, 10, 12, and 14. The altitudes of

these passes for the model calculations are 1420 m, 1125 m, and 1600 m for passes 5 and 6, passes 9 and 10, and passes 12 and 14, respectively.

Since neither the MDM or METS programs currently provide information on instantaneous concentrations, direct comparisons between the predicted values and the airborne measurements were made only for the ADPIC, TREATS and DISF models. Figures 22 and 23 show the comparative results. The solid lines in the figures are the values calculated from the model on the path as shown in Figs. 20 and 21 at the appropriate time. The dotted lines are the experimental results. Because many uncertainties are involved in both the calculations and the measurements, it is difficult to derive any conclusions as to the validity of the absolute values at any spatial location in either case; for example, the wind velocity used in the model calculation is certainly not the real wind velocity which transports the ground cloud at the launch. This uncertainty could cause the model-predicted cloud to be far from the real cloud, i.e., the path of measurements is not the same as that simulated. Therefore two additional calculations for each pass have been made by simply moving the whole path of each pass 500 m downwind and 500 m upwind. The results are drawn in dashed lines for the upwind relocation and in dashed-dotted lines for the downwind case in Figs. 22 and 23. The data bars on the solid lines from TREATS represent the range of variation obtained using different vertical eddy diffusivities as given in the previous section. Surprisingly, the values fall in a quite narrow band.

Comparisons of concentrations on flight passes between the airborne measurement and TREATS model are given in Fig. 22(a) and comparisons for the ADPIC model are given in Fig. 22(b). The comparisons for TREATS on passes 9 and 10 are not plotted in the figure because this model produces a value of 0 ppm on all three paths for both passes, i.e., the "exact" path, the path moved 500 m downstream, and the path moved 500 m upstream. This is not surprising in view of the comparisons for other passes. From the plots for passes 5, 6, 12, and 14 in Fig. 22(a), it may be seen that the maximum concentration in the TREATS-simulated clouds during the time of each flight pass is much higher than the measurement. As mentioned before, these four passes are presumed to have traversed the maximum concentration region of the cloud. Therefore, the higher values obtained from the model imply that diffusion in the TREATS model is not as fast as in the real cloud. In

other words, the eddy diffusivity used in the TREATS model may be inaccurate. The slower rate of diffusion prevents the cloud from becoming large enough to produce any concentration for passes far away from the cloud center such as passes 9 and 10. The comparisons for ADPIC results shown in Fig. 22(b), imply the same conclusion as for the TREATS model. No exact calculations were made for passes 5, 6, 9, and 10.

As shown in Fig. 23, concentrations calculated from DISF correlate, in general, quite well with flight measurements. On the basis of comparisons between calculations and data for passes 5 and 6, we can conclude that the cloud is actually located a little further downwind than the model indicates. This apparent dislocation, however, raises the question of what the maximum predicted concentrations from DISF would be on a path through or near the center of the modeled cloud where both passes 5 and 6 are presumed to lie. The answer is that the maximum predicted concentration anywhere in the cloud will be very close to (although definitely somewhat higher than) the value of the dashed lines in Fig. 23. This conclusion is based on the observation that although the exact location of any of the calculated curves with respect to the cloud coordinates is unknown, that position can be reasonably estimated by assuming a bell-like spatial distribution at any point in time and then comparing the relative concentrations of the three profiles which are separated by 500 m. Thus, in pass 5, it may be concluded that the "exact" profile (solid line) and the upwind profile (dashed line) both lie fairly close to the center of the cloud since this is the only portion of the cloud where fairly high concentrations can be encountered and a 500 m shift in position does not change the maximum value significantly. Similarly, in pass 6 three curves appear to be on the upwind side of the centerline profile but, since the differences between them are small, the two highest curves, at least, are not far from the center. The 3 ppm maximum in the profile farthest upwind therefore is a fair approximation of the absolute maximum attainable.

On the other hand, passes 9 and 10 exhibit very low concentration profiles and display a monotonic increase in maximum concentration as cuts are taken further and further upwind. This indicates that this region of the cloud lies near its edge where the concentration vs. time distribution is characterized by the flat tail portion of the curves and low absolute values.

Considering the comparisons of flight passes 12 and 14 in Fig. 23, it is found that the peak value of downwind (dash-dot) profile is higher than that for the solid and dashed lines, directly opposite to the results of the other passes in the figure. This is because the wind speed used in the DISF calculation at the altitude of these two flight passes is the average value for the upper 700 m of the PBL and the actual wind speed at 1600 m is higher than the average. The argument concerning the differences between plotted results for passes 5, 6, 9, and 10 is not applicable to passes 12 and 14 because the separation distance between the two paths in the calculations (500 m) is smaller than the standard deviation of the cloud spreading when the cloud is better mixed after long times; the better mixing (i.e., wider spread) is apparent from the data (dotted lines) for passes 12 and 14.

There is an additional interesting point in the ADPIC comparisons for pass 12 in Fig. 22(b), this plot gives an excellent example supporting the argument used above in the DISF flight comparisons to qualitatively determine the maximum concentration via analysis of the differences of the peak values of the plotted results. As shown in the plot, the calculated maxima on the given three paths increase rapidly and progressively, in the upwind direction. Using the argument cited before, the maximum value at the centerline of the cloud should be located even further upwind and its value will be significantly higher than the maximum in the dashed curve--how much cannot be accurately determined. In fact, detailed calculations of the entire cloud using ADPIC yield a centerline maximum value of 10 ppm.

b. August 20 Case - Ground-Based Measurements - For the August launch there were five ground-based HCl monitoring sites indicated by black spots in Fig. 15. No HCl was detected at any of these sites except P-10 near the coast line. "No HCl" means that the HCl level is less than the lower detection limit, 0.005 ppm, of the instrument. As shown in Fig. 15, the ground level calculations using TREATS and ADPIC predicted that the path of maximum concentration would be closer to P-2, P-5, P-7, and P-8 where no HCl was detected than to site P-10; TREATS, in particular, predicts a path that is farthest from P-10. If a direct comparison is made between the measurements and the results calculated for these sites by ADPIC and TREATS, great disagreement is seen; ADPIC did not give a larger value than the instrument limit on sites

P-7, P-8, and P-10 but gave measurable values at sites P-2 and P-5; TREATS gave no HCl on site P-10 but gave measurable values at the other four sites.

In order to test these models with less demanding requirements, one can ignore the direction of cloud travel and simply assume that all paths of maximum concentration for different models coincide along the path predicted by MDM because the MDM (as well as DISF) predicted path is closest to P-10. The comparison of results for site P-10 under such circumstances is shown in Table VIII. DISF gives a value near that of the observed maximum concentration but a value which is a factor of 5.6 higher than the measurement for the dosage.

In contrast to DISF, the TREATS model showed an excellent agreement with the observed dosage value but a factor of two lower than the measured maximum concentrations. Compared to the data, ADPIC predicted too low and MDM predicted conservatively high on both concentration and dosage. It should also be mentioned that the MDM model is the only one of the four models (excluding METS) which predicted the HCl value larger than 0.005 ppm at those "no HCl" detected sites with these adjustments; in fact, it is quite high (about 0.2 ppm).

c. December 10 Case - Airborne Measurement - During this launch, there were 12 sampling flight passes through the lower cloud below 660 m, the PLB height in this case. Most were at altitudes between 550 m and 600 m. From the flight measurements, the portion of the cloud between altitudes 550 m and 600 m was located between 180° to 185° from the launch pad. The actual path is indicated by the shaded area in Fig. 24 and is about 10° to 15° off the cloud paths predicted by the models as indicated by the dashed and solid lines in the same figure. The predicted cloud path was calculated using wind direction measured at 40 min before launch (see Appendix C). The lack of correlation between the measurements and predictions may be attributed solely to the change in the wind. Furthermore, the cloud path at the 1400 m level, observed using IR measurements and the dashed line in Fig. 24, is also found to have a 10° to 15° difference from the wind direction used in the calculation at that 1400 m level. Therefore, we have compared the predicted concentration in the maximum core region directly to the measured airborne sampling data. The maximum core region was taken as the disc-like volume between altitudes 550 m and 600 m and with radius 550 m. Its volume is approximately equivalent to the cell size used in the ADPIC model. To make such comparisons, we have

assumed that the airplane average speed was 55 m sec^{-1} and the concentration of the core region was well mixed, i.e., the average value of the concentrations within the 22 sec interval during which the highest levels were measured was used to represent the measurement value of the core region at the time of the flight pass. Surprisingly, it was found that the measured value at 28.52 min after launch was a factor of three greater than the initial value used in the model calculations at stabilization time. This meant that either the total source strength assigned to the initial cloud (below the PBL height) using the preprocessor program was less than 30% of the strength of the real cloud, or the lower portion of the cloud near the ground was unrealistically given too much strength. The latter situation is impossible because the total source strength of the portion of the cloud in the calculation below 600 m was less than three times the assigned source strength of the portion of the cloud between 550 m and 600 m. In other words, the preprocessor program underestimates the total amount of pollutants left in the nocturnal PBL. This probably occurs whenever the predicted cloud stabilization height is above the estimated PBL.

Further comparisons between the predictions and measurement data were made for the so-called "dilution ratio" that is, the ratio of the average concentration in the core region at time t to the concentration at time $t-\Delta t$. Table IX shows the ratios calculated from different models and airborne measurements. The earlier time refers to the times at stabilization and 10 min after. The later time refers to 26 min and 36 min after stabilization; 26 min after stabilization is the time of the first airborne sample pass made between altitudes 550 m and 600 m. This table shows that: (1) ADPIC and DISF models dilute the cloud very slowly at the upper portion of the PBL, that is, they move only small amounts of pollutants from the upper highly concentrated region to the ground; (2) TREATS seems to predict slightly faster diffusion than the real situation; and (3) MDM definitely diffuses too fast during the first 10 min at the upper level. The fast diffusion predicted by MDM at the earlier time explains why the highest ground concentration resulted at the near field of the launch pad using MDM. Most importantly, it shows that the high peak of maximum ground concentrations predicted by MDM is caused by moving the upper level pollutants to the ground too fast. It should be noted that the results shown in Table IX from MDM

were based on calculations using the vertically uniform σ_{A_o} and σ_{E_o} (see Section III.A.1).

d. December 10 Case - Ground-Based Measurements - Locations of the four ground monitoring sites and the predicted paths of ground maximum concentration are given in Fig. 25. The measurements have shown that no HCl was detected at site P-1 but 19.5 (ppm-sec), 6.2 and 15.2 were collected at sites P-2, P-3, and P-4, respectively. With this information, the ADPIC program clearly demonstrates its capability to predict the maximum ground concentration path of pollutants more accurately than the other models. This is probably due to its ability to model the advection effect; the December case was in a nocturnal condition with strong advective wind and weak turbulence. In the comparisons made for the December case, we assumed that all paths of maximum ground concentration for different models coincided in one path given by ADPIC and then compared the concentrations at locations P-2, P-3, and P-4 between the model predictions and the measurements. The results are shown in Table X. Since in the airborne measurement comparisons, the total source strength of the cloud used in the calculations is about a factor of three less than that of the real cloud, the values in the table have been multiplied by three.

We have also given three sets of values for MDM in the comparisons. They were calculated using the vertically uniform $\sigma_A = 8°$, $\sigma_A = 4°$ and a monotonic decay profile for σ_A as cited in Section III, respectively. Apparently, none of these three sets of values gave trends similar to those observed. This may be attributed to the improper dispersion by MDM at the upper portion of the PBL. The ADPIC results are clearly lower than the measured data. The paradox of why ADPIC gives lower predictions of ground instantaneous concentration than DISF, while the former has a greater dispersion than the latter in the upper portion (as shown in the airborne comparison), can be resolved in two ways: (1) DISF assumes higher turbulence than ADPIC in the middle portion of the PBL and (2) the imposed assumption of incompressibility of the fictitious flow field, which would reduce the diffusion rate, in the ADPIC model may be improper. Although the maximum instantaneous concentrations predicted by TREATS and DISF were notably lower than the measurements at sites P-2 and P-4, the predictions from these two models seem to be adequate. However, from the

overall view of the prediction capabilities of these five models by comparison with data, TREATS gives the best results for this nocturnal launch case. This may be because (1) since the shear of the wind speed in the PBL is negligible in this night case, ignoring off-diagonal eddy diffusivity terms in TREATS is valid, (2) the Blackadar type vertical eddy diffusivity and the mixing length scale are proper for the shallow PBL as in the December case, and (3) the empirical Pasquill-Gifford type curves were obtained from measurements at the lower portion of the layers; when the layer is shallow, the eddy diffusivity derived from these curves may be adequate.

E. CALCULATIONS AND COMPARISONS FOR AN OBSERVED GROUND CLOUD

The comparative studies described in the previous sections were made utilizing as input the description of the stabilized cloud provided by the MDM preprocessor program. (For simplification, we will call it the "modeled cloud".) As mentioned before, the uncertainties included in such input may seriously affect the downwind predictions of concentration distributions. Hence a comparative study of diffusion models using more realistic input was desired. Of the three launch cases examined in this study, the August case is the only one for which the most complete observation and airborne sampling data are available. The most detailed comparison based on stabilized cloud characteristics as interpreted from both observation data and airborne measurements (collectively called the observed cloud data) was therefore made for the August case. Because the previous comparative results for this case showed that the DISF model yielded the best predictions compared to measurements, this set of calculations and comparisons for the observed cloud focused on the DISF and MDM models only. The assumptions and procedures incorporated in this analysis are:

(1) The cloud location and volume are directly interpolated from the photographs of the stabilized cloud taken by three Askania tracking cameras. An ellipsoid shape for the cloud in each sector is assumed.

(2) A Gaussian concentration distribution is used for each ellipsoid cloud. The concentration at the edge of the cloud is assumed to be 1% of that at the center.

(3) The total amount of pollutant is taken to be that resulting from 17 sec of exhaust. The number 17 was chosen since early airborne samples show that the average HCl monitored is about 4 ppm; this concentration, when combined with the observed volume of the cloud, 2.2×10^9 m^3, gives a total mass of HCl in the stabilized cloud of about 15×10^6 g, which equals that from about 17 sec of exhaust. In addition, from the camera observations, the cloud left in the PBL is that portion of exhaust which reaches the ground between firing and the attainment of 500 m altitude. Using the trajectory function for Titan III, 17 sec is required for the rocket to reach the altitude 500 m.

(4) Since the camera observations show that the cloud contains two cloud portions, amounts corresponding to 14 sec and 3 sec of exhaust are assigned to the higher and lower portions respectively; this distribution ratio is based solely on the observed volumes of the two portions.

Figure 26 shows the comparative results of the maximum ground dosages obtained using MDM and DISF. Compared to the results of calculations using the modeled cloud as input (Fig. 14) the results based on actual observed cloud characteristics show lower peaks and more rapid convergence of predictions from MDM and DISF at downwind distances. A comparison between this set of DISF calculations and airborne measurements is shown in Fig. 27 and a comparison of the ground measurements and model predictions at monitoring site P-10 is shown in Table XI. Better agreement between airborne measurements and calculated results using the observed cloud rather than the modeled cloud (in Figs. 27 and 23, respectively) justifies our efforts. The maximum ground concentration path predicted from DISF using improved observed cloud characteristics as input is close to the ADPIC predictions in Fig. 15; we have presented the predicted results before and after adjustment to the MDM predicted path as described in the previous section on ground-based measurement comparison.

F. DISCUSSION

The comparisons made during this program demonstrate that the MDM generally overpredicts concentrations (or dosages) of exhaust constituents at the ground. This occurs principally because the model assumes that the standard deviation of wind azimuth angle σ_A is vertically uniform, whereas it varies with height. The concentration predictions are about an order of magnitude higher than the values indicated by the use of other models which give results in better agreement with the available data. For example, the DISF model gave good agreement with the data for the daylight August launch. The difference in concentrations predicted by MDM and DISF is about an order of magnitude, the same difference between TREATS and MDM for the December nighttime launch case, where TREATS gave values of the same order of magnitude as the measured data. Therefore, the ground level pollutant concentration predictions from MDM may be treated as conservatively high.

As shown, the input of σ_A is a dominant parameter for the MDM predictions. Direct measurements of σ_A vary rapidly over wide ranges, especially in nighttime cases; it appears more useful to utilize the value of σ_A given by an interpolation method based on similarity theory which gives consistently higher predictions for a variety of meteorological conditions.

There is no detailed information presently available on the cloud at stabilization; the description of the stabilized cloud given by MDM (more precisely, by its preprocessor) seems to be reasonable when the center of the cloud mass is below the top of the PBL, although even under these conditions, MDM still tends to overpredict ground concentrations and dosages (see Section IV.E). On the other hand, when the cloud center penetrates the top of the PBL, which usually happens with a shallow PBL ($\lesssim$ 700 m) the total calculated source strength seems to be lower than that in the real cloud. This is a serious problem, because in this case the pollutant level is artificially decreased and the assumption of conservatively high estimates may be nullified.

Recent efforts by SAI to modify the preprocessor program to more exactly account for the mixing rate of the exhaust plume and the rocket trajectory resulted in even greater overpredictions for ground concentrations.

The following conclusions were reached concerning the other models used in this study:

(1) The moment scheme (TREATS), coupled with the Blackadar formula for the vertical diffusivity and the horizontal eddy diffusivities deduced from the Pasquill-Gifford curves, did not properly model the cloud diffusion in the August case, but gave favorable comparisons with data for the nighttime December case. The probable explanation is that the eddy diffusivities used may not adequately describe the deep PBL (August case) which is driven mainly by sea breeze rather than the usual thermal and mechanical forces. The Blackadar formula and Pasquill-Gifford curves having been based on the lower portion of the PBL, would be inadequate for the deep PBL existing during the August launch but valid for the shallow PBL of the December case.

(2) The inherent ability of ADPIC to treat the advection effects due to wind variation is clearly exhibited in this study, particularly in the December nighttime case. However, this model showed very slow diffusion of the exhaust clouds; this is probably due to its implicit assumption of incompressibility of the pseudovelocity flow field which ignores cell expansion and consequently reduces the diffusion rate. However, some of the Lawrence Livermore Laboratory researchers believe that the grid was too large to resolve the source well--the numerical technique in these cases acted to further dampen the diffusion.

(3) DISF gives the best agreement with the data for the August daylight launch case probably because of its use of off-diagonal diffusivities and its physically sound Lagrangian approach to the diffusion parameters. However, the predictions of this model do not correlate very well with data for the December nighttime launch case, especially in comparisons of the path of maximum ground level concentrations. The probable cause is the inability of DISF to physically describe wind direction changes. This is not an important factor in the August case with its low level of advection wind and high turbulence but it is important in the December case which was characterized by high wind and low turbulence.

(4) The limited calculational results from METS do not provide sufficient information to judge its capability. However, its extremely low predictions for the dosage field on the ground for the December case indicate the need for a more detailed examination of this model.

V. DRY DEPOSITION AND AEROSOL COAGULATION STUDY

During its initial history the Space Shuttle ground cloud contains both an aerosol, chiefly alumina, emitted by the solid state rocket motors, and a large amount of debris swept up by the rocket exhaust. In order to describe the evolution of particulate matter in the cloud during its early history (before cooling and condensation occurs), the following model of particle growth via coagulation including (i) agglomeration among the exhaust alumina particles, (ii) agglomeration between debris and alumina, and (iii) agglomeration among the debris particles has been formulated. The model allows the chemical composition of the evolving alumina/debris aerosol (debris is considered to be a homogeneous substance) and the rate of sedimentation of this aerosol to be followed.

A. FORMULATION OF THE PROBLEM

Consider an aerosol containing (i) a chemical component made up of particles containing both a material A and a material B, referred to as component A/B, and (ii) a component of pure B particles, called B.

Both components are divided into sets of particles having discrete masses, m_i, where

$$m_i = \alpha^{i-1} m_1 \qquad i = 1,2,\ldots q \tag{46}$$

where α is the mass fraction ratio. The number densities (particles ml^{-1}) of the two components are then described by the sets of numbers $\{n_i^{A/B}(m_i)\}$ for component A/B and $\{n_i^{B}(m_i)\}$ for component B. Aerosol A/B is also described by a set of numbers $\{b_i\}$ where b_i is the average mass fraction of material B in ith-sized particles of A/B ($0 \leq b_i \leq 1$). In order to obtain the set of particle number densities $\{n_i(m_i)\}$ from a general particle number distribution, $n(m)$,* one uses

$$n_i = \int_{(m_{i-1}m_i)^{1/2}}^{(m_{i+1}m_i)^{1/2}} n(m)\, dm = \int_{m_i\alpha^{-1/2}}^{m_i\alpha^{1/2}} n(m)dm \tag{47}$$

* When discussing properties of distributions, which are generally true for both A/B and B components, no superscripts are used.

If, as is often the case, n(m) is described by a power law

$$n(m) = n_o\, m^{-x} \qquad \text{(particles ml}^{-1}\text{ g}^{-1}\text{)} \tag{48}$$

then

$$n_i = n(m_i)m_i \frac{\sinh(x'\log\,\alpha)}{x'} \tag{49}$$

where

$$x' = \frac{x-1}{2} \tag{50}$$

The mass density of particles in the ith mass class is given by

$$\int_{m_i\alpha^{-1/2}}^{m_i\alpha^{1/2}} n(m)m\,dm = n_i m_i + \int_{m_i\alpha^{-1/2}}^{m_i\alpha^{1/2}} n(m)(m-m_i)\,dm \tag{51}$$

or, for the power law particle distribution,

$$\int_{m_i\alpha^{-1/2}}^{m_i\alpha^{1/2}} n(m)m\,dm = n_i m_i\left[\frac{x'}{x'-1/2}\,\frac{\sinh[(x'-1/2)\log\,\alpha]}{\sinh[x'\log\,\alpha]}\right] \tag{52}$$

For rough estimates of the mass density of ith-sized particles, the term in brackets in Eq. (52) is nearly unity and the product $n_i m_i$ may be used; for $\alpha \lesssim 10$ and x in the range of 1.0 to 2.0 errors of up to 30% may occur if $n_i m_i$ is assumed to be the particle mass in the ith mass class. Since the calculations which describe the coagulation process (see Eq. (74) below) rigorously conserve mass (if sedimentation losses are negligible), any error in mass introduced by dividing the (continuum) initial mass spectrum into discrete mass classes is maintained throughout the calculation. If the shape of a power law distribution does not change significantly, the correct mass in each class can be recovered accurately from Eq. (52). Generally, however, one must reconstruct a continuum distribution n(m) from the n_i and then use Eq. (51) to obtain the actual mass in each class.

In order to obtain expressions for the rate of change of the particle density, the following rates are defined:

L_{ij} = rate of collision between particles of component A/B, size i, with particles of A/B, size j. (L_{ii} = twice the actual collision rate.)

L'_{ij} = rate of collision of particles of component B, size i, with particles of component B, size j. (L'_{ii} = twice the actual collision rate.)

L''_{ij} = rate of collision of particles of component A/B, size i, with particles of component B, size j.

Collision kernels, $K(m_i, m_j) \equiv K^c_{ij}$, are defined by

$$L_{ij} = K^c_{ij}\, n_i^{A/B} n_j^{A/B} \tag{53}$$

$$L'ij = K^c_{ij}\, n_i^{B} n_j^{B} \tag{54}$$

$$L''_{ij} = K^c_{ij}\, n_i^{A/B} n_j^{B} \tag{55}$$

The form of the collision kernels has been given by Fuchs.[52] The collision kernels considered here incorporate the effects of two processes: (i) the rate of Brownian coagulation and (ii) the rate of scavenging of light particles by falling heavy particles, i.e.,

$$K^c_{ij} = K_{B,ij} + K_{S,ij} \tag{56}$$

$K_{S,ij}$, the contribution to the kernel from heavy particle sedimentation, is given by

$$K_{S,ij} = \pi\, \zeta_{ij}\, r_{max}^2 |v_{S,i} - v_{S,j}| \tag{57}$$

where r_{max} is the radius of the larger of the two particle sizes (r_i or r_j), where

$$r_i = \left(\frac{3\, m_i}{4\pi\rho}\right)^{1/3} \tag{58}$$

and ζ_{ij} is a factor accounting for the fact that small particles slip around falling larger particles.[52]

$$\zeta_{ij} = (1 + r_{min}/r_{max})^2 - \frac{1}{1 + r_{min}/r_{max}} \tag{59}$$

where r_{min} is the smaller of r_i or r_j. The particle density (assumed the same for all particles) is denoted by ρ; the sedimentation velocity $v_{S,i}$ of small particles is given by

$$v_{S,i} = \frac{m_i g D_i}{k_B T} \tag{60}$$

where D_i is the particle diffusion coefficient (see below), k_B is Boltzmann's constant (1.38×10^{-16} ergs K^{-1}) and T is temperature. For larger falling particles, for which the particle Reynolds number approaches and exceeds unity, the boundary flow around the particle separates and drag increases more rapidly with particle size than is implied by Eq. (60). In this case the sedimentation velocity is obtained from an empirical relation given by Fuchs[53]:

$$C_{D,i} = \frac{24}{Re_i} + \frac{4}{(Re_i)^{1/3}} \tag{61}$$

where the drag coefficient $C_{D,i}$ is given by

$$C_{D,i} = \frac{2 m_i g}{\pi \rho_g v_{S,i}^2 r_i^2} \tag{62}$$

and the particle Reynolds number is

$$Re_i = \frac{2 r_i \rho_g v_{S,i}}{\mu} \tag{63}$$

Using Eqs. (62) and (63) and Eqs. (64) and (65) which follow, for the density and viscosity of air (ρ_g and μ, respectively)

$$\rho_g = 0.353\ (P/T) \qquad (g\ ml^{-1}) \tag{64}$$

$$\mu = 1.055 \times 10^{-5}\ T^{1/2} \qquad (g\ cm\ sec^{-1}) \tag{65}$$

where P is in atm and T in K, Eq. (61) may be written in terms of P, T, $v_{S,i}$, r_i, and m_i as

$$v_{S,i} + 2.74 \times 10^2\ P^{2/3}\ r_i^{2/3}\ T^{-1}\ v_{S,i}^{5/3} - 4.93 \times 10^6\ m_i\ r_i^{-1}\ T^{-1/2} = 0 \tag{66}$$

In practice, the simpler Eq. (60) is used for particles with $r_i \leq 25$ μm and Eq. (66) is solved to obtain $v_{S,i}$ for larger particles.

The Brownian coagulation kernel is given by[52]

$$K_B(m_i, m_j) = 4\pi(r_i + r_j)(D_i + D_j) \times \left\{ \frac{r_i + r_j}{r_i + r_j + \delta_{ij}} + \frac{4(D_i + D_j)}{(r_i + r_m) G_{ij}} \right\}^{-1} \tag{67}$$

where, the diffusion coefficient,

$$D_i = \frac{kT}{6\pi \mu r_i} \left[1 + 1.257 \, Kn_i + 0.40 \, Kn_i \exp\left(-\frac{1.10}{Kn_i} \right) \right] \tag{68}$$

and

$$Kn_i = \frac{\text{gas molecule mean free path}}{\text{particle radius}} = \frac{\lambda}{r_i}$$

G_{ij} is the mean thermal speed of ith and jth sized particles,

$$G_{ij} = \{G_i^2 + G_j^2\}^{1/2} \tag{69}$$

$$G_i = \left(\frac{8 \, kT}{\pi \, m_i} \right)^{1/2} \tag{70}$$

δ_{ij} is a "mean free path" for particles:

$$\delta_{ij} = (\delta_i^2 + \delta_j^2)^{1/2} \tag{71}$$

$$\delta_i = \frac{(2)^{1/2} \pi \, G_i}{48 \, D_i \, r_i} \left\{ \left(2r_i + \frac{8 \, D_i}{\pi \, G_i} \right)^3 - \left[4r_i^2 + \left(\frac{8 \, D_i}{\pi \, G_i} \right)^2 \right]^{3/2} \right\} - 2^{3/2} \, r_i \tag{72}$$

For air at a temperature T(K) and pressure P(atm), the expression for the molecular mean free path, λ, is:

$$\lambda = 2.2 \times 10^{-8} \left(\frac{T}{P} \right) \text{ cm} \tag{73}$$

In order that mass be conserved and that particle number be accurately counted, the following method due to Kritz[54] is used to divide the mass of a newly formed particle among the mass classes: If a particle of mass m_j collides with one of mass m_i ($i \geq j$), the resultant particle is divided and a fraction F_{ij} assigned to mass class i and a fraction $(1 - F_{ij})$ assigned to mass class $i + 1$. Since mass must be conserved

$$F_{ij} m_i + (1 - F_{ij}) m_{i+1} = m_i + m_j \tag{74}$$

or

$$F_{ij} = - \frac{m_{i+1} - (m_i + m_j)}{m_{i+1} - m_i} = 1 - \frac{m_j}{(\alpha - 1) m_i} \tag{75}$$

Using the expression for collision rates developed above, changes which occur in $\{n_i^{A/B}\}$, $\{n_i^{B}\}$ and $\{b_i\}$ in a time interval Δt may be calculated. Changes due to coagulation are computed as follows (losses due to sedimentation from the cloud will be taken into account later):

$$\Delta n_i^{A/B} = \left\{ - \sum_{j=1}^{i} (L_{ij} + L''_{ij}) + \sum_{j=1}^{i} (S_{ij} L_{ij} + L''_{ij}) F_{ij} \right.$$

$$+ \sum_{j=1}^{i-1} [(S_{i-1,j} L_{i-1,j} + L''_{i-1,j})(1 - F_{i-1,j}) + L''_{ji} F_{ij}]$$

$$\left. + \sum_{j=1}^{i-2} L''_{j,i-1} (1 - F_{i-1,j}) \right\} \Delta t \tag{76}$$

$$\Delta n_i^{B} = \left\{ - \sum_{j=1}^{i-1} (L'_{ij} + L''_{ji}) + \sum_{j=1}^{i} S_{ij} L'_{ij} F_{ij} \right.$$

$$\left. + \sum_{j=1}^{i-1} S_{i-1,j} L'_{i-1,j} (1 - F_{i-1,j}) \right\} \Delta t \tag{77}$$

where

$$S_{ij} = \begin{cases} 1/2 & i=j \\ 1 & i \neq j \end{cases} \tag{78}$$

The factor S_{ij} is required for correct counting. L_{ii} and L'_{ii} are twice the actual collision rate for ith-sized particles with one another. Each such collision removes two of these particles from the ith class and places a fraction F_{ii} of a particle in the ith class and $(1 - F_{ii})$ in the $(i + 1)$th class.

The mass of material B added to the ith class of A/B in time Δt is given by:

$$\Delta M_i^{A/B}(B) = \Bigg\{ - \sum_{j=1}^{q} (L_{ij} + L''_{ij})\, m_i b_i + \sum_{j=1}^{i} [S_{ij} L_{ij} (m_i b_i + m_j b_j) + L''_{ij}(m_i b_i + m_j)] \frac{m_i}{m_i + m_j} F_{ij} + \sum_{j=1}^{i-1} [S_{i-1,j} L_{i-1,j} (m_{i-1} b_{i-1} + m_j b_j) + L''_{i-1,j} (m_{i-1} b_{i-1} + m_j)] \frac{m_i}{m_{i-1} + m_j} (1 - F_{i-1,j}) + \sum_{j=1}^{i-1} L^n_{j,i} (m_i + m_j b_j) \frac{m_i}{m_i + m_j} F_{ij} + \sum_{j=1}^{i-2} L^n_{j,i-1} (m_{i-1} + m_j b_j) \frac{m_i}{m_{i-1} + m_j} (1 - F_{i-1,j}) \Bigg\} \times \Delta t \tag{79}$$

To calculate the change in b_i in Δt,

$$\Delta b_i = \frac{M_i^{A/B}(B) + \Delta M_i^{A/B}(B)}{m_i (n_i^{A/B} + \Delta n_i^{A/B})} - \frac{M_i^{A/B}(B)}{m_i\, n_i^{A/B}} \tag{80}$$

or

$$\Delta b \left\{ = \frac{1 + \Delta M_i^{A/B}(B)/m_i n_i^{A/B} b_i}{1 + \Delta n_i^{A/B}/n_i^{A/B}} - 1 \right\} b_i \tag{81}$$

To obtain the total changes in the $\{n_i^{A/B}\}$ and $\{n_i^{B}\}$, $\{\Delta n_i^{A/B}\}$ and $\{\Delta n_i^{B}\}$, we must add to the changes caused by coagulation, those caused by

sedimentation. These latter losses, assuming the cloud to be well-stirred (homogeneous), are given by

$$\Delta'' n_i^{A/B} = - \frac{v_{S,i}\, n_i^{A/B}}{h} \Delta t \tag{82}$$

$$\Delta'' n_i^{B} = - \frac{v_{S,i}\, n_i^{B}}{h} \Delta t \tag{83}$$

where h is the cloud height. The total changes are then given by

$$\Delta n_i^{A/B} = \Delta' n_i^{A/B} + \Delta'' n_i^{A/B} \tag{84}$$

$$\Delta n_i^{B} = \Delta' n_i^{B} + \Delta'' n_i^{B} \tag{85}$$

It remains to specify Δt. In order for the calculation to accurately follow the evolution of the aerosol, $\Delta n_i / n_i$ must be much less than 1 for all i. It can be seen that (Eqs. (76), (77)) this will be the case if

$$\left\{ K_{ij}^c\, n_j - K_{ij}^c\, n_j\, F_{ij} \right\} \Delta t << 1/q, \quad j \leq i \tag{86}$$

and

$$K_{ij}^c\, n_j\, \Delta t << 1/q \qquad j > i$$

for all i (and both B and A/B aerosol components). Thus one sets

$$\Delta t = \min(\Delta t_1, \Delta t_2) \tag{87}$$

where

$$\Delta t_1 = \frac{\tau q^{-1}}{\left\{ K_{ij}^c \frac{m_j}{m_i} n_j \right\}_{max}} \left(\leq \frac{\tau q^{-1}}{\left\{ (1 - F_{ij})\, K_{ij}^c n_j \right\}_{max}} \text{ for } \alpha \geq 2 \right) \qquad j \leq i \tag{88}$$

where the subscript (max) indicates the maximum for all i (and all $j < i$). Also,

$$\Delta t_2 = \frac{\tau q^{-1}}{\{K_{ij}^c\, n_j\}_{max}} \qquad j > i \tag{89}$$

where (max) indicates the maximum for all i (and $j > i$) and the time step size parameter, τ, is chosen in such a manner (i.e., large enough) that times required for computation are practical, but small enough that the desired accuracy is obtained.

B. CODE VERIFICATION

The equations developed in the previous section were coded and a series of calculations was performed on model systems in order to test how accurately the evolution of a cloud of coagulating particles is followed and what effects the time step and mass class size parameters, τ and α, have on this accuracy.

Figures 28 and 29 show the results of calculations performed on a model, single component system for which the integro-differential equation governing the rate of coagulation,[52]

$$\frac{\partial}{\partial t} n(m, t) = \int_0^{m/2} K\, n(m - m', t)\, n(m', t)\, dm' - \int_0^{\infty} K\, n(m, t)\, n(m', t)\, dm' \qquad (90)$$

has an analytical solution. This model system is one in which K is a constant and the initial (t = 0) distribution is

$$n(m, 0) = 4 \frac{n_o\, m}{\bar{m}_o^2} \exp(-2\, m\, \bar{m}_o^{-1}) \qquad (91)$$

where n_o is the initial (total) particle number density and $\bar{m}_o$ is the initial average particle mass. At later times, the particle distribution follows the equation

$$n(m, t) = 8 \frac{n_o \exp(-2\, m\, \bar{m}_o^{-1})}{\bar{m}_o (n_o K t)^{1/2} (n_o K t + 2)^{3/2}} \times \left[\sinh 2\, m\, \bar{m}_o^{-1} \left(\frac{n_o K t}{n_o K t + 2}\right)^{1/2}\right] \qquad (92)$$

For the case considered in Figs.28 and 29, $K = 6 \times 10^{-10}$ ml particles^{-1} sec^{-1}, $n_o = 1 \times 10^6$ particles ml^{-1} and $\bar{m}_o = 5.24 \times 10^{-10}$ g (corresponding to a 10 μm particle with unity density); times of t = 0, 1.25×10^5 sec, and 1.7×10^6 sec are considered which correspond to a dimensionless time ($K\, n_o\, t$) of 0, 75

and 1020. The analytical solution of Eq. (90) in the form of

$$N(d,t) \equiv \text{particles ml}^{-1} \text{ with diam} > d = \int_d^\infty n(m) \frac{dm}{d(d)} d(d) \quad (93)$$

and

$$N'(d,t) \equiv \text{particles ml}^{-1} \text{ with diam} < d = \int_0^d n(m) \frac{dm}{d(d)} d(d) \quad (94)$$

are shown as curves in Figs. 28 and 29, respectively. These are compared to machine calculations giving values for

$$N_i((d_i d_{i+1})^{1/2}) = \sum_{j=i+1}^{r} n_j \quad (95)$$

and

$$N_i((d_i d_{i+1})^{1/2}, t) = \sum_{j=1}^{i} n_j \quad (96)$$

which were performed using the values for the mass class ratio, α, and the time step parameter, τ, indicated in the figure captions and also in Table XII which summarizes the results shown in Figs. 28 and 29.

Figures 28 and 29 and Table XII show that the numerical solutions yield, to a good approximation, the actual solution to the coagulation rate equation. Numerical solutions were obtained using the following pairs of values for the mass class ratio, α, and the time step parameter, τ: $\alpha = 2$, $\tau = 0.01$; $\alpha = 2$, $\tau = 0.1$ and $\alpha = 10$, $\tau = 0.1$. The total number of particles and the mean mass or, equivalently the mass-average diameter $d_{\overline{m}} = (6\overline{m}/\pi\rho)^{1/3}$ are accurately calculated.* However, it is apparent from Figs. 28 and 29 that

---

* The mean mass at time t is obtained from the output by the formula

$$\overline{m}(t) = \left(\sum_{j=1}^{r} n_j(t)\, m_i \Big/ \sum_{i=1}^{r} n_i(t) \right) \times \left(M_{total} \Big/ \sum_{i=1}^{r} n_i(0) m_i \right)$$

i.e., it is assumed that the second term on the right hand side of Eq. (51) remains a constant percentage of the first term. Here M_{total} is the actual initial mass of the aerosol as given by the left hand side of Eq. (51). Since, if no sedimentation losses occur, mass is conserved in the calculations, the correct calculation of $\overline{m}(t)$ depends only on the correct calculation of the total particle number.

the numerical solution tends to overestimate the number of light and very heavy particles. The tendency becomes very noticeable for the larger mass class ratio of $\alpha = 10$. Since mass is rigorously conserved in the numerical calculation, the overestimation of numbers of heavy particles necessitates that the mass of the remaining lighter particles be underestimated. This can be seen clearly in Fig. 29 and in Table XII where the values of $d_{N,90}$, $d_{N,50}$ and $d_{N,10}$, the particle diameters for which N (Eq. 93) is 90%, 50%, and 10% of the total number of particles, are all found to be smaller than their true values.

For the user of this code interested in keeping computational time to a minimum it is important to note that the use of $\tau = 0.1$ instead of $\tau = 0.01$ with $\alpha = 2$ leads to no noticeable decrease in accuracy. On the other hand, increasing α from 2 to 10 leads to a marked decrease in accuracy; with $\alpha = 10$ the numerical solution (while still having accurate values for total particle number and $d_{\overline{m}}$) has become badly "smeared" with, e.g., $d_{N,50}$, the median particle diameter, being only 70% of the correct value at $t = 1.7 \times 10^6$ sec (see Table XII). Since calculations such as these can often require several minutes on a modern computer (a CDC 6600 in this case) it is clear that setting τ as large as possible ($\tau \gtrsim 0.1$) is desirable since little or no accuracy is lost. On the other hand setting α much greater than 2 results in a very substantial loss in accuracy and one must then weigh this loss against the cost of machine time.

Before suggesting what would appear to be good practical values for τ and α it is worthwhile to examine the results of calculations on a less artificial system. In Fig. 30 the results of calculations on a system in which the coagulation of an aerosol initially containing 1×10^8 particles ml^{-1} is followed. The initial size spectrum of the aerosol is of a form often obtained in practice,

$$n(m) = n_o' m^{-2} \qquad 5.24 \times 10^{-19} \text{ g} \leq m \leq 5.24 \times 10^{-13} \text{ g}$$

or

$$n(d) = n_o d^{-4} \qquad 0.01 \text{ μm} \leq d \leq 1.0 \text{ μm}$$

In this case the collision kernel K_{ij}^c is of the form given by Eqs. (56), (57) and (67) and, for selected values of particle masses, is tabulated in

Table XIII. No analytical solution of the coagulation rate equation (Eq. (90)) can be obtained for this case and we will assume that the numerical solution using $\alpha = 2.07$ and $\tau = 0.01$ is accurate. As with the case just discussed, it can be seen that no great error is incurred by increasing τ to 0.1 and indeed, in the calculation at t = 250 sec, no major errors (assuming here that the $\tau = 0.1$ calculation is correct) appear when τ is increased to 1.0 except for the two lightest mass classes. (At heavy masses, $d \gtrsim 1 \mu m$, there are no significant differences in any of the cases.) For $\alpha = 10$ at 130 sec, errors are very apparent at light masses, but no significant error is noted in the total particle number of the median particle size ($d_{N,50}$). At $t = 1.3 \times 10^4$ sec only results for $\tau = 1.0$ are shown; excessive computational times would have been required to obtain results using $\tau = 0.1$. This curve, if the trends noted at t = 250 sec are maintained, underestimates the number of very small particles but should yield approximately correct values for total particle number and mass average particle size.

From these examples the following "rules of thumb" regarding the selection of α and τ are apparent. First, since values of τ up to 1.0 have little effect on the sample calculations, it is probably true that use of values of 0.1 to 0.5 will not result in meaningful errors. Only where the size spectrum is very rapidly changing, as in the smallest size classes of Fig. 30 where small particles are rapidly being consumed, would any significant errors result. (The calculated rate of decrease of these very small particles has little or no physical significance anyway, since in any real system no sharp cut off at 0.01 μm would exist.) Secondly, the size of α, the mass class size ratio, should be kept as small as possible consistent with economical computation. Use of $\alpha = 2$ yields very accurate results. For $\alpha = 10$, total number and mean particle mass are computed accurately but the shape of the calculated particle distribution may tend to become incorrect if a rapidly varying size spectrum such as the exponentially varying one of Figs. 28 and 29 is treated.

As a rule, then, the use of α in the range of 2 to at most 5 is indicated. It should be kept in mind that the computational time will be inversely proportional to α^2 and thus, if extended calculations are required, every effort should be made to make α as large as is consistent with the demands to be made on the results. A particular example of some

importance is that in which it is desired to accurately predict sedimentation losses. In this case the possible overprediction of the production of very large particles, such as was seen in the comparison with the analytical solution (Figs. 28 and 29), may lead to an overestimation of the amount of material lost. Unfortunately, time did not permit us to systematically quantify this observation; a few calculations where this comparison could be made indicated that sedimentation losses could be overestimated by as much as a factor of 2 when $\alpha = 10$ was used instead of $\alpha = 2$ with power law distributions of the type used in Fig. 30.

Both of the verification tests shown in Figs. 28, 29 and 30 deal only with coagulation of a single component aerosol. In order to check that the mixing of two components is correctly treated the following simple test was conducted. A calculation was performed in which the initial aerosol was one containing two components, A and B, with identical size spectrum. As this aerosol coagulates, those particles which are mixtures of A and B should display equal amounts of material A and material B, i.e, the following relationship should hold

$$b_i = 0.5(n_i^{A/B} - n_i^{B})/n_i^{A/B}$$

Calculations performed over several thousand time steps showed this relationship to hold rigorously.

C. DRY DEPOSITION FROM THE GROUND CLOUD

The coagulation code has been used to compute the loss of alumina from the ground cloud of the May 20 Titan launch during the cloud rise period. It is assumed that no particle growth by means other than coagulation occurs, i.e., the warm cloud remains above the dew point. The cloud is considered to be well-mixed and thus to have a uniform density of particulate matter throughout. The expansion of the cloud via entrainment and the pressure decrease during cloud rise, as discussed in Section II, are incorporated into the calculations.

The calculations, performed over a time interval in which the cloud grows from an initial volume of 6.5×10^7 m^3 to 5×10^9 m^3 when stabilization occurs at 525 sec at an altitude of about 1800 m, are obtained by using Briggs'

formula. The mass of alumina deposited in the cloud by the Titan is 2.2×10^7 g and thus the initial density of particulate matter is 0.340 mg m^{-3}. The density of the alumina (and the swept-up debris) is taken to be 3.0 g ml^{-1}.

Uncertainty as to the actual size spectra of the alumina and debris particles and the mass of debris swept up requires that a range of values for these parameters be treated. Calculations were thus performed (i) using three alumina distributions from different sources, (ii) assuming that, for particles less than 1 μm in size, the mass of the debris is 10 times the mass of the alumina, and (iii) assuming the total mass of debris is either 100 or 1000 times that of the alumina. The three alumina particle size distributions are those of Varsi,[55] obtained from Titan flight measurements, and those of Dawborn[56] and Kreautle[57] which were obtained from measurements on particles produced in small motor firings in tanks. These distributions are given in Table XIV. The measurements of Kreautle include rapidly settling particles collected from the floor of the tank and are thus noticeably different from the other two measurements of airborne particles in having considerably more large ($\gtrsim$ 1 μm) particles. Thus the Kreautle data would represent a worst case situation with regard to sedimentation early in the cloud history if no debris were present. (As will be seen below the presence of debris modifies this conclusion somewhat.) The assumption that, below 1 μm, there will be about 10 times as much debris as alumina is based on airborne measurements of the Titan ground cloud. The assumption that either 100 or 1000 times as much debris as alumina is to be found in the cloud initially is simply a guess. The results of calculations presented here are for a factor of 1000 for calculations with the Varsi and Dawborn alumina distributions and both 100 and 1000 with the Kreautle alumina distribution. (It will be seen that the amount of alumina carried down is not overly sensitive to this ratio and thus the accuracy of these calculations is probably not limited by this unknown factor so much as by such simplifying assumptions and errors as that of assuming a uniform distribution of particulate material in the cloud.) Table XIV also summarizes the size distributions used for the debris. The median particle diameter $d_{N,50}$ and the mass-average diameter $d_{\overline{m}}$ of all distributions are also given. The calculations were performed using a time step parameter, $\tau = 0.01$, and a mass class size ratio, $\alpha = 10$. As discussed above, this results in some overestimation of the rate of formation of large

particles and thus tends to be a worst case calculation with regard to the amount of sedimentation. Figures 31 to 34 show the particle number distribution, $N^{\dagger}(d)$ (particle with diam $<$ d) and mass distribution, M(d) (mass of particles with diam $<$ d) for total mass and alumina for the four test calculations. Note that for the Kreautle distribution the initial mass distribution for alumina is very nearly a step function, dropping rapidly from its maximum at 340 mg m^{-3} to zero between 2 and 7 μm. The Varsi and Dawborn initial distributions have more curvature with most of the mass being contained in particles less than 1 μm in size.

At stabilization the cloud has expanded by a factor of 72. Total particle number densities have dropped factors of 250 to 600. As can also be seen in Figs. 31 to 34 the larger debris particles which are still airborne at stabilization have captured about 2% to 5% of the alumina. This effect is denoted by the rather abrupt change in slope of the M_{Al} curves occurring at $d \gtrsim 5$ μm in the figures. (In the Varsi data case the change is not so noticeable as in the other three cases.) This process of scavenging of small alumina particles by large, rapidly falling, debris particles is responsible for most of the removal of alumina from the cloud. For example, using the Kreautle alumina distribution with the debris mass being 1000 times the alumina mass at 525 sec (stabilization) the rate at which alumina is carried down from the cloud by large debris particles with diameter $>$ 10 μm is about 10^4 times the rate of loss of alumina by the sedimentation of pure alumina or small alumina/debris particles. It is important to note from these figures that the amount of alumina coating the larger debris particles is not very dependent (i) on the particular alumina distribution used or (ii) on the amount of debris present. This is further exemplified in Figs. 35 and 36. In these figures the amounts of sedimentation, both total and of alumina, are plotted. The Kreautle distribution with 1000 times as much debris as alumina and the Dawborn distribution with the same mass of debris lead to the deposition of 3×10^6 g and 2×10^6 g, respectively, of alumina in the first 525 sec (375 sec for the Dawborn case). The use of the Varsi distribution with 1000 times as much debris and Kreautle distribution with 100 times as much debris as alumina, deposit about 1×10^6 g. The greater deposition from the Kreautle distribution with the larger amount of debris is expected;

thus that the Dawborn distribution would yield about the same amount of deposited alumina is not so easy to explain. Apparently the amount of material which settles is a relatively strong function of the average size of the debris particle (more so, for example, than of debris particle number) which is larger for the Dawborn and Kreautle (1000) distributions. In any case, the differences are not great between any of the cases. However, if debris had not been present, large differences would have been noted with the Kreautle distribution yielding about an order of magnitude more sedimentation than the other two.

If one assumes that the stabilized cloud were stationary, spherical and uniform with a volume of 5×10^9 m^3 and the deposited alumina were spread evenly over the ground under the cloud, the worst case loading of alumina, averaged over the ground beneath the cloud would be 0.8 g m^{-2} at the end of 525 sec. The drift of the cloud will, of course, tend to decrease actual loadings, but the nonhomogeneity of the cloud and the fact that early in the cloud's history it is smaller would tend to raise the loading level near the launch pad. Although the calculations do not take into account the movement of the cloud, which tends to reduce loading at any particular point on the ground, the rate of loss of material due to sedimentation throughout the cloud rise period is calculated. It is possible to integrate this rate and thus calculate the loading at the point on the ground below the center of the (stationary) cloud. These maximum time-integrated loadings, at the end of the cloud rise period, are given in Table XV. The trends are similar to those for total loadings of Figs. 35 and 36. The Kreautle distributions with heavy debris loading give the heaviest alumina loading at the ground, 5 times that of the Kreautle distribution with less debris.

VI. CONCLUSIONS AND RECOMMENDATIONS

A. CONCLUSIONS

This study, which was undertaken to investigate the complex interactions between the turbulent flow field in the lower portion of the troposphere (the PBL) and the rocket exhaust ground cloud resulting from Space Shuttle/Titan III rocket launches, comprises two separate tasks: (1) an attempt to identify and minimize the uncertainties and potential inaccuracies of the NASA Multilayer Diffusion Models using data from selected Titan III launches at KSC, and (2) a systematic analysis of the physical/chemical processes taking place during the cloud rise, and formulation of a realistic time-dependent model. The former study is based on detailed parametric calculations using the MDM code and a comparative study of several more exactly formulated diffusion models, the MDM, and NASA measurements.

The results of the comparative studies of diffusion models and the parametric calculations are as follows:

(1) If the input standard deviation of the azimuth angle, σ_A, is chosen appropriately, the MDM consistently overpredicts the ground level concentrations and dosages for the cases examined in this study (cf. data and other models). However, it should be noted that the MDM predicted results at ground level are strong functions of σ_A; the peak maximum ground level concentration (or dosage) predicted by MDM, using an interpolated σ_A based on similarity theory and assuming that σ_A is vertically uniform in the entire PBL, is an order of magnitude larger than the value indicated by the available data. Therefore the peak in maximum ground level concentrations predicted by MDM seems to be a conservative input for analyzing ground level environmental hazards (such as the environmental constraint for Shuttle launches).

(2) MDM overpredictions at ground level are mainly due to rapid transport of more highly concentrated pollutants from the upper portion of the PBL. This results from the assumption of strong turbulence (large values of σ_A) in the upper portion of the PBL. Conversely, the possibility must therefore be considered that pollutant concentrations above the ground level may be underestimated. Environmental hazard

analyses, e.g. weather modification studies, which require, as input, pollutant concentrations throughout the entire PBL, must employ MDM with caution.

(3) In a shallow PBL condition, the present study shows that the uncertainty in the entrainment constant used in the cloud rise formula can cause a factor of three ($\overset{\times}{\div}$ 3) error in the downwind ground level concentration predictions (Section III.A.2). It is also found under such PBL conditions that the MDM-simulated initial cloud contains lower pollutant concentrations than does the real cloud. Although the latter deficiency may occasionally nullify the "conservative" prediction ((1), above) the problem can be resolved by simply assuming that the center of the exhaust cloud mass (stabilization height) is located below the PBL height.

(4) Compared to the more exactly formulated models, TREATS, ADPIC, and DISF, the MDM model has less potential for including nonhomogeneous and nonstationary features such as variations of wind direction and wind speed, non-uniform surfaces, land-sea interactions, etc., or for incorporating microphysical and chemical processes (such as aerosol mechanics and heterogeneous chemistry as well as kinetic chemistry). Nevertheless, it should be kept in mind that the MDM model, because of its ability to consistently overpredict ground level concentrations, can certainly serve as an acceptable engineering tool for use in environmental hazard analyses at ground level.

(5) The TREATS, ADPIC and DISF models although they serve only as reference tools in this study, do contribute to an understanding of the relative merits of the different diffusion modeling techniques. For example, the moment scheme of TREATS demonstrates the mathematical relationship between the vertical nonhomogeneous nature of turbulence and the moments of the pollutant concentration distribution; the trajectory technique of ADPIC provides a description of advection effects due to wind variations in time and space. Although the model in its present form predicts lower pollutant concentrations at ground level than indicated by available data, it can give a good description of the exhaust cloud transit path. The ADPIC-predicted

ground level pollutant concentration can also be treated as a lower bound. The DISF model demonstrated the necessity of including off-diagonal diffusivities and indicated the advantages of the physically sound Lagrangian approach for the derivation of diffusion parameters. The overall merit of the DISF model has been shown in its favorable comparisons with airborne measurements in a strong turbulence condition. The various strengths of these three models may serve as valuable guidelines for the future development of a new and advanced diffusion model.

(6) The current lack of micrometeorological information concerning the PBL at KSC causes many difficulties in making diffusion calculations and results in wide uncertainties in the calculated results. Based on the MDM parametric study, the MDM-predicted results are found to be more sensitive to those parameters relating to the micrometeorological information, such as σ_A and PBL height than to uncertainties in the description of initial cloud and ground surface effects. For example, the peak of the maximum ground level concentration from MDM can vary by an order of magnitude depending on the value of σ_A (Fig. 4) chosen. A factor of two error is encountered due to the uncertainties of the PBL height.

The major conclusions of the calculations on the physical/chemical processes during cloud rise are as follows:

(1) The value used in the MDM for the heat release from the Shuttle solid fuel (or Titan III) is reasonable.

(2) Deluge water injected into the exhaust plume from the AWSS for the Shuttle, or from the trench for Titan, has little effect on subsequent concentration predictions if wet chemistry is not an important factor.

(3) It was found that an average loading of about 1 g m^{-2} of alumina (about 15% of the alumina initially in the cloud), with respect to the particle size distributions tested, will be deposited on the ground in a worst case example, as in the Titan III launch of 20 May 1975.

(4) Beneath the center of a rising cloud with no horizontal movement, loadings as large as 4.5 g m^{-2} are calculated. Horizontal movement of the cloud will lower the loading and thus there is good reason to believe that the calculated results include the worst case situation.

(5) In dry deposition alumina settles predominantly via coagulation with rapidly falling debris particles. While more information on the alumina and debris particle size distributions and the mass of debris would be useful, the amount of alumina deposition is not critically sensitive to these parameters.

B. RECOMMENDATIONS

The following recommendations are based on our study of the interactions between the rocket ground cloud and the atmosphere:

(1) This comparative study of diffusion models focused on a sea breeze daylight case and a nighttime case. An extension of this type of study to additional meteorological conditions would be useful.

(2) At this stage, the models adopted in this program, with the exception of the MDM, have not been fully documented and some of them (e.g. ADPIC) can only be used in the developer's computer system. Therefore efforts should be made to fully document those models and/or to convert them into a more widely used computer system.

(3) A simulation model to provide micrometeorological information on the PBL at KSC, with special emphasis on determining the diffusion parameters and the thickness of the PBL, should be developed. This model must take into account the land-sea interaction feature at KSC, but should retain its less complex features for routine usage.

(4) This study showed that the calculation and comparisons which use, as input, a description of the stabilized cloud based on observed cloud location and volume, gave better agreement with the data than those which use the MDM modeled cloud. Therefore, an engineering formula or modifications of the cloud model in MDM on the basis of empirical correlations between the meteorological characteristics and available observed data of Titan III clouds should be implemented.

(5) Heat flux, $\overline{w'q'}$ near ground height (say 4 m) should be measured at existing tower locations at KSC, because it is a fundamental quantity in determining the physical scales in the PBL, such as characteristic wind speed, characteristic temperature, Monin-Obukhov length, etc.

(6) At present, the measurement data on the size distribution and composition of aerosols associated with the ground cloud for validation and refinement of the models are scarce. Efforts to obtain such data should be encouraged.

(7) In this study, only limited calculations on cloud dry deposition were made. Extended calculations for the various meteorological conditions and for different rocket exhausts such as from the Shuttle should be carried out. Some modifications and refinements of this model, accounting for the different densities of two kinds of particles and turbulence-induced coagulation, and incorporating wet chemistry (condensation) should be made.

APPENDIX A

CLOUD RISE AEROSOL MODEL (CRAM) COMPUTER PROGRAM

I. PROGRAM DESCRIPTION

This program is used to calculate coagulation between two types of aerosols in a spherical buoyant atmospheric cloud, or in a group of buoyant clouds in which the lower clouds are spherical and the upper clouds are cylindrical. The changes in the cloud, i.e., the increase in size, and the decrease in temperature and pressure, are taken into account. The aerosols are divided into a set number of discrete mass sizes.

For calculation purposes, one aerosol is kept pure, while the other contains a fraction of materials from each type of aerosol. A separate fraction is kept for each mass class. Both sedimentation and Brownian coagulations are calculated, as well as sedimentation loss through fallout. If the multi-cloud option is used, sedimentation loss in one cloud is added to the cloud below.

For generalization of application, two other options are included:

(1) PTVC option: Pressure, temperature and volume are kept constant.

(2) KKC option: The collision kernel is kept constant.

Output provided historically:

(1) Mass and size distribution for each aerosol.

(2) Sedimentation loss: Sedimentation velocity, total mass loss, number lost in each mass class, and mass loss rate are included.

(3) Physical properties of each cloud, including the entrained air mass from which the water content in the cloud can be calculated.

II. PROGRAM INPUT

A. FORMAT DESCRIPTION

Input must be in the form:

<title card>

<namelist JIM>

<namelist JIM1>

Where the title card is one line of alphanumeric data, Columns 2-80 are printed at the top of the output.

Namelist data has the form:

$<namelist name> <variable lists> $END

Column 1 must always be left blank. The variable list has the form:

<variable name> = <constant>, or

<array name> = <string of constants (separated by commas)>

Every variable list (including the last one) must be followed by a comma. If two or more constants in a string have the same value, they can be represented as n*(value), where n is the (integer) number of repetitions. Blanks must not appear inside variable or namelist names, but they can be used anywhere else. Constant strings can be continued from one line to the next. Variables can be defined in any order inside the namelist, but the two namelists must be in the proper order. Namelist JIM1 is not used if the PTVC option (constant pressure, temperature, and volume) is selected.

If the variable has a default value and is not defined in the namelist, the default value is used by the program.

If the multicase option is used, then complete sets of data, including the title card, must be given for each case. However, after the first set of data, input values do not have to be defined if they are the same as the values defined in the first set, except for the arrays ANP, BNP, and BNEW (which must be defined every time) and variables with a default value (which must be defined any time a value other than the default value is desired).

B. VARIABLES

Name	Type	Units	Value Restriction	Array Size	Default Value
			NAMELIST JIM		
ALFA	real	---	≥ 2	---	---
ANP	real	no-ml^{-1}	---	30 × 20	---
BNEW	real	---	---	30 × 20	---
BNP	real	no-ml^{-1}	---	30 × 20	---
CNH	real	cm^{-1}	---	---	---
CNOMX	real	no-ml^{-1}	---	---	---
CNPRES	real	atm	---	---	---
CNTEM	real	°K	---	---	---
CNVOL	real	m^3	---	---	---
FACTRA	real	---	---	20	1.0
FACTRB	real	---	---	20	1.0
IOINT	integer	---	≥ 1	---	---
IR	integer	---	≤ 30	---	---
KKC	logical	---	---	---	.FALSE.
NCLTI	integer	---	---	---	---
NLAY	integer	---	$1 \leq n \leq 20$	---	1
NT	integer	---	---	---	---
NT1	integer	---	---	---	1000
NT2	integer	---	---	---	1000
NZS	integer	---	---	---	1
PTVC	logical	---	---	---	.FALSE.
RHO	real	g-cm^{-1}	---	---	---
RMO	real	g	---	---	---
RN2M	real	---	---	---	1.0
TEND	real	sec	---	---	---
TI	real	---	---	---	---
XKCON	real	ml-sec^{-1}	---	---	---
			NAMELIST JIM1		
BZN	real	m	---	20	---
CORTM	logical	---	---	---	.FALSE.
DPHZ	real	k-m^{-1}	---	---	---
DT	real	sec	---	---	---
DWATER	real	cal	---	---	3.2557E9
GAMTWO	real	---	---	---	0.49
INTPR	logical	---	---	---	.TRUE.
IPINT	integer	---	---	---	5
NLAY	integer	---	≤ 20	---	1
P	real	atm	---	100	---
QC	real	cal sec^{-1}	---	---	1.1883E10
T	real	°K	---	100	---

Name	Type	Units	Value Restriction	Array Size	Default Value
TF	real	sec	---	---	---
TFA	real	---	---	---	---
TFB	real	---	---	---	---
U	real	m sec^{-1}	---	100	---
ZP,ZU,ZT	real	m	---	100	---

C. DESCRIPTION OF VARIABLES

Name	Symbol	Description
		NAMELIST JIM (MAIN PROGRAM)
ALFA	α	Mass ratio of consecutive mass sizes.
ANP,BNP,BNEW	n_i^B	Arrays giving A/B distributions, B distributions, and fraction B in A/B, respectively. Each array has 600 elements; 1-30 for the bottom cloud, 31-60 for the second cloud, up to 20 clouds; elements 1, 31, 61, etc. give number for smallest mass particle in each cloud.
	$n_i^{A/B}$	
	b_i	
CNH	h	Used only with PTVC option (normally calculated in CLDRIS routine). Vertical thickness of cloud. (Used only for calculating sedimentation loss). Sedimentation loss can be rendered insignificant by making CNH very large.
CNOMX	---	Used only with PTVC option. Minimum value for mass distributions. (Values less than CNOMX are set equal to CNOMX at the end of each time interval.)
CNPRES	P	Used only with PTVC option. Cloud atmospheric pressure.
CNTEM	T	Used only with PTVC option. Cloud temperature.
CNVOL		Used only with PTVC option. Cloud volume.
FACTRA,FACTRB	---	At the start of the program, the A/B and B mass distributions of cloud number are multiplied by FACTRA (n) and FACTRB (n), respectively, for all n up to NLAY. (This provides a convenient scaling factor.)
IOINT		Number of time intervals between printouts.
IR	q	Number of mass sizes.
KKC		Logical variable. When TRUE, the collision kernel is set equal to a constant.
NCLTI		Number of time intervals between recalculations of delta time ("DT").
NLAY		Number of clouds (can be defined in CLDRIS routine, but it must be defined here if it is not equal to 1 and the PTVC option is used).
NT	---	Number of time intervals to be calculated, if cloud rise time (TEND) is not exceeded first.
NT1		Increment value for NT2 when time interval NT2 is reached.
NT2		Number of time intervals at which to first revise TI; then counter for subsequent revisions of TI.
NZS		Multicase option. If NZS is not equal to 1, CRAM expects another complete case of input data.
PTVC	---	This is a logical variable. When it is TRUE, the constant pressure, volume, and temperature option is used.
RHO	ρ	Density of particle material.

Name	Symbol	Description
RMO	m_1	Mass of the smallest particle (smallest mass size).
RN2M		Revised value for TI (TI=*RN2M).
TEND		Time at which to stop calculations (cloud rise time), if NT not exceeded first.
TI	τ	Initial value for time step size index.
XKCON	K_{ij}	Value of collision kernel when KKC option is used.

NAMELIST JIM1 (CLDRIS ROUTINE)

BZN		Array giving initial altitudes of bottom of each cloud, and top of top cloud, (BZN(1) normally equals 0).
CORTM		Logical variable; if TRUE, the time correction for Briggs' formula is included in order to account for the instantaneous cloud formation.
DPHZ	$\Delta\phi/\Delta z$	Ratio of ambient potential pressure to altitude.
DT		Time interval for cloud rise calculations. Note that this "DT" is different from the "DT" in the main program.
DWATER		Cooling effect of the deluge water on the bottom cloud.
GAMTWO	γ	Entrainment constant.
INTPR		This logical variable if TRUE, causes additional printouts in the CLDRIS routine.
IPINT		Number of CLDRIS calculation intervals between CLDRIS printouts.
NLAY		Number of clouds.
P,U,T	P_{amb}, U_{amb}, T_{amb}	Ambient pressure, wind velocity, and temperature arrays, respectively.
QC	Q	Heat content of the exhaust per second of fire.
TF	t_f	Time of fire for bottom cloud.
TFA, TFB		Values used to calculate time of fire for upper clouds; t = TFA × (ALTITUDE)**TFB.
ZP, ZU, ZT		Altitudes at which pressure, wind velocity, and temperature are given in P, U, and T arrays.

III. EXPLANATION OF IMPORTANT VARIABLES

Name	Symbol	Description
		MAIN PROGRAM
AN, BN, B		These are temporary storage arrays for the mass distributions. They correspond to ANP, BNP, and BNEW, but they only hold the values for one cloud
ASLAB, ASLB		These arrays keep track of the total number of particles lost through sedimentation for each mass class, over the entire cloud (material A/B and B, respectively).
DAN, DBN, DB	$\Delta N_i^{A/B}$, ΔN_i^{B}, ΔB_i	Change in number A/B, number B, fraction B in A/B for a given mass class, for a given cloud.
DT	Δt	Length of (main routine) time interval.
F	$F_{i,j}$	This array is used to calculate how a particle formed in a collision is reclassified, i.e., if 2 particles, m_i and m_j ($m_i > m_j$) collide, the new particle (mass = $m_i + m_j$) is split up: $F_{ij}*m_i$ into mass class i; $(1-F_{ij})*m_{i+1}$ into mass class i + 1.
G	G_i	Array of the mean thermal speed of the i'th size particle.
H	h	Vertical thickness of the cloud.
IP		Pointer for printout, when N=IP, the mass distributions are printed, and IP is incremented by IOINT.
L		Counter for cloud number.
N		Counter for time interval.
NCLT		When N=NCLT, DT is recalculated, and NCLT is incremented by NCLTI.
PMB		Array storing total original mass of material B in each cloud.
RABSED, RBSED		For a given mass class, rate of sedimentation loss (number/second/ml) for A/B and B, respectively.
RAD, RM		Arrays storing the radius and the mass, respectively, of each mass class particle.
RL, RLP, RLPP,	L_{ij},L'_{ij},L''_{ij}	Collision rate arrays: RL, between A/B size i and A/B size j; RLP, between B_i and B_j; KLPP, between A/B_i and B_j.
RMAA		Array storing total original mass of material A in each cloud.
SIG	L_i	"Mean free path" for particle values returned.
TLIM, TOLD		Values returned from CLDRIS. TLIM is the time of the most recent CLDRIS calculation; TOLD is the time of the previous calculation. Values at time TIME are linearly interpreted between these two.

Name	Symbol	Description
U	μ	Viscosity of air.
VLBEG, VLEND		Cloud volume at beginning and end of (main routine) time interval.
VSED	$V_{s,i}$	Sedimentation velocity array.
YK	K_{ij}	Collision kernel array.

CLDRIS ROUTINE

ARMO AIRMO	m_{air}	This array stores the mass of air in each cloud. This is the amount of air in the cloud, from the previous calculation (from ARMO array).
AIRMP	M_o	Total mass of cloud at the beginning of the interval.
AIRN	$m_{air,new}$	Mass of new air entrained in cloud.
API, AVI	P, V	Arrays storing original pressure and volume, respectively, in each cloud.
AZN	Z_c	Stores the height of the center of each cloud.
CPA	Cp_i	Specific heat of each pollutant at 100° K intervals, from 200° to 1300° (set by DATA statement).
CPB, CPC		Arrays calculated to provide easy calculation of the specific heat of a pollutant at a given temperature.
CPD, CPE, CPF		Calculated to provide the integral of the mass times the specific heat of a pollutant with respect to temperature, over any range from 298° to 1300° K.
CPMIX	$C_{p,mix}$	Specific heat of the cloud.
FRACA	F_i	Rate of mass flow of each pollutant into the cloud from rocket exhaust (set by DATA statement).
I	i	Used in loops; points to one of the 6 pollutants.
IPR		Pointer for output; when N = IPR, cloud parameters are printed, and IPR is incremented by IPINT.
J	j	Refers to a temperature range of 100° K: from 100*(J+1) to 100*(J+2).
L		Sub-cloud number.
N		(CLDRIS) time interval counter.
PAMB, UAMB, TAMB	P_{amb}, U_{amb}, T_{amb}	Ambient pressure, wind velocity, and temperature, respectively, at the cloud altitude.
PMAS	M_p	Mass of pollutant I in cloud L.
Q	Q	Heat content of each cloud.

Name	Symbol	Description
QL	Q_l	Energy loss due to adiabatic expansion.
RMW	M_{wi}	Molecular weight of each pollutant.
TFAR	t_f	Length of time interval over which rocket fires exhaust into each cloud.
VOBS	V_{obs}	Volume of cloud.
WN	w	Increase in height of cloud in (CLDRIS) time interval.
PROR, DPR, VOL, DVOL, TEMP, DTK		These arrays return values to the main routine for pressure, temperature, and volume in each cloud. PROR and DPR are for pressure, VOL and DVOL are for volume, TEMP and DTK are for temperature. PROR, VOL and TEMP contain values for the end of the interval, DPR, DVOL, and DTK return the change in the quantities over the interval.

IV. SAMPLE PROBLEM INPUT DATA

CASE 1

```
CONSTANT PRESSURE, TEMPERATURE, & VOLUME (PTVC OPTION) TESTING
$JIM
PTVC=.TRUE.,CNVOL=1.0,TEND=1.E10,CNTEM=300.0,CNPRES=1.,NLAY=1,
KKC=.TRUE.,XKCON=6.E-10,
CNOMX=1.E-20,BNEW=30*0.0,
RHO=1.,CNH=1.E10,ANP=30*0.0,
RMO=5.23E-14,ALFA=10.0,IR=10,NT=5000,TI=.01,IOINT=500,
NCLTI=50,NZS=0,
BNP=.180,19.71,1.897E3,1.308E5,8.54E5,1.312E4,30*0.0,
$END
```

CASE 2

```
VARSI AL2O3 DISTRIBUTION,DEBRIS =100*AL2O3 MASS
$JIM
BNP=1.944E7,2.11E7,8.907E7,1.388E7,7.4o4E5,4.022E4,2153.,115.8,
     o.23o,15*0.0,
ANP=2*0.0,9.595E7,9.354E7,1.13E7,1.3o5Eo,1.648E5,1.991E4,
       2404.,290.3,35.07,4.23o,.5117,.oo18,7.466E-3,10*0.0,
NZS=0,
RMO=1.E-17,ALFA=10.0,IR=1o,RHO=3.0,NT=5000,
TI=.1,IOINT=100,TEND=525.077,NCLTI=10,BNEW=30*0.0,
$END
$JIM1
  TF=17.0,TFA=.635,TFB=.484,DPHZ=.001098,
BZN=0.0,656.0,
DT=1.0,NLAY=1,IPINT=25,
 ZP=0.0,141.46,304.88,471.04,589.63,609.76,847.26,914.63,970.73,1056.7,
    1219.51,1524.39,1542.99,1829.27,2051.82,2134.15,2203.96,2331.4,2439.02,
 ZT=0.0,141.46,304.88,471.04,589.63,609.76,847.26,914.63,970.73,1056.7,
    1219.51,1524.39,1542.99,1829.27,2051.82,2134.15,2203.96,2331.4,2439.02,
 ZU=0.0,141.46,304.88,471.04,589.63,609.76,847.26,914.63,970.73,1056.7,
    1219.51,1524.39,1542.99,1829.27,2051.82,2134.15,2203.96,2331.4,2439.02,
 P=1.002,.987,.9o9,.951,.938,.936,.91,.903,.898,.888,.872,.841,.839,.811,
     .79,.782,.776,.764,.754,
 T=300.5,298.2,29o.6,295.1,294.7,294.6,293.4,292.5,291.9,291.2,289.6,287.2,
     287.1,285.3,284.1,283.5,283.0,283.7,284.2,
 U=2.57,3*3.o,2*3.08,5*3.6,2*3.08,3.6,2*4.63,5.15,6.18,7.72,
$END
```

V. SAMPLE OUTPUT

CASE I

```
CONSTANT PRESSURE, TEMPERATURE, & VOLUME (PTVC OPTION) TESTING
                  AEROSOL PROGRAM

DENSITY OF PARTICLE MATERIAL =    1.000  G/ML
NO. OF PARTICLE CLASSES =     10
TIME STEP SIZE INDEX =      .0100
MASS OF SMALLEST PARTICLE =    .52300E-13  GM.
RATIO OF CONSECUTIVE MASS CLASSES(ALFA) =  10.0000
NO. OF TIME STEPS = 5000


LAYER =      1


INITIAL MASS OF A/B =     0.           G.
INITIAL MASS OF B =     522.110      G
INITIAL MASS =     522.110
          SEDIMENTATION VELOCITIES
CLASS              MASS, PG        DIAM, MICRO-M     VELOCITY, CM/SEC/
    1        .52300000E-01         .46396088              .872355E-03
    5         523.00000            9.9957342              .302669
   10         52300000.            463.96088              187.083


          SAMPLE COAGULATION CONSTANTS
               K(I,J) = 1.0E-10  ML/PARTICLE/SEC
CLASS                1              5              10              15              20              25              30

    1        6.000000
    5        6.000000       6.000000       6.000000
   10        6.000000       6.000000       6.000000
```

TIME = 0.0000
TIME INTERVAL = 0
DELTA TIME = 0.00000
CLOUD 1

PARTICLE SIZE AND COMPOSITION SPECTRUM

CLASS	MASS, PG	DIAM, MICRO-M	N(A,B), PER ML	FRACTION B IN A/B	N(B), PER ML	********** SEDIMENTATION ********** LOSS (NO/ML/SEC) A/B	B	ACCUMULATED (NO) A/B	B
1	.52300E-01	.46396	0.	0.	.1800				
2	.52300	.99957	0.	0.	19.71				
3	5.2300	2.15352	0.	0.	1897.				
4	52.300	4.63961	0.	0.	.1308E+06				
5	523.00	9.99573	0.	0.	.8540E+06				
6	5230.0	21.53516	0.	0.	.1312E+05				
7	52300.	46.39609	0.	0.	0.				
8	.52300E+06	99.95734	0.	0.	0.				
9	.52300E+07	215.35156	0.	0.	0.				
10	.52300E+08	463.96088	0.	0.	0.				

TIME = 135072.6961
TIME INTERVAL = 5000
DELTA TIME = 117.63110
CLOUD 1

PARTICLE SIZE AND COMPOSITION SPECTRUM

CLASS	MASS, PG	DIAM, MICRO-M	N(A,B), PER ML	FRACTION B IN A/B	N(B), PER ML	********** SEDIMENTATION ********** LOSS (NO/ML/SEC) A/B	LOSS (NO/ML/SEC) B	ACCUMULATED (NO) A/B	ACCUMULATED (NO) B
1	.52300E-01	.46396	0.	0.	.1038E-03	0.	.9054E-17	0.	.5099E-04
2	.52300	.99957	0.	0.	.1136E-01	0.	.3945E-14	0.	.2222E-01
3	5.2300	2.15352	0.	0.	1.096	0.	.1631E-11	0.	9.177
4	52.300	4.63961	0.	0.	85.42	0.	.5675E-09	0.	3002.
5	523.00	9.99573	0.	0.	4324.	0.	.1309E-06	0.	.2150E+06
6	5230.0	21.53516	0.	0.	.1349E+05	0.	.1879E-05	0.	.5770E+06
7	52300.	46.39609	0.	0.	5876.	0.	.3580E-05	0.	.4190E+06
8	.52300E+06	99.95734	0.	0.	261.0	0.	.6350E-06	0.	.4172E+05
9	.52300E+07	215.35156	0.	0.	1.031	0.	.7902E-08	0.	344.7
10	.52300E+08	463.96068	0.	0.	.2975E-03	0.	.5567E-11	0.	.1793

NO. OF A/B PARTICLES = 0. NO./ML
NO. OF B PARTICLES = 24042.607 NO./ML

ALL MASSES IN MICRO-G/ML
MASS OF A/B PARTICLES = 0.
MASS OF B PARTICLES = 522.06170

MASS FRACTION OF B IN A/B = I

ACCUMULATED SEDIMENTATION LOSSES (G)
MASS OF MATERIAL B LOST = .48675006E-01 (G)
MASS OF MATERIAL A LOST = 0.
TOTAL MASS LOST = .48675006E-01

SEDIMENTATION LOSS RATE (G/SEC)
A/B PARTICLES = 0.
B PARTICLES = .57083384E-06

H, VOLUME AT BEGINNING AND END OF INTERVAL = .10000000E+11 1.0000000 1.0000000

CASE 2

```
VARSI AL203 DISTRIBUTION,DEBRIS =100*AL203 MASS
 CRAM CALLED
RMW(I)=    18.016000
RMW(I)=    36.465000
RMW(I)=    44.054000
RMW(I)=    101.96100
RMW(I)=    28.013400
RMW(I)=    159.69200
UAMB,ASPS,RTS=    0.
    2.26232          .598401E-02
A,TIMEO=    .52298548E+13    .99510503
TIMEO=    .98984565E-01
INTERMEDIATE OUTPUT=  NOIT,CM1F,CZ,C1,CPD,CPE(L,M1)
CPF(L,M1),TO1,TO2,TNEW,TF1,TF2,F1,F2
FNEW,RKP
   21     -.11113E+16      .35929E+13     -.43768E+08     -.13310E+11      .41897E+08
     9288.2           310.43           310.43           310.43
    -.19769E+13      .27193E+13      .27193E+13     -.19769E+13
     .67241E+07      .27045E-05
************************************************

TIME INTERVAL =      1
LAYER =    1
NEW TEMPERATURE =       310.43
TIME =       1.0000
DELTA TIME =       1.0000
MASS OF NEW AIR INGESTED INTO CLOUD =       .50536E+11
MASS OF OLD AIR IN CLOUD =       0.
NO. OF ITERATIONS =     21
OBSERVED VOLUME =       .44663E+08
HEIGHT OF CLOUD =       449.18
CLOUD VELOCITY =       49.185
GL =      0.
ADDITIONAL VARIABLES=  ZM,CPMIX,GAM,Q(L),PAMB,     TAMB,PMT,PI,VI,AIRMT(L)
    .329814E-01    0.               0.              .198755E+12     .953368
    295.297         .182367E+09     .958696         .315396E+08     0.
INTERMEDIATE OUTPUT=  NOIT,CM1F,CZ,C1,CPD,CPE(L,M1)
CPF(L,M1),TO1,TO2,TNEW,TF1,TF2,F1,F2
FNEW,RKP
   21     -.13289E+16      .43255E+13     -.43768E+08     -.13310E+11      .41897E+08
     9288.2           308.14           308.14           308.14
    -.23321E+13      .62584E+12      .62584E+12     -.23321E+13
     .52881E+06      .28209E-05
```

```
TIME INTERVAL =      2
LAYER =    1
NEW TEMPERATURE =       308.14


TIME =       2.0000
DELTA TIME =       1.0000
MASS OF NEW AIR INGESTED INTO CLOUD =       .10306E+11
MASS OF OLD AIR IN CLOUD =       .50536E+11
NO. OF ITERATIONS =     21
OBSERVED VOLUME =       .55862E+08
HEIGHT OF CLOUD =       483.96
CLOUD VELOCITY =       34.778
QL =      .131207E+10
ADDITIONAL VARIABLES:  ZM,CPMIX,GAM,Q(L),PAMB,     TAMB,PMT,PI,VI,AIRMT(L)
     .344016E-01     .272567         1.33475         .198755E+12     .949583
     295.056         .182367E+09     .958696         .315396E+08     .149233E+14
                     AEROSOL PROGRAM

DENSITY OF PARTICLE MATERIAL =    3.000  G/ML
NO. OF PARTICLE CLASSES =     16
TIME STEP SIZE INDEX =      .1000
MASS OF SMALLEST PARTICLE =    .10000E-16  GM.
RATIO OF CONSECUTIVE MASS CLASSES(ALFA) =  10.0000
NO. OF TIME STEPS = 5000


LAYER =      1


INITIAL MASS OF A/B =     .122936E+10 G.
INITIAL MASS OF B =     .121232E+08 G
INITIAL MASS =     .124149E+10
         SEDIMENTATION VELOCITIES
CLASS              MASS, PG        DIAM, MICRO-M     VELOCITY, CM/SEC/
    1        .10000000E-04         .18532772E-01          .402300E-04
    5        .10000000E+00         .39927647              .203856E-02
   10        10000.000             18.532772              3.04753
   15        .10000000E+10         860.21508              699.450
```

SAMPLE COAGULATION CONSTANTS
K(I,J) * 1.0E-10 ML/PARTICLE/SEC

CLASS	1	5	10	15	20	25	30
1	15.32860						
5	413.9299	8.378283	5418.733	.5660900E+08			
10	20796.19	5418.733	6.164520	.2616289E+10			
15	3578971.	.5660900E+08	.2616289E+10	6.142154			

****

TIME = 0.0000
TIME INTERVAL = 0

DELTA TIME = 0.00000
CLOUD 1

PARTICLE SIZE AND COMPOSITION SPECTRUM

CLASS	MASS, PG	DIAM, MICRO-M	N(A,B), PER ML	FRACTION B IN A/B	N(B), PER ML	SEDIMENTATION LOSS (NO/ML/SEC) A/B	SEDIMENTATION LOSS (NO/ML/SEC) B	SEDIMENTATION ACCUMULATED (NO) A/B	SEDIMENTATION ACCUMULATED (NO) B
1	.10000E-04	.01653	0.	0.	.1944E+08				
2	.10000E-03	.03993	0.	0.	.2110E+08				
3	.10000E-02	.08602	.9595E+08	0.	.8907E+08				
4	.10000E-01	.18533	.9354E+08	0.	.1388E+08				
5	.10000E+00	.39928	.1130E+08	0.	.7464E+06				
6	1.0000	.86022	.1365E+07	0.	.4022E+05				
7	10.000	1.85328	.1648E+06	0.	2153.				
8	100.00	3.99276	.1991E+05	0.	115.8				
9	1000.0	8.60215	2404.	0.	6.236				
10	10000.	18.53277	290.3	0.	0.				
11	100000	39.92765	35.07	0.	0.				
12	.10000E+07	86.02151	4.236	0.	0.				
13	.10000E+08	185.32772	.5117	0.	0.				
14	.10000E+09	399.27647	.6180E-01	0.	0.				
15	.10000E+10	860.21508	.7466E-02	0.	0.				
16	.10000E+11	1853.27720	0.	0.	0.				

INTERMEDIATE OUTPUT: NUIT,CMIF,CZ,C1,CPD,CPE(L,M1)
CPF(L,M1),T01,T02,TNEW,TF1,TF2,F1,F2
FNEW,RKP

21	-.15721E+16	.51488E+13	-.43768E+08	-.13310E+11	.41897E+08
	9298.2	306.11	306.11	306.11	
	-.27251E+13	.74636E+12	.74636E+12	-.27251E+13	
	-.82063E+06	.26210E-05			

```
TIME INTERVAL =   500
LAYER =    1
NEW TEMPERATURE =      287.40
TIME =      500.00
DELTA TIME =      1.0000
MASS OF NEW AIR INGESTED INTO CLOUD =      .11988E+10
MASS OF OLD AIR IN CLOUD =      .45593E+13
NO. OF ITERATIONS =    21
OBSERVED VOLUME =      .47230E+10


HEIGHT OF CLOUD =      2124.1
CLOUD VELOCITY =      .20132
QL =     .293159E+11
ADDITIONAL VARIABLES:  ZM,CPMIX,GAM,Q(L),PAMB,    TAMB,PMT,PI,VI,AIRMT(L)
    .344067E-01    .240356        1.39753        .198755E+12    .782974
    283.573        .182367E+09    .958696        .315396E+08    .130962E+16


************************************************************
 TIME =    522.2967
TIME INTERVAL =   240
DELTA TIME =      5.25077
CLOUD    1
```

PARTICLE SIZE AND COMPOSITION SPECTRUM

CLASS	MASS, PG	DIAM, MICRO-M	N(A,B), PER ML	FRACTION B IN A/B	N(B), PER ML	SEDIMENTATION LOSS (NO/ML/SEC) A/B	SEDIMENTATION LOSS (NO/ML/SEC) B	SEDIMENTATION ACCUMULATED (NO) A/B	SEDIMENTATION ACCUMULATED (NO) B
1	.10000E-04	.01853	0.	0.	0.	0.	0.	0.	.1552E+12
2	.10000E-03	.03993	0.	0.	5.441	0.	.2783E-08	0.	.2024E+13
3	.10000E-02	.08602	.2726E+05	.1776	.1620E+05	.3341E-04	.1986E-04	.2645E+15	.1749E+15
4	.10000E-01	.18533	.2624E+06	.1432	.1201E+05	.8667E-03	.3967E-04	.3603E+16	.2066E+15
5	.10000E+00	.39928	.1008E+06	.1069	482.0	.1071E-02	.5117E-05	.3590E+16	.2784E+14
6	1.0000	.86022	.1139E+05	.4869E-01	3.695	.4566E-03	.1482E-06	.1494E+16	.1470E+13
7	10.000	1.85328	1099.	.1597E-01	.2020E-02	.1837E-03	.3374E-09	.6291E+15	.5758E+11
8	100.00	3.99276	120.1	.6485E-02	.6905E-08	.8818E-04	.5071E-14	.3094E+15	.3806E+10
9	1000.0	8.60215	13.20	.3076E-02	0.	.4382E-04	0.	.1570E+15	.1737E+09
10	10000.	18.53277	1.404	.6185E-03	0.	.2138E-04	0.	.7879E+14	130.9
11	100000	39.92765	.1484	.5787E-03	0.	.1043E-04	0.	.3986E+14	0.
12	.10000E+07	86.02151	.1572E-01	.4534E-03	0.	.3815E-05	0.	.1556E+14	0.
13	.10000E+08	185.32772	.1552E-02	.3210E-03	0.	.1110E-05	0.	.5222E+13	0.
14	.10000E+09	399.27647	.1248E-03	.1993E-03	0.	.2083E-06	0.	.1344E+13	0.
15	.10000E+10	860.21508	.5968E-05	.1154E-03	0.	.2049E-07	0.	.2642E+12	0.
16	.10000E+11	1853.27720	.3207E-07	.9419E-04	0.	.2468E-09	0.	.8836E+10	0.

NO. OF A/B PARTICLES = 403086.29 NO./ML
NO. OF B PARTICLES = 28697.606 NO./ML

ALL MASSES IN MICRO-G/ML
MASS OF A/B PARTICLES = .13921375
MASS OF B PARTICLES = .18818338E-03
MASS FRACTION OF B IN A/B = .16807E-01

ACCUMULATED SEDIMENTATION LOSSES (G)
MASS OF MATERIAL B LOST = 142091.33 (G)
MASS OF MATERIAL A LOST = .58063631E+09
TOTAL MASS LOST = .58077840E+09

SEDIMENTATION LOSS RATE (G/SEC)
A/B PARTICLES = 284446.31
B PARTICLES = .51176011E-02

H,VOLUME AT BEGINNING AND END OF INTERVAL = 208399.41 .47390261E+10 .47395908E+10

APPENDIX B

PROGRAM LISTING

```
      PROGRAM CRAM(INPUT,OUTPUT,PUNCH,TAPE5,TAPE5=INPUT,TAPE6=OUTPUT,
     1  TAPE7=PUNCH)
      DIMENSION AN(30),ANP(30,20),ASLAB(20,30),ASLB(20,30),B(30),
     1  BN(30),BNEW(30,20),BNP(30,20),D(30),DPR(20),DTK(20),DVOL(20),
     2  F(30,30),G(30),PM(20),PMAA(20),PMB(20),PROR(20),RAD(30),
     3  RL(30,30),RLP(30,30),RLPP(30,30),RM(30),SIG(30),
     4  TEMP(20),TITLE(79),VOL(20),VSED(30),XK(30,30)
      DIMENSION FACTRA(20),FACTRB(20)
      LOGICAL PTVC,KKC
      COMMON /CA/CNOMX,NLAY,VOL,DVOL,TEMP,DTK,
     1  PROR,DPR
      NAMELIST /JIM/ ALFA,ANP,BNEW,BNP,CNH,CNOMX,CNPRES,CNTEM,CNVOL,
     1  FACTRA,FACTRB,
     2  IDINT,IR,KKC,NCLTI,NLAY,NT,NT1,NT2,NZS,PTVC,RMO,RN2M,
     3  RHO,TEND,TI,XKCON
C  THIS PROGRAM IS INTENTED TO CALCULATE THE COAGULATION OF TWO TYPES OF
C  PARTICLES IN THE EXHAUST CLOUD OF A ROCKET BLAST OFF.  THE PARTICLES ARE
C  DIVIDED INTO A NUMBER OF DISCREET MASS SIZES.
C  JIM IS THE INPUT DATA NAMELIST FOR THE MAIN PROGRAM; THE VARIABLES ARE:
C  RMO = MASS OF THE SMALLEST PARTICLE (SMALLEST MASS SIZE)
C  ALFA = MASS RATIO OF CONSECUTIVE MASS SIZES
C  IR = NUMBER OF MASS SIZES
C  RHO =: DENSITY OF PARTCILE MATERIAL
C  NT = NUMBER OF TIME INTERVALS TO BE CALCULATED, IF CLOUD RISE TIME (TEND)
C       IS NOT EXCEEDED FIRST
C  ANP,BNP,BNEW = ARRAYS GIVING A/B DISTRIBUTIONS, B DISTRIBUTIONS, AND
C    FRACTION B IN A/B,RESPECTIVELY.  EACH ARRAY HAS 600 ELEMENTS;  1-30 FOR
C    THE BOTTOM CLOUD, 31-60 FOR THE 2'ND CLOUD, UP TO 20 CLOUDS;  ELEMENTS 1,
C    31, 61, ETC. GIVE NUMBER FOR SMALLEST MASS PARTICLE IN EACH CLOUD.
C  TI = INITIAL VALUE FOR TIME STEP SIZE INDEX.
C  IDINT = NUMBER OF TIME INTERVALS BETWEEN PRINT OUTS.
C  TEND = TIME AT WHICH TO STOP CALCULATIONS (CLOUD RISE TIME), IF NT NOT
C    EXCEEDED FIRST.
C  NT2 = NUMBER OF TIME INTERVAL AT WHICH TO FIRST REVISE TI;  THEN COUNTER
```

```
C     FOR SUBSEQUENT REVISIONS OF TI.
C   NT1 = INCREMENT VALUE FOR NT2 WHEN TIME INTERVAL NT2 REACHED
C   RN2M = REVISE VALUE FOR TI ( TI=TI*RN2M)
C   NCLTI = NUMBER OF TIME INTERVALS INBETWEEN RECALCULATIONS OF DELTA TIME
C     ('DT').
C   END OF NAMELIST VARIABLES.
C   FOR ANY DO LOOPS USING N ,L, OR I, N IS THE COUNTER FOR THE TIME INTERVAL,
C   L POINTS TO THE CLOUD, AND I IS THE MASS SIZE POINTER.
C   IP IS THE COUNTER FOR THE PRINTOUT, IE, WHEN IP=N, MASS DISTRIBUTIONS ARE
C   PRINTED, AND WHEN THE TOP LAYER HAS BEEN PRINTED, IP IS INCREMENTED BY
C   'IDINT'.
C   'NCLT' IS THE COUNTER FOR RECALCULATIONS OF 'DT', WHEN NCLT=N, 'DT' IS
C   RECALCULATED, AND 'NCLT' IS INCREMENTED BY 'NCLTI'.
C   'TIME' POINTS TO THE BEGINNING OF THE INTERVAL BEING EXAMINED.
C   'CLDRIS' IS A SUBROUTINE THAT CALCULATES TEMPERATURE, PRESSURE, AND
C   VOLUMEOF EACH CLOUD.  THE FIRST TIME IT IS CALLED AS 'CLDRIS', AFTER
C   THAT, AS 'POINT', WHICH IS AN ENTRY POINT IN 'CLDRIS'.  'CLDRIS' SETS
C   VALUES IN 6 ARRAYS, 'VOL,TEMP,PROR,DVOL,DTK,DPR'.  THE FIRST THREE GIVE
C   THE VALUES OF VOLUME, TEMPERATURE, AND PRESSURE, RESPECTIVELY, IN EACH
C   CLOUD, AT TIME 'TLIM'.  THE SECOND THREE GIVE THE CHANGES IN VOLUME,
C   TEMPERATURE, AND PRESSURE, RESPECTIVELY, IN EACH CLOUD, SINCE THE LAST
C   TIME THEY WERE CALCULATED ('TOLD').  ALL THREE CHANGE ARRAYS SHOULD CONTAIN
C   POSITIVE VALUES, ASSUMING DROPS IN TEMPERATURE AND PRESSURE, AND A RISE
C   IN VOLUME.  WHENEVER 'TLIM' IS EXCEEDE BY 'TIME', 'POINT' IS CALLED.
1     READ(5,111) (TITLE(I),I=1,79)
      DO 2 I=1,20
      FACTRA(I)=1.0
      FACTRB(I)=1.0
      DO 2 J=1,30
      ASLAB(I,J)=0.0
2     ASLB(I,J)=0.0
111   FORMAT(1X,79A1)
      WRITE(6,111) (TITLE(I),I=1,79)
      NT2=1000
      NZS=1
      NT1=1000
      RN2M=1.0
      NLAY=1
      PTVC=.FALSE.
      KKC=.FALSE.
```

```
      READ (5,JIM)
      DO 112 J=1,NLAY
      DO 112 I=1,IR
      ANP(I,J)=ANP(I,J)*FACTRA(J)
112   BNP(I,J)=BNP(I,J)*FACTRB(J)
      IP=IOINT
      TKOLD=100000.0
      T1PER=TEND/100.0
      NCLT=1
      TIME=0.0
C  FOR PTVC; WHEN THIS IS SET TRUE BY THE INPUT DATA (DEFAULT VALUE=
C  FALSE), CONSTANT PRESSURE,TEMPERATURE, AND VOLUME ARE ASSUMED.GIVEN
C  IN INPUT AS CNPRES(ATM.), CNTEM(K), CNVOL(M**3), ALSO, NLAY MUST BE
C  GIVEN IN THE INPUT DATA BECAUSE CLDRIS IS NOT CALLED.  CNOMX MUST BE
C  GIVEN, AND HEIGHT(CNH) MUST ALSO BE GIVEN.(HEIGHT IN CM)
      IF(PTVC) GO TO 80
      CALL CLDRIS(TLIM)
      GO TO 81
80    TLIM=TEND+1.0
      DO 82 I=1,NLAY
      VOL(I)=CNVOL
      DVOL(I)=0.0
      PROR(I)=CNPRES
      DPR(I)=0.0
      TEMP(I)=CNTEM
82    DTK(I)=0.0
81    TOLD=0.0
      DO 30 N=1,NT
      IF(N.NE.NT2) GO TO 11
      NT2=NT2+NT1
      TI=TI*RN2M
C  FOLLOWING IS THE CLOUD LOOP, IE, EVERY TIME THROUGH THIS LOOP, THE
C  DISTRIBUTIONS FOR ANOTHER CLOUD ARE CALCULATED.
C  'TK'  AND 'P' ARE VALUES OF TEMPERATURE AND PRESSURE, INTERPOLATED FOR
C  TIME  'TIME'. 'U' IS THE VISCOCITY OF AIR, 'RLAMDA' IS THE MOLECULAR MEAN FREE
C  FREE PATH.  'ALFC' IS A DUMMY VARIABLE EQUAL TO THE MASS OF THE PARTICLE
C  IN QUESTION.  'RK' IS BOLTZMANN'S CONSTANT.
11    DO 60 L=1,NLAY
```

```
                TK=TEMP(L)+(TLIM-TIME)/(TLIM-TOLD)*DTK(L)
                P=PRDR(L)+(TLIM-TIME)*DPR(L)/(TLIM-TOLD)
  115           U=1.055E-5*SQRT(TK)
                RLAMDA=2.2E-8*TK/P
                ALFC=1./ALFA*RMO
                RK=1.38E-16
                V1=RK*TK/18.85/U
  120           V2=1.257*RLAMDA
                V3=.4*RLAMDA
                V4=-1.1/RLAMDA
              C  FOLLOWING IS A LOOP TO CALCULATE VALUES DEPENDANT ON MASS SIZE. 'AN, BN, AND
              C  B' ARE USED TO STORE THE MASS DISTRIBUTIONS FOR THE LAYER BEING
  125         C  CALCULATED, ALLOWING NEW VALUES TO BE STORED IN 'ANP, BNP, AND BNEW' AND
              C  STILL HAVE THE OLD VALUES AVAILABLE.
               C  'RM(I)' = THE MASS, 'RAD(I)' = THE RADIUS, AND 'VSED(I)' = THE
               C  SEDIMENTATION VELOCITY OF A PARTICLE OF MASS CLASS I.
               C  'SIG(I)' = VALUES USED TO CALCULATE THE COLLISION KERNEL ARRAYS.
  130             DO 10 I=1,IP
                  AN(I)=ANP(I,L)
                  BN(I)=BNP(I,L)
                  B(I)=BNEW(I,L)
                  ALFC=ALFC*ALFA
  135             RM(I)=ALFC
                  RADI=(.2387*ALFC/RHO)**(1./3.)
                  RAD(I)=RADI
                  TEST=V4*RADI
                  IF (TEST.LE.-500.) TEST=-500.0
  140             DI=V1/RADI*(1.+V2/RADI+V3/RADI*EXP(TEST))
                  D(I)=DI
                  GS=2.546*RK*TK/ALFC
                  G(I)=GS
                  GR=SQRT(GS)
  145             DUM=2.546*DI/GR
                  SIG(I)=.09256*GR/DI/RADI*((2.*RADI+DUM)**3.0-(4.*RADI*RADI
                 1  +DUM*DUM)**1.5)-2.828*RADI
               10   IF(RADI.LE.2.0E-3) VSED(I)=980.0*ALFC*DI/RK/TK
                  IF(.96.LE.TK/TKOLD.AND.1.04.GT.TK/TKOLD) GO TO 43
  150             TKOLD=TK
                  DO 44 I=1,IR
                  RADI=RAD(I)
                  IF(RADI.LE.2.0E-3) GO TO 44
```

```
                TERM1=2.74E2*((P*RADI)**0.666667)/TK
155             TERM2=4.93E6*RM(I)/(SQRT(TK))/RADI
                EN=TERM2/20.0
                EP=TERM2
                DO 47 J=1,25
                VSEDI=(EN+EP)/2.0
160             FNEW=VSEDI+TERM1*(VSEDI**1.666667)-TERM2
                IF(FNEW.GT.0.0) GO TO 48
                EN=VSEDI
                GO TO 47
           48   EP=VSEDI
165        47   CONTINUE
                VSED(I)=VSEDI
           44   CONTINUE
           43   A=0.0
           C  THE FOLLOWING LOOP CALCULATES THE F ARRAY, THE 'XK' (COLISSION KERNEL)
170        C  ARRAY, AND SOME OF THE VALUES USED FOR CALCULATING 'DT'.
                DO 20 I=1,IR
                DO 20 J=1,I
                RSUM=RAD(I)+RAD(J)
                DSUM=D(I)+D(J)
175             DUM=1.+RAD(J)/RAD(I)
                XKI=(DUM*DUM-1./DUM)*3.1416*RAD(I)*RAD(I)*(VSED(I)-VSED(J))+
               1  12.57*RSUM*DSUM/(RSUM/(RSUM+SQRT(SIG(I)*SIG(I)+SIG(J)*SIG(J)))
               2    +4*DSUM/RSUM/SQRT(G(I)+G(J)))
                IF(KKC)XKI=XKCON
180             XK(I,J)=XKI
                XK(J,I)=XKI
                F(I,J)=1-RM(J)/(ALFA-1.0)/RM(I)
                IF (L.NE.1.OR.N.NE.NCLT) GO TO 20
                ATT=XKI*RM(J)/RM(I)
185             A=AMAX1(A,ATT*AN(J),ATT*BN(J))
           20   CONTINUE
           C  THE FOLLOWING (UP TO STMT 28) CALCULATE SOME OF THE INITIAL MASSES,
           C  AND PRINT OUT THE INITIAL CONDITIONS.  'H' ( THE THICKNESS OF THE CLOUD)
           C  IS SET AT 100 METERS, EXCEPT FOR CLOUD 1, WHERE IT IS SET AS THE RADIUS.
190        C  'DT' IS CALCULATED, IF 'N=NCLT', AND 'L=1'.
                IF(N.NE.1) GO TO 28
                PM(L)=0.0
```

```
                PMBB=0.0
                PMAB=0.0
      195       PMAA(L)=0.0
                DO 25 I=1,IR
                PMBB=PMBB+RM(I)*BN(I)
                PMAB=PMAB+RM(I)*AN(I)
                PMAA(L)=PMAA(L)+RM(I)*AN(I)*(1-B(I))
      200   25  PM(L)=PM(L)+RM(I)*(AN(I)+BN(I))
                PMB(L)=PM(L)-PMAA(L)
                H100=H/100
                IF(L.EQ.1)WRITE(6,400)RHO,IR,TI,RMO,ALFA,NT
                WRITE(6,405) L
      205   405 FORMAT(* LAYER = *I5)
                DUM=(VOL(L)-DVOL(L))*1.0E6
                PMAA(L)=PMAA(L)*DUM
                PMB(L)=PMB(L)*DUM
                WRITE(6,406) PMAB*DUM,PMBB*DUM,PM(L)*DUM
      210   406 FORMAT(//* INITIAL MASS OF A/B = *G14.6* G.*/
               1  * INITIAL MASS OF B = *G14.6* G*/* INITIAL MASS = *G14.6)
                WRITE(6,410)
                I=1
                WRITE(6,420)I,RM(1)*1.E12,RAD(1)*2.E4,VSED(1)
      215       DO 500 I=5,IR,5
                RMI=RM(I)*1.0E12
                RADI=RAD(I)*2.0E4
      500   WRITE(6,420) I,RMI,RADI,VSED(I)
                WRITE(6,430)
      220       I=1
                WRITE(6,440) I,XK(1,1)*1.E10
                DO 510 I=5,IR,5
      510   WRITE(6,440) I,XK(I,1)*1.E10,(XK(I,J)*1.E10,J=5,IR,5)
      400   FORMAT(20X*AEROSOL PROGRAM*//
      225      2  * DENSITY OF PARTICLE MATERIAL = *F7.3*  G/ML*/
               3  * NO. OF PARTICLE CLASSES = *I5/* TIME STEP SIZE INDEX = *
               4  F9.4/* MASS OF SMALLEST PARTICLE = *G12.5*  GM.*/
               5  * RATIO OF CONSECUTIVE MASS CLASSES(ALFA) = *F8.4/
               6  * NO. OF TIME STEPS =*I5//)
      230   410  FORMAT(10X,*SEDIMENTATION VELOCITIES*/* CLASS*12X*MASS, PG*
               1  7X*DIAM, MICRO-M*4X*VELOCITY, CM/SEC/*)
      420   FORMAT(1X,I5,2(5X,G15.8),5X,G15.6)
      430   FORMAT(//10X,*SAMPLE COAGULATION CONSTANTS*/15X,
```

```
     1  33HK(I,J) * 1.0E-10  ML/PARTICLE/SEC/1X,*CLASS*14X*1*14X*5*
     2  13X*10*13X*15*13X*20*13X*25*13X*30*/)
440   FORMAT(1X,I5,4X,7(1X,G14.7))
      NZERO=0
      WRITE(6,450) TIME,NZERO,DT,L
      DO 730 I=1,IR
730   WRITE(6,460) I,RM(I)*1.0E12,RAD(I)*2.0E4,AN(I),B(I),BN(I)
28    H=10000.0
      IF(L.NE.1) GO TO 29
      H=((VOL(L)-(TLIM-TIME)*DVOL(L)/(TLIM-TOLD))**(1.0/3.0))*124.07
      IF(N.NE.NCLT) GO TO 29
      NCLT=NCLT+NCLTI
      DT=TI/A/IR
      IF(DT.GT.T1PER)DT=T1PER
      IF (DT.GT.T1PER/3.0) IOINT=INT(T1PER*5/DT)
C  THE COLLISION RATE ARRAYS ARE CALCULATED.
29    DO 50 I=1,IR
      DO 50 J=1,I
      XKI=XK(I,J)
      DUM=XKI*AN(I)*AN(J)
      RL(I,J)=DUM
      RL(J,I)=DUM
      DUM=XKI*BN(I)*BN(J)
      RLP(I,J)=DUM
      RLP(J,I)=DUM
      RLPP(I,J)=XKI*AN(I)*BN(J)
50    RLPP(J,I)=XKI*AN(J)*BN(I)
C  THIS IS THE MAIN LOOP FOR CALCULATING NEW MASS DISTRIBUTIONS.
      VLEND=VOL(L)-DVOL(L)*(TLIM-TIME-DT)/(TLIM-TOLD)
      VLBEG=VOL(L)-DVOL(L)*(TLIM-TIME)/(TLIM-TOLD)
      IF(PTVC) H=CNH
      DO 100 I=1,IR
      DAN=0.0
      DBN=0.0
      DB=0.0
      IM=I-1
      IF(I.EQ.1) GO TO 55
      RMM=RM(IM)
      DUM=B(IM)
      RMMBM=RMM*DUM
```

```
      55    RMI=RM(I)
275         RMBI=RMI*B(I)
      C  THIS LOOP PERFORMS THE SUMMATIONS FOR EACH MASS SIZE 'I'.
            DO 200 J=1,IR
            S=1.0
            IF(I.EQ.J) S=.5
280         SM=1.0
            IF (IM.EQ.J) SM=0.5
            RLV=RL(I,J)*DT
            RLPV=RLP(I,J)*DT
            RLPPV=RLPP(I,J)*DT
285         RLPPR=RLPP(J,I)*DT
            DBN=DBN-RLPV-RLPPR
            DUM=RLV+RLPPV
            DAN=DAN-DUM
            DB=DB-DUM*RMBI
290         IF (J.GT.I) GO TO 200
            RMJ=RM(J)
            RMBJ=RMJ*B(J)
            DUM=RMI/(RMJ+RMI)
            FV=F(I,J)
295         SFV=S*FV
            SLFV=SFV*RLV
            FLPPV=FV*RLPPV
            DAN=DAN+SLFV+FLPPV
            DB=DB+SLFV*DUM*(RMBI+RMBJ)+FLPPV*DUM*(RMBI+RMJ)
300         DBN=DBN+SFV*RLPV
             IF(J.GE.I.OR.I.EQ.1) GO TO 200
            DUM2=RMI/(RMM+RMJ)
            FMV=1-F(IM,J)
            SFMV=FMV*SM
305         SLFMV=SFMV*RL(IM,J)*DT
            FLPPM=RLPP(IM,J)*FMV*DT
            FLPPR=RLPPR*FV
            DAN=DAN+SLFMV+FLPPM+FLPPR
            DB=DB+SLFMV*DUM2*(RMMBM+RMBJ)+FLPPM*DUM2*(RMMBM+RMJ)
310        1  +FLPPR*DUM*(RMI+RMBJ)
            DBN=DBN+SFMV*RLP(IM,J)*DT
            IF(J.GE.IM.OR.I.LE.2) GO TO 200
            FLPPMR=RLPP(J,IM)*FMV*DT
            DAN=DAN+FLPPMR
```

```
315               DB=DB+FLPPMR*DUM2*(RMM+RMBJ)
              200 CONTINUE
                C  STORE NEW MASS DISTRIBUTIONS AN 'ANP,BNP,BNEW', TAKING INTO ACCOUNT
                C  THE INCREASE IN VOLUME, THE SEDIMENTATION LOSS, AND THE SEDIMENTATION
                C  GAIN, (WHERE APPLICABLE).
320               DUM=AN(I)
                  DUM2=DUM+DAN
                  DUM3=BN(I)+DBN
                  IF(DUM2.LT.CNUMX) DUM2=0.0
                  IF(DUM3.LT.CNUMX) DUM3=0.0
325           35  IF (DUM2.EQ.0.0) GO TO 92
                  BNEW(I,L)=(RMI*DUM*B(I)+DB)/RMI/DUM2
                  GO TO 95
              92  BNEW(I,L)=0.0
              95  VSEDIH=VSED(I)/H
330               VSEDFR=VSEDIH*DT
                  IF(VSEDFR.LE.1.0) GO TO 37
                  WRITE(6,36)VSEDFR,DT,H,VSED(I)
                  VSEDIH=1.0/DT
              36  FORMAT(* SEDIMENTATION FRACTION .GT. 1, =*G14.6* DT= *G14.6
335              1  * H= *G14.6* VSED(I)= * G14.6)
              37  RABSED=DUM2*VSEDIH
                  ABSED=RABSED*DT
                  RBSED=DUM3*VSEDIH
                  BSED=RBSED*DT
340               DTL=(TLIM-TIME-DT)/(TLIM-TOLD)
                  ASLAB(L,I)=ASLAB(L,I)+ABSED*VLBEG*1.0E6
                  ASLB(L,I)=ASLB(L,I)+BSED*VLBEG*1.0E6
                  IF(L.EQ.1) GO TO 62
                  DVL=VLEND/(VOL(L-1)-DTL*DVOL(L-1))
345               ANP(I,L-1)=ANP(I,L-1)+ABSED*DVL
                  BNP(I,L-1)=BNP(I,L-1)+BSED*DVL
              62  G(I)=RABSED
                  D(I)=RBSED
                  DVL=VLBEG/VLEND
350               ANP(I,L)=(DUM2-ABSED)*DVL
                  BNP(I,L)=(DUM3-BSED)*DVL
             100  CONTINUE
                C  PRINT OUT IF 'N=NP', OTHERWISE GO TO NEXT CLOUD.
                  IF(N.NE.IP) GO TO 60
```

```
      IF(L.EQ.NLAY)IP=IP+IDINT
      SLRAB=0.0
      SLRB=0.0
      ABND=0.0
      BND=0.0
      SMAB=0.0
      SMB=0.0
      FMBINA=0.0
      WRITE(6,450)TIME,N,DT,L
  700 DO 70 I=1,IR
      RMI=RM(I)
      SLRAB=SLRAB+RMI*G(I)
      SLRB=SLRB+RMI*D(I)
      BI=BNEW(I,L)
      ANI=ANP(I,L)
      BNI=BNP(I,L)
      ABND=ABND+ANI
      DUM=ANI*RMI
      SMAB=SMAB+DUM
      FMBINA=FMBINA+DUM*BI
      BND=BND+BNI
      SMB=SMB+BNI*RMI
      RMI=RMI*1.E12
      RADI=RAD(I)*2.0E4
      WRITE(6,460)I,RMI,RADI,ANI,BI,BNI,G(I),D(I),ASLAB(L,I),ASLB(L,I)
   70 CONTINUE
      SMBINA=FMBINA/SMAB
      BSEDL=PMB(L)-(FMBINA+SMB)*VLEND*1.0E6
      ASEDL=PMAA(L)-(SMAB-FMBINA)*VLEND*1.0E6
      SLRAB=SLRAB*1.0E6*VLEND
      SLRB=SLRB*1.0E6*VLEND
      SMB=SMB*1.0E6
      SMAB=SMAB*1.0E6
      TSEDL=BSEDL+ASEDL
      WRITE(6,470) ABND,BND,SMAB,SMB,SMBINA,BSEDL,ASEDL,TSEDL,
     1  SLRAB,SLRB,H,VLBEG,VLEND
  450 FORMAT(//1X,15(4H****)/*  TIME = *F11.4/* TIME INTERVAL = *
     1  I5/* DELTA TIME = * F12.5/* CLOUD*
     1  I5///10X,*PARTICLE SIZE AND COMPOSITION SPECTRUM*/
     7 71X,12(1H*),*   SEDIMENTATION  *,12(1H*)/* CLASS*6X*MASS,*9X
```

```
      8  *DIAM,*5X*N(A,B),*3X*FRACTION*6X*N(B),*6X*LOSS (NO/ML/SEC)*
      9  7X*ACCUMULATED (NO)*/14X*PG*9X*MICRO-M*5X*PER ML*4X*B IN A/B*
      1  4X*PER ML*,2(8X*A/B*10X*B*))
  460  FORMAT(1X,I3,5X,G12.5,F11.5,4X,7G11.4)
  470  FORMAT(/* NO. OF A/B PARTICLES = *G16.8*  NO./ML*/
     1  * NO. OF   B PARTICLES = *G16.8*  NO./ML*//* ALL MASSES IN *
     2  *MICRO-G/ML*/* MASS OF A/B PARTICLES = *G16.8/
     3  * MASS OF   B PARTICLES = *G16.8/* MASS FRACTION OF B IN A/B = *
     4  G12.5//* ACCUMULATED SEDIMENTATION LOSSES (G) */
     5  * MASS OF MATERIAL B LOST = *G16.8*   (G)*/
     6  * MASS OF MATERIAL A LOST = *G16.8/* TOTAL MASS LOST = *
     8  G16.8//* SEDIMENTATION LOSS RATE (G/SEC)*
     9 /* A/B PARTICLES = * G16.8/* B PARTICLES = *
     7  G16.8//* H,VOLUME AT BEGINNING AND END OF INTERVAL = *
     8  3G16.8///)
   60  CONTINUE
       TIME=TIME+DT
       IF (TIME.GT.TEND) GO TO 31
       IF(TIME.LE.TLIM) GO TO 30
   32  TOLD=TLIM
       CALL POINT(TLIM)
       IF (TIME.GT.TLIM) GO TO 32
   30  CONTINUE
   31  IF(NZS.NE.1) GO TO 1
       STOP
       END
```

SUBROUTINE CLDRIS

```
      SUBROUTINE CLDRIS(TIME)
      DIMENSION CPA(6,12),CPB(6,11),CPC(6,11),CPD(20,11),CPE(20,11),
     1  CPF(20,11),FRACA (6),P(100),PMAS(20,6),RMW(6),T(100),U(100),
     2  ZP(100),ZT(100),ZU(100)
      DIMENSION  AIRMT(20),API(20),APMT(20),ARMO(20),ASPS(20),
     1  AVI(20),AZN(20),BZN(20),DPR(20),DTK(20),DVOL(20),PROR(20),
     2  Q(20),RTS(20),TEMP(20),TFAR(20),VOL(20)
      LOGICAL CORTM,INTPR
      COMMON /CA/CNOMX,NLAY,VOL,DVOL,TEMP,DTK,
     1  PROP,DPR/CB/ZT,T
      COMMON /CC/ZP,P/CD/ZU,U
      DATA FRACA/1.397oE6,9.0168E5,1.7441E6,1.2626E6,5.0773E6,1.664E4/,
     1  RMW/18.016,36.465,44.054,101.961,28.0134,159.692/
      DATA ((CPA(I,J),J=1,12),I=1,6)/
     1 7.969,8.027,8.[illegible],8.415,8.676,8.954,9.246,9.547,9.851,
     2   10.152,10.444,10.723,
     3 6.961,6.964,6.973,7.004,7.069,7.167,7.289,7.423,7.559,
     4   7.693,7.819,7.936,
     5 7.714,8.896,9.877,10.666,11.31,11.846,12.293,12.667,12.988,
     6   13.243,13.466,13.656,
     7 12.22,13.98[illegible],22.965,25.366,26.899,27.946,28.713,29.317,29.821,
     8   30.26,30.653,31.008,
     9 6.957,6.961,6.99,7.069,7.196,7.35,7.512,7.67,7.815,
     1   7.945,8.061,8.162,
     1 16.3,24.9,28.71,31.5,33.74,35.786,37.815,39.792,36.0,
     2   33.646,33.822,33.998/
      NAMELIST /JIM1/ BZN,DPHZ,DT,DWATER,GAMTWO,IPINT,NLAY,P,QC,TF,
     1  TFA,TFB,T,U,ZP,ZT,ZU,CORTM,INTPR
C  THIS SUBROUTINE CALCULATES THE TEMPERATURE,PRESSURE, VOLUME, AND HEIGHT
C  OF THE CLOUD AS IT RISES.  THE TEMPERATURE, PRESSURE, AND VOLUME ARE
C  RETURNED TO THE MAIN PROGRAM.
C  JIM1 IS THE INPUT DATA NAMELIST;  THE VARIABLES ARE:
C  TF = TIME OF FIRE FOR BOTTOM CLOUD.
C  TFA = X  VALUES USED TO CALCULATE TIME OF FIRE FOR UPPER CLOUDS;
C  TFB = X  TIME = TFA * (ALTITUDE) EXP (TFB).
C  BZN = ARRAY GIVING INITIAL ALTITUDES OF BOTTOM OF EACH CLOUD, AND TOP OF
C    TOP CLOUD (BZN(1) NORMALLY EQUALS 0)
C  DPHZ = RATIO OF AMBIANT POTENTIAL PRESSURE TO ALTITUDE.
```

```
C  DT = TIME INTERVAL FOR CLOUD RISE CALCULATIONS.  NOTE THAT THIS 'DT' IS
C    DIFFERENT FROM THE 'DT' IN THE MAIN PROGRAM.
C  NLAY = NUMBER OF CLOUDS.
C  ZP = /  ALTITUDES AT WHICH PRESSURE, WIND VELOCITY, AND TEMPERATURE ARE
C  ZU = /  GIVEN IN P, U, AND T ARRAYS RESPECTIVELY.
C  ZT = /
C  P = +
C  U = +  AMBIANT PRESSURE, WIND VELOCITY, AND TEMPERATURE ARRAYS, RESPECTIVELY
C  T = +
C  END OF NAMELIST
C  THE FIRST PART OF THE PROGRAM, UP TO 'ENTRY POINT', IS EXECUTED ONLY
C  ONCE.
C  FOR ALL LOOPS IN THIS ROUTINE, 'L' POINTS TO A CLOUD, 'I' POINTS TO ONE
C  OF 6 POLLUTANTS, AND 'J'  REFERS TO A TEMPERATURE RANGE OF 100 DEGREES K,
C  FROM 100J+100, TO 100J +200 K.
C  QC IS THE HEAT OF THE EXHAUST RELEASED PER SECOND.
C  THE FOLLOWING ONE DIMENSIONAL ARRAYS ARE INITIALIZED, DEPENDANT ON 'L'.
C  'Q' IS THE HEAT CONTENT OF EACH CLOUD.
C  'RTS' IS THE SQUARE ROOT OF 'S', USING TEMPERATURE AT THE GROUND, FOR
C  BOTTOM CLOUD, OR AT THE BOTTOM OF THE CLOUD OTHERWISE.
C  'ASPS' IS A PARTIAL CALCULATION OF THE Z EQUATION, INCLUDING 'A'.
C    TEMP. AND PRESSURE (FOR RHO OF AIR) TAKEN AT GROUND OR BOTTOM OF CLOUD,
C    WIND VELOCITY ( L NOT EQUAL 1) AT MIDDLE OF LAYER.
C  'TFAR'  IS THE TIME OF FIRE FOR THE CLOUD.
C  'AVI'  IS THE ORIGIONAL CLOUD VOLUME.
C  'API' IS THE ORIGIONAL PRESSURE ( AT THE CENTER OF THE CLOUD).
C  'AZN' IS THE HEIGHT OF THE CENTER OF THE CLOUD.
C  'APMT'  IS THE TOTAL POLLUTANT MASS IN EACH CLOUD.
C  'PMAS', A VARIABLE DEPENDANT ON 'I' AS WELL AS 'L', IS THE MASS OF EACH
C    POLLUTANT IN EACH CLOUD.
      QL=0.0
      N=0
      DO 1 I=1,20
      VOL(I)=1.0
      PROR(I)=5.0
      TEMP(I)=1225.0
      ARMG(I)=0.0
      AIRMT(I)=0.0
      APMT(I)=0.0
```

```
      DO 1 J=1,11
      CPD(1,J)=0.0
80    CPE(1,J)=0.0
    1 CPF(I,J)=0.0
      IPINT=5
      CORTM=.FALSE.
      INTPR=.TRUE.
85    GAMTWO=0.49
      QC=1.1883E10
      DWATER=3.2557E9
      READ(5,JIM1)
      IPR=IPINT
90    RK=8.2E-5
      P=1.9671
      Q(1)=TF*QC-DWATER
      RTS(1)=SQRT(9.8*DPHZ/T(1))
      ASPS(1)=.25*RTS(1)*((.13822*Q(1)*RK*T(1)/P(1)/DPHZ)**.25)
95   1  /GAMTWO**0.75
      IF (NLAY.EQ.1) GO TO 6
      DO 5 L=2,NLAY
      CALL TFIND(TAMB,BZN(L))
      CALL PFIND(PAMB,BZN(L))
100   PTS(L)=SQRT(9.8*DPHZ/TAMB)
      AZN(L)=(BZN(L)+BZN(L+1))/2.0
      CALL UFIND(UAMB,AZN(L))
      ASPS(L)=1.0/3.0*RTS(L)*((.5529*QC*RK*TAMB/PAMB/DPHZ/UAMB)
     1  **(1.0/3.0))
105   TFAR(L)=TFA*((BZN(L+1)**TFB)-(BZN(L)**TFB))
      Q(L)=QC*TFAR(L)
    5 AVI(L)=((BZN(L+1)-BZN(L))**3.0)*0.19635
    6 AZN(1)=(BZN(2)-BZN(1))/1.64
      AVI(1)=((AZN(1)*GAMTWO)**3.0)*4.18879
110   CNDMX=.01/AVI(1)
      TFAR(1)=TF
      TIME=-DT
      DO 7 L=1,NLAY
      CALL PFIND(PAMB,AZN(L))
115   API(L)=PAMB
      DO 7 I=1,6
```

```
                PMASI=FRACA(I)*TFAR(L)
                IF (I.EQ.1.AND.L.EQ.1) PMASI=PMASI+5.565E6
                APMT(L)=APMT(L)+PMASI
120         7   PMAS(L,I)=PMASI
            C  'CPB & CPC' ARE CALCULATED SO THAT THE SPECIFIC HEAT OF POLLUTANT 'I'
            C  AT TEMPERATURE 'T' CORRESPONDING TO THE TEMPERATURE RANGE 'J' IS EQUAL TO
            C  'CPB(I,J) + CPC(I,J) * T'.
            C  'CPD, CPE, CPF' ARE CALCULATED TO FIND THE INTEGRAL OF
125         C  (MASS POLLUTANT * SPECIFIC HEAT) WITH RESPECT TO HEAT, OVER THE
            C  TEMPERATURE RANGE FROM 298 K TO ANY TEMPERATURE UP TO 1300 K.
            C  'CUMI' IS THE SUMATION OF THE INTEGRALS OF THE PREVIOUS ( OR LOWER)
            C  TEMPERATURE RANGES, 'T1' IS THE BOTTOM TEMPERATURE OF THE RANGE, AND
            C  'S1' IS THE SLOPE OF SPECIFIC HEAT/TEMPERATURE.
130         C  'CPA(I,J)' IS THE SPECIFIC HEAT OF POLLUTANT'I'
            C    IN TEMPERATURE RANGE 'J'.
                DO 8 I=1,6
                CUMI=-49.0*(2*CPA(I,1)+.98*(CPA(I,2)-CPA(I,1)))
                DO 8 J=1,11
135             T1=100.0*J+100.0
                CPAJ=CPA(I,J)
                CPAJP=CPA(I,J+1)
                S1=(CPAJP-CPAJ)/100.0
                CPB(I,J)=CPAJ-S1*T1
140             CPC(I,J)=S1
                IF (J.NE.1) CUMI=CUMI+(CPAJ+CPA(I,J-1))*50.0
                DO 8 L=1,NLAY
                CPD(L,J)=CPD(L,J)+(CUMI-T1*CPAJ+S1*T1*T1/2.0)*PMAS(L,I)/RMW(I)
                CPE(L,J)=CPE(L,J)+(CPAJ-T1*S1)*PMAS(L,I)/RMW(I)
145         8   CPF(L,J)=CPF(L,J)+(S1/2.0)*PMAS(L,I)/RMW(I)
                IF(INTPR)WRITE(6,212) UAMB,(ASPS(L),RTS(L),L=1,NLAY)
            212 FORMAT (* UAMB,ASPS,RTS:*G15.6,/(1X,2G15.6))
                A=(ASPS(1)*4.0/RTS(1))**4.0
                TIMEO=1-2.56E10/A
150             IF(TIMEO.LT.-1.0)TIMEO=-1.0
                TIMEO=ACOS(TIMEO)
                ENTRY POINT
            C  ABOUT TIME:  THE TIME USED IN THE FOLLOWING SECTION OF THE PROGRAM IS
            C  SET TO THE END OF THE INTERVAL, BUT THE TEMPERATURE RETURNED IS FOR THE
```

```
155         C  BEGGINNING, AND THE CORRESPONDING TIME RETURNED AS 'TLIM' IN THE MAIN
            C  PROGRAM MUST BE THE BEGGINNING.  HENCE, 'DT' IS SUBTRACTED FROM 'TIME'
            C  BEFORE RETURN.
            C  'N' IS THE TIME INTERVAL.
            C  THIS PROGRAM USES A BINARY APROXIMATION ROUTINE, SETTING TO1 ( THE LOWER
160         C  RANGE) TO 200 K, AND TO2 (THE UPPER) TO THE PREVIOUS TEMPERATURE (1275
            C ORIGIONALY).  'AIRMO' IS THE MASS OF AIR IN THE OLD CLOUD, 'PMT' IS THE
            C  POLLUTANT MASS, 'VI,PI' ARE THE ORIGIONAL VOLLUME AND PRESSURE.  'ZTE'
            C  IS THE RISE IN THE CLOUD SINCE TIME 0.  'DPR & PROR' ARE CALCULATED FROM
            C  THE PRESSURE OF THE HEIGHT AZN(L), BEGINNING OF INTERVAL, CENTER OF CLOUD.
165         15    TIME=TIME+DT*2.0
                  N=N+1
                  DO 10 L=1,NLAY
                  TO1=200.0
                  TO2=TEMP(L)+50.0
170               AIRMO=ARMO(L)
                  PMT=APMT(L)
                  VI=AVI(L)
                  PI=API(L)
                  ZTE=AZN(L)-BZN(L)
175               CALL PFIND(PAMB,AZN(L))
                  DPR(L)=PROR(L)-PAMB
                  PROR(L)=PAMB
                  TS=TIME*RTS(L)
                  IF(CORTM.AND.N.EQ.1) TS=TIMEO
180         C  THE EQUATIONS FOR VOLUME AND VELOCITY ARE DIFFERENT FOR 'L=1'.
            C  'VOL & DVOL' ARE CALCULATED FOR THE BEGINNING OF THE INTERVAL,
            C  'WN' IS THE VELOCITY, 'ZN' IS THE HEIGHT, AND 'VOBS' IS THE NEW VOLUME.
                  IF (L.NE.1) GO TO 18
                  VOBS=((ZTE*GAMTWO)**3.0)*4.18879
185               DVOL(L)=VOBS-VOL(L)
                  VOL(L)=VOBS
                  WN=ASPS(1)*SIN(TS)*((1-COS(TS))**(-.75))
                  ZN=AZN(1)+WN*DT
                  AZN(1)=ZN
190               VOBS=4.18879*((ZN*GAMTWO)**3.0)
                  GO TO 19
            18    TT=BZN(L+1)-BZN(L)
                  VOBS=TT*ZTE*ZTE*0.7854
                  DVOL(L)=VOBS-VOL(L)
```

```
      VOL(L)=VOBS
      WN=ASPS(L)*SIN(TS)*((1-COS(TS))**(-2.0/3.0))
      ZN=AZN(L)+WN*DT
      AZN(L)=ZN
      ZTE=ZN-BZN(L)
      VOBS=TT*ZTE*ZTE*.7854
19    CALL PFIND(PAMB,AZN(L))
      CALL TFIND(TAMB,AZN(L))
C   'CPMIX' IS THE SPECIFIC HEAT OF THE CLOUD,
C   'ZM' IS ONE OVER THE MOLECULAR WEIGHT,
C   'AIRMP' IS THE TOTAL MASS,
C   'M1' POINTS TO A TEMPERATURE RANGE EACH TIME THE FUNCTION IS CLACULATED.
C   'CI' IS THE MASS FRACTION OF A GIVEN POLLUTANT,
C   'QL' (Q LOSS) IS CALCULATED IF 'N' NOT EQUAL TO 1.
C   'PVRK, CM1F, CZ, &C1" ARE INTERMEDIATE VARIABLES INDEPENDANT OF
C   TEMPERATURE USED IN THE HEAT BALANCING EQUATION.
C   THE FIRST VALUES OF THE FUNCTION ARE CALCULATED, FOR 'T01' AND 'T02',
C   AND THEY ARE CHECKED TO MAKE SURE THEY ARE OF OPPOSITE SIGNS.   IF NOT,
C   THE INTERVAL BETWEEN 'T01' AND 'T02' IS DIVIDED INTO 50 SECTIONS, AND THE
C   VALUE OF THE FUNCTION IS PRINTED OUT AT EACH SECTION.  IF THE VALUE EVER
C   CHANGES SIGN, THE PROGRAM BRANCHES ON, IF NOT, IT RETURNS.
      CPMIX=0.0
      ZM=0.0
      AIRMP=AIRM0+PMT
      M1=INT(T02/100.0)-1
      DO 20 I=1,6
      CI=PMAS(L,I)/AIRMP
      ZM=ZM+CI/RMW(I)
      IF(N.EQ.1) GO TO 20
      CPMIX=CPMIX+CI*(CPB(I,M1)+CPC(I,M1)*T02)
20    CONTINUE
      IF (N.EQ.1) GO TO 25
      C02=AIRM0*0.21/AIRMP
      CN2=AIRM0*0.78/AIRMP
      ZM=ZM+C02/32.0+CN2/28.013
      CPMIX=CPMIX+AIRM0*.24/AIRMP
      GAM=CPMIX/(CPMIX-R*ZM)
      GAMR=1.0/GAM
      QL=(GAMR*VI*PI-GAMR*VI*(PI**GAMR)*(PAMB**(1-GAMR)))*2.421E4
25    RKP=RK*ZM
```

```
      PVRK=PAMB*VOBS/RKP
      CM1F=PVRK*(-.24*TAMB+WN*WN/8368.0)
      CZ=.24*(TAMB*AIRMP+PVRK-AIRMT(L))+QL-Q(L)
       C1=-.24*PMT
      M1=INT(T01/100.0)-1
      TF1=CM1F/T01+CZ+CPD(L,M1)+T01*(C1+CPE(L,M1))+T01*T01*CPF(L,M1)
      M1=INT(T02/100.0)-1
      TF2=CM1F/T02+CZ+CPD(L,M1)+T02*(C1+CPE(L,M1))+T02*T02*CPF(L,M1)
      F1=AMAX1(TF1,TF2)
      F2=AMIN1(TF1,TF2)
      IF(F1.GT.0.0.AND.F2.LT.0.0) GO TO 70
      DO 90 NOIT=1,50
      TT=T01+NOIT*(T02-T01)/50.0
      M1=INT(TT/100.0)-1
      TF1=CM1F/TT+CZ+CPD(L,M1)+TT*(C1+CPE(L,M1))+TT*TT*CPF(L,M1)
      F1=AMAX1(TF1,TF2)
      F2=AMIN1(TF1,TF2)
      WRITE(6,210)NOIT,F1,F2
210   FORMAT(* SSO; FUNC:*I5,2G15.5)
      IF(F1.GT.0.0.AND.F2.LT.0.0) GO TO 92
90    CONTINUE
      IF(INTPR)
     1 WRITE(6,200) NOIT,CM1F,CZ,C1,CPD(L,M1),CPE(L,M1),CPF(L,M1),T01,
     1  T02,TNEW,TF1,TF2,F1,F2,FNEW,RKP
      N=1
      TNEW=T02
      STOP
92    T01=TT
70    IF (TF1.GT.0.0) GO TO71
      TNEW=T02
      T02=T01
      T01=TNEW
C   'T01 & T02'  ARE SET SO THAT 'T01' CORRESPONDS TO THE POSITIVE VALUE AND
C   'T02' TO THE NEGATIVE (ABOVE).
C   IN THE MAIN ITERATION LOOP, THE FUNCTION IS CALCULATED FOR THE MIDDLE OF
C   THE INTERVAL, AND EITHER 'T01' OR 'T02' IS SET TO THE MIDDLE OF THE
C   INTERVAL, DEPENDING ON THE FUNCTIONS' POLARITY.  THE NEW MASS OF THE CLOUD
C   IS CALCULATED AND STORED, AND THE 'TEMP' AND 'DTK' ARRAYS ARE FILLED.
71    DO 75 NOIT=1,20
      TNEW=(T01+T02)/2.0
```

```
      M1=INT(TNEW/100.0)-1
      FNEW=CM1F/TNEW+CZ+CPD(L,M1)+TNEW*(C1+CPE(L,M1))+TNEW*TNEW*
     1  CPF(L,M1)
      IF (FNEW.GT.0.0) GO TO 72
      TO2=TNEW
      GO TO 75
72    TO1=TNEW
75    CONTINUE
81    AIRN=PVRK/TNEW-AIRMP
      IF(N.GT.5.AND.N.NE.IPR) GO TO 33
      IF(N.EQ.IPR.AND.L.EQ.NLAY) IPR=IPR+IPINT
      IF(INTPR)
     1 WRITE(6,200) NOIT,CM1F,CZ,C1,CPD(L,M1),CPE(L,M1),CPF(L,M1),TO1,
     1  TO2,TNEW,TF1,TF2,F1,F2,FNEW,RKP
200   FORMAT(* INTERMEDIATE OUTPUT:  NOIT,CM1F,CZ,C1,CPD,CPE(L,M1)*
     1  /* CPF(L,M1),TO1,TO2,TNEW,TF1,TF2,F1,F2*/* FNEW,RKP*/
     2  1X,I5,5G15.5,2(/1X,4G15.5)/1X,5G15.5)
      WRITE(6,100) N,L,TNEW,TIME,DT,AIRN,AIRMO,NOIT,VOBS,ZN,WN,QL,ZM,
     1  CPMIX,GAM,Q(L),PAMB,TAMB,PMT,PI,VI,AIRMT(L)
33    AIRMT(L)=AIRMT(L)+AIRN*TAMB
      ARMO(L)=AIRMO+AIRN
      DTK(L)=TEMP(L)-TNEW
      TEMP(L)=TNEW
10    CONTINUE
      TIME=TIME-DT
      IF(N.EQ.1) GO TO 15
100   FORMAT(1X,12(4H****)//* TIME INTERVAL = *I5/* LAYER =*I5/
     1  * NEW TEMPERATURE = *G15.5/* TIME = *G15.5/
     2  * DELTA TIME = *G15.5/* MASS OF NEW AIR INGESTED INTO CLOUD = *
     3  G15.5/* MASS OF OLD AIR IN CLOUD = *G15.5/
     4  * NO. OF ITERATIONS = *I5/* OBSERVED VOLUME = *G15.5/
     5  * HEIGHT OF CLOUD = *G15.5/* CLOUD VELOCITY = *G15.5/
     6  * QL = *G15.6/* ADDITIONAL VARIABLES:  ZM,CPMIX,GAM,Q(L),PAMB,
     7  TAMB,PMT,PI,VI,AIRMT(L)*2(/1X,5G15.6))
110   FORMAT(//1X,70(1H*)//* NO CONVERGENCE *//1X,70(1H*))
80    RETURN
      END
```

```
      SUBROUTINE TFIND(TF,ZA)
      COMMON/CB/ATZ,ATF
      DIMENSION ATZ(100),ATF(100)
      DO 10 I=1,100
      IP=I+1
      ZHI=ATZ(IP)
      IF(ZA.LT.ZHI) GO TO 12
   10 CONTINUE
   12 TLOW=ATF(I)
      THI=ATF(IP)
      ZLOW=ATZ(I)
      TF=TLOW+(ZA-ZLOW)*(THI-TLOW)/(ZHI-ZLOW)
      RETURN
      END

      SUBROUTINE PFIND(TF,ZA)
      COMMON/CC/APZ,APF
      DIMENSION APZ(100),APF(100)
      DO 10 I=1,100
      IP=I+1
      ZHI=APZ(IP)
      IF(ZA.LT.ZHI) GO TO 12
   10 CONTINUE
   12 TLOW=APF(I)
      THI=APF(IP)
      ZLOW=APZ(I)
      TF=TLOW+(ZA-ZLOW)*(THI-TLOW)/(ZHI-ZLOW)
      RETURN
      END
      SUBROUTINE UFIND(TF,ZA)
      COMMON/CD/AUZ,AUF
      DIMENSION AUZ(100),AUF(100)
      DO 10 I=1,100
      IP=I+1
      ZHI=AUZ(IP)
      IF(ZA.LT.ZHI) GO TO 12
   10 CONTINUE
   12 TLOW=AUF(I)
      THI=AUF(IP)
      ZLOW=AUZ(I)
      TF=TLOW+(ZA-ZLOW)*(THI-TLOW)/(ZHI-ZLOW)
      RETURN
      END
```

APPENDIX C

SOURCE DATA

December 10, 1974
0710 Z (0310 EDT) KSC

VOL	CENTER LOCATION x	y	SHAPE z (meters)	r	ΔD	POLLUTANT STRENGTH IN EACH VOLUME CO	CO_2	HCl (milligrams)	Al_2O_3
1	33.12	-46.4	96.5	533.9	193	9.393893E+07	9.76426 E+06	7.070670E+07	1.023564E+08
2	42.88	-73.1	209.8	533.9	33.6	4.384055E+07	4.556904E+06	3.299827E+07	4.776892E+07
3	67.45	-153.7	265.7	533.9	78.4	1.784056E+08	1.854395E+07	1.342838E+08	1.943917E+08
4	174.38	-553.1	431	533.9	252.1	2.213516E+09	2.300787E+08	1.666087E+09	2.411860E+09
5	197.9	-685.6	586.9	533.9	59.8	1.119119E+09	1.163242E+08	8.423483E+08	1.219399E+09
6	208.8	-807.5	639.1	533.9	44.6	1.004438E+09	1.04401 E+08	7.560287E+08	1.094442E+09

UPPER AIR METEOROLOGICAL DATA
Dec. 10, 1974 0631Z

BOUNDARY LAYER meters	WIND DIRECTION degrees	WIND SPEED met/s	TEMPERATURE degrees C	PRESSURE mb	RELATIVE HUMIDITY percent
4.88	310.0	3.08	7.9	1023.0	62.0
192.99	339.0	9.77	9.1	1000.0	66.0
226.52	341.0	9.77	9.5	996.0	67.0
304.88	345.0	10.80	8.9	986.6	68.0
557.01	345.0	10.28	6.7	957.0	60.0
616.77	355.0	10.28	7.8	950.0	57.0
661.28	354.0	10.28	8.6	945.0	55.0
914.63	346.0	10.28	7.9	916.5	40.0
1063.11	340.0	11.31	7.4	900.0	40.0
1219.51	332.0	11.83	7.1	883.2	39.0
1524.39	314.0	12.85	6.5	851.1	37.0
1533.23	314.0	12.85	6.4	850.0	37.0
1829.27	306.0	13.88	5.8	820.1	37.0
1870.73	305.0	13.88	5.8	816.0	37.0
2028.96	318.0	13.88	4.3	800.0	37.0
2134.15	319.0	13.88	3.6	790.1	37.0
2238.72	310.0	15.42	3.0	780.0	37.0

Stability Category: Stable Air
Brunt Voisala Frequency = 0.0172 (sec^{-1})

Mixing Layer Depth: 665 (meters)

SOURCE DATA
August 20, 1975
2122 Z KSC

VOL	CENTER LOCATION x	y	z	SHAPE r	ΔD	POLLUTANT STRENGTH IN EACH VOLUME CO	CO_2	HCl	Al_2O_3
	(meters)					(milligrams)			
1	-25.6	5.7	83.3	831.4	166.5	4.0331436E+07	4.1927008E+06	3.0401153E+07	4.3937757E+07
2	-43.2	6.6	193.3	831.4	53.6	2.2114947E+07	2.2989848E+06	1.6669872E+07	2.4092402E+07
3	-78.5	6.6	262.5	831.4	84.8	5.7781849E+07	6.0067785E+06	4.3554979E+07	6.2948537E+07
4	-237.2	-4.6	457.4	831.4	304.9	7.6493345E+08	7.9519535E+07	5.7659387E+08	8.3333160E+08
5	-252.7	-6.6	624.1	831.4	28.6	1.5260289E+08	1.5864009E+07	1.1502948E+08	1.6624821E+08
6	-377.2	-18.5	776.5	831.4	276.2	2.7565466E+09	2.8655998E+08	2.0778381E+09	3.0030291E+09
7	-425.1	-23.8	1002.6	831.4	176	3.1968884E+09	3.3233620E+08	2.4097604E+09	3.4827450E+09
8	-461.3	-21	1155.1	831.4	128.9	2.9295459E+09	3.0454432E+08	2.2082421E+09	3.1914975E+09
9	-529.9	13.9	1374	784.8	308.9	9.0534840E+09	9.4116533E+08	6.8243627E+09	9.8630206E+09
10	-131.7	594	1553.8	668.7	58.8	1.6301156E+09	1.6946054E+08	1.2287535E+09	1.7758758E+09
11	-167.7	584.4	1706.3	570.8	246.1	5.3512145E+09	5.5629164E+08	4.0336548E+09	5.8297048E+09
12	-243.9	879.6	1908.6	441.4	158.5	2.2781997E+09	2.3683287E+08	1.7172683E+09	2.4819098E+09

UPPER AIR METEOROLOGICAL DATA
Aug. 20, 1975 2046Z

BOUNDARY LAYER meters	WIND DIRECTION degrees	WIND SPEED met/s	TEMPERATURE degrees C	PRESSURE mb	RELATIVE HUMIDITY percent
4.88	110.0	3.60	28.7	1018.3	75.0
166.50	95.0	4.11	26.8	1000.0	84.0
220.12	91.0	4.11	26.2	994.0	83.0
304.90	89.0	4.11	25.5	984.5	83.0
609.80	83.0	2.60	24.5	951.1	62.0
638.41	82.0	2.60	24.5	948.0	62.0
914.60	87.0	1.03	21.8	918.5	69.0
1090.60	80.0	.51	20.6	900.0	74.0
1219.50	109.0	.51	20.0	886.9	69.0
1524.40	169.0	1.54	17.7	856.1	68.0
1583.20	166.0	1.54	17.4	850.0	69.0
1829.30	162.0	1.54	16.3	826.1	70.0
1987.80	167.0	3.08	15.4	811.0	70.0
2100.30	170.0	4.11	15.5	800.0	71.0
2211.30	171.0	5.66	15.6	790.0	73.0
2439.00	159.0	4.63	11.7	769.0	77.0

Stability Category: Stable Air
Brunt Voisala Frequency = 0.008 (sec^{-1})

Mixing Layer Depth: 1988 (meters)

SOURCE DATA
March 14, 1976
0127 Z March 15 KSC

VOL	CENTER LOCATION x	y	z	SHAPE r	ΔD	POLLUTANT STRENGTH IN EACH VOLUME CO	CO_2	HCl	Al_2O_3
	(meters)					(milligrams)			
1	-10.5	-29.0	91.5	608.7	182.3	6.74629 E+07	7.0123 E+06	5.07786 E+07	7.3508 E+07
2	-64.3	-73.9	244.2	608.7	122.6	1.61505 E+08	1.6787 E+07	1.215631E+08	1.75977E+08
3	-336.9	-154.9	457.4	608.7	304.9	2.095226E+09	2.17783E+08	1.577052E+09	2.28297E+09
4	-354.6	-155.7	617.4	608.7	15.2	2.186213E+08	2.27241E+07	1.645537E+08	2.38211E+08
5	-831.6	-105.1	769.8	608.7	289.6	6.607105E+09	6.86790E+08	4.973090E+09	7.19914E+09
6	-987.1	-56.9	1001.4	576.	173.5	6.203409E+09	6.44799E+08	4.669233E+09	6.75927E+09

UPPER AIR METEOROLOGICAL DATA
March 14, 1976
0127Z, March 15, 1976 (2027 EDT, March 14, 1976)

BOUNDARY LAYER meters	WIND DIRECTION degrees	WIND SPEED met/s	TEMPERATURE degrees C	PRESSURE mb	RELATIVE HUMIDITY percent
4.88	0.0	1.54	19.9	1020.7	87.0
182.30	40.0	6.17	19.9	1000.0	98.0
304.88	60.0	5.66	19.6	985.9	97.0
609.76	87.0	5.66	18.2	951.8	99.0
625.00	87.0	5.15	18.1	950.0	99.0
914.63	105.0	3.60	16.9	918.6	84.0
1088.10	130.0	3.08	15.3	900.0	98.0
1219.50	154.0	3.08	14.9	886.4	97.0
1524.40	211.0	3.60	13.1	855.1	100.0
1572.60	218.0	4.12	12.8	850.0	100.0
1829.30	233.0	5.66	11.5	824.7	95.0
2081.10	239.0	6.70	10.0	800.0	94.0
2134.20	240.0	6.70	9.6	795.2	95.0
2439.00	248.0	7.20	7.9	766.6	77.0
2615.50	252.0	7.20	6.2	750.0	79.0

Stability Category: Stable Atmosphere

Brunt Voisala Frequency = S

$$= \left(\frac{g}{T_o} \frac{\partial \phi}{\partial z}\right)^{1/2}$$

$$0.014 \ (\sec^{-1})$$

Mixing Layer Depth: 1088 (meters)

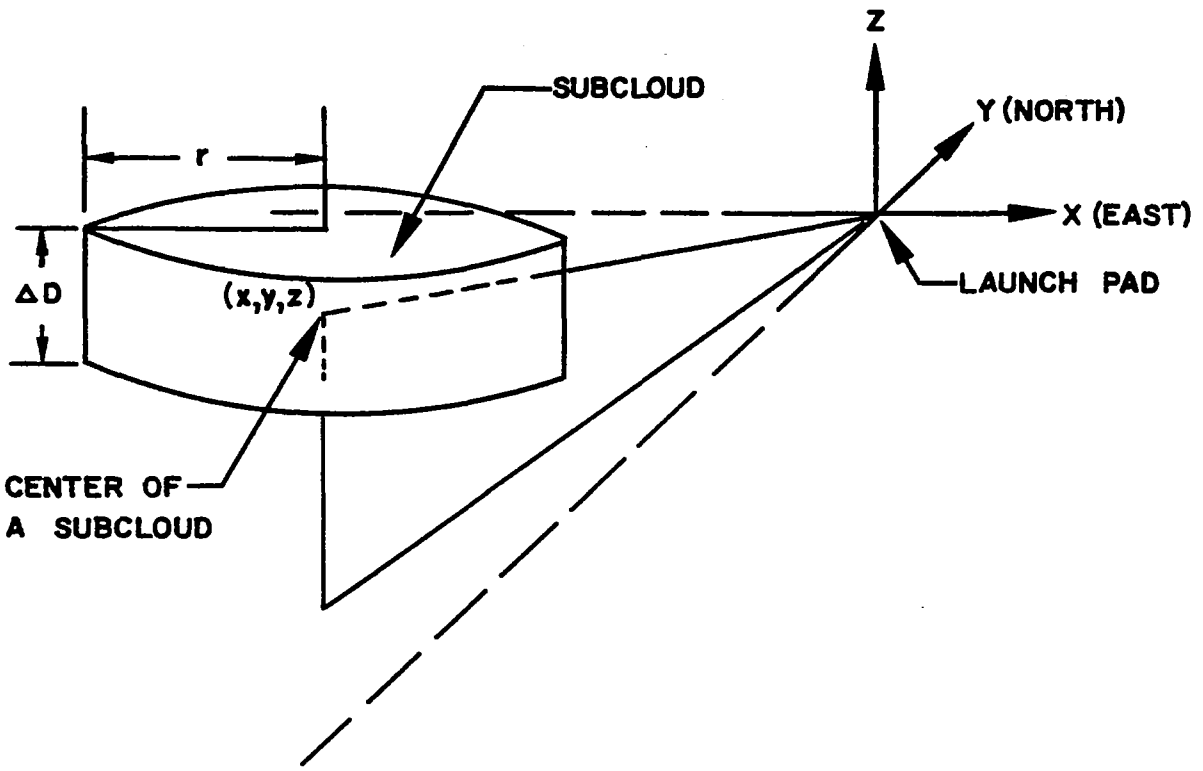

FIGURE C-1 DESCRIPTION OF THE SOURCE DATA

The stabilized cloud is layered into several subclouds, each of which resembles a pancake. The center (x,y,z), the height ΔD and the radius r of each subcloud are given by means of referring to a cartesian coordinated system set at the launch pad. The total amount of each pollutant species in each subcloud is given in the source data tables. It has been assumed that the concentration distribution in each subcloud is Gaussian in the horizontal plane, xy, and uniform in the vertical z direction.

APPENDIX D

SYMBOLS

$\overline{C}$	mean concentration of contaminant
$C_{D,i}$	drag coefficient for particle size class i
C_i	mass fraction of species i in cloud
C_p	specific heat at constant pressure
C_v	specific heat at constant density
c'	fluctuating concentration
D_i	particle diffusion coefficient ($cm^2\ sec^{-1}$)
$d_{\overline{m}}$	mass average diameter (cm)
e_s	saturation vapor pressure (mb)
f	Coriolis parameter (sec^{-1})
G_{ij}	mean thermal speed of ith and jth sized particles ($cm\ sec^{-1}$)
g	gravity constant ($cm\ sec^{-2}$)
H	thickness of flow field
h	cloud thickness
h_L	effective heat release per unit mass of liquid propellant ($cal\ g^{-1}$)
h_s	effective heat release per unit mass of solid propellant ($cal\ g^{-1}$)
h_w	latent heat of water vaporization at room temperature ($cal\ g^{-1}$)
K_{gas}	gas constant ($atm \cdot m^3 \cdot K^{-1}$)
K_{ij}	eddy diffusivity tensor ($m^2\ sec^{-1}$)
K^c_{ij}	collision kernel
K_x, K_y, K_z	eddy diffusivities ($m^2\ sec^{-1}$)
k	Von Karman constant
k_B	Boltzmann's constant ($ergs\ K^{-1}$)
L	Monin-Obukhov length scale
L_{ij}	rate of collision between particles of component A/B, size i, with particles of A/B, size j
L'_{ij}	rate of collision of particles of component B, size i, with particles of component B, size j

L''_{ij}	rate of collision of component A/B, size i, with particles of component B, size j
ℓ	mixing length (m)
$\dot{M}_L$	mass flow rate of liquid engine (g sec^{-1})
M_s	mass flow rate of solid engine (g sec^{-1})
M_w	mass flow rate of poured water (g sec^{-1})
MW_i	molecular weight of species i in cloud
M_{total}	actual initial mass of aerosol (g) (see eq. 14)
m	mass (g)
m_{air}	mass rate of air entrained due to turbulent mixing (g sec^{-1})
$\bar{m}_o$	initial average particle mass (g)
N'(d)	initial particle number distribution
n	number of moles in a unit volume
n_o	initial (total) particle number density
P	pressure in cloud (atm)
P_{amb}	ambient environmental pressure (atm)
Q	source strength (ppm)
Q_h	effective available heat (total effective heat content in cloud) (cal)
Re_i	particle Reynolds number
R_f	flux Richardson number
R_g	gradient Richardson number
RH	relative humidity (%)
R_{ij}	Lagrangian correlation tensor
S	constant mean shear gradient (sec^{-1})
s	Brunt Vaisala frequency (sec^{-1})
T	absolute temperature (K)
T_{22}, T_{33}	Lagrangian integral time scales in crosswind and vertical direction respectively (sec)
T_R	absolute temperature of ambient air near ground (K)
t	time
t_f	firing time during which cloud is formed (sec)
t_I	time for initial cloud rise speed (sec) (see eq. 5)
$\tilde{U}_p$	pseudovelocity (m sec^{-1})
u'_i	fluctuating velocity component in i direction (m sec^{-1})

u_*	friction velocity (m sec^{-1})
V	wind speed (m sec^{-1})
V_g	geostrophic wind speed (m sec^{-1})
V_{obs}	observed cloud volume (m^3)
V'	mixed Eulerian/Lagrangian fluctuation velocity (m sec^{-1})
$v_{s,i}$	sedimentation velocity of i size particle (cm sec^{-1})
W	cloud rise speed (m sec^{-1})
W_m	mixing ratio
$\overline{w'q'}$	heat flux
X_o	alongwind distance from pollutant point source
$\tilde{x}_o$	point source location
$\tilde{x}_{oo}$	fictitious point source location
z_o	initial cloud center location
Z_i	thickness of the PBL
Z_m	predicted stabilization height
Z(t)	cloud altitude at time t
z	height of source location
z_o	roughness length
α	mass class size
γ	entrainment constant
γ'	specific heat ratio
γ_d	adiabatic lapse rate (K m^{-1})
γ_g	constant for absorption strength of lower boundary
γ_p	absorption factor
γ_T	eddy conductivity (m sec^{-1})
γ_u	constant for absorption strength of upper boundary
δ	mean free path for particles (cm)
ε	rate of energy dissipation (m^4 sec^{-1})
θ_{oo}	total mass of pollutants at altitudes z and time t
λ	molecular mean free path (cm)
μ	viscosity of air (g cm sec^{-1})
ν	eddy viscosity (m^2 sec^{-1})
P	set of post-afterburning chemical species
ρ	particle density (g m^{-3})

ρ_{air}	density of ambient air near ground (g m^{-3})
ρ_g	density of air (g ml^{-1})
σ_0	initial standard deviation
σ_A	standard deviation of wind azimuth angle
σ_{A_o}	standard deviation of wind azimuth angle at a reference height near ground
σ_E	standard deviation of wind elevation angle
σ_{E_o}	standard deviation of wind elevation angle at a reference height near ground
σ_{ij}	dispersion tensor
σ_v	standard deviations of turbulent wind fluctuation components in cross-wind direction
σ_w	standard deviations of turbulent wind fluctuation components in vertical direction
σ_x, σ_y σ_z	standard deviations of mean concentration dispersions in x, y, z directions
σ_{x_o}	standard deviation of initial pollutant distribution in alongwind direction
σ_{y_o}	standard deviation of initial pollutant distribution in crosswind direction
σ_{z_o}	initial standard deviation of initial pollutant distribution in vertical direction
τ	time step size (sec)
ϕ	nondimensional wind shear
$\Delta\phi/\Delta z$, $\partial\phi/\partial z$	vertical gradient of virtual potential temperature

Subscripts:

air	ambient air
amb	ambient
obs	observed
max	maximum

REFERENCES

1. Dumbauld, R.K. and Bjorklund, J.R., "NASA/MSFC Multilayer Diffusion Models and Computer Programs - Version 5," NASA CR-2631, 1975.

2. Stephens, J.B., "Atmospheric Diffusion Predictions for the Exhaust Effluents from the Launch of a Titan 3C, December 13, 1973," NASA TM X-64925, 27 September 1974.

3. Stewart, R.B. and Grose, W.L., "Parametric Studies with an Atmospheric Diffusion Model that Assesses Toxic Hazards Due to the Ground Clouds Generated by Rocket Launches," NASA TN D-7852, May 1975.

4. "Panel Reports from the Shuttle Environmental Evaluation Symposium (Tropospheric)," 24-26 February 1975.

5. Hwang, B.C. and Pergament, H.S., "Environmental Effects of Space Shuttle Solid Rocket Motor Exhaust Plumes," AeroChem TP-343, NASA CR-145079, July 1976.

6. Glasser, M.E. and Siler, R.K., "Diffusion Estimates for Space Shuttle Launches from KSC," NASA/JSC 12507, February 1977.

7. Slade, D.H., Ed., "Meteorology and Atomic Energy," USAEC-TID-24190,1968.

8. Monin, A.S. and Yaglom, A.M., Statistical Fluid Mechanics, Vol. 1 (MIT Press, Cambridge, 1971), Chap. 5.

9. Stern, A.C., ed., "Proceedings of the Symposium on Multiple-Source Urban Diffusion Models," EPA Publ. AP-86, 1970.

10. Cramer, H.E., "Engineering Estimates of Atmospheric-Dispersion Capacity," presented at Annual Meeting of the American Industrial Hygiene Association, Chicago, IL, April 1959.

11. Gregory, G.L., Wornom, D.C., Bendura, R.J., and Wagner, H.S., "Hydrogen Chloride Measurements from Titan III Launches at the Air Force Eastern Test Range, FL, 1973 thru 1975," NASA TM X-72832, 1976.

12. Lee, R.W. and Elliott, R.W., "Effluent Transport: Model Description and Program Software," EG & G 5-611-R, 1974.

13. Chandler, M.W., "The Development of a Numerical Model (TREATS) to Simulate Atmospheric Dispersion from an Instantaneous Source in a Non-homogeneous Atmosphere," NUS-1197, 1974.

14. Lange, R., "ADPIC - A Three-dimensional Computer Code for the Study of Pollutant Dispersal and Deposition under Complex Conditions," UCRL-51462, 1973.

15. Hwang, B. C., Peskin, R.L., and So, R.M.C., "Concentration Distribution in Turbulent Shear Flow," AeroChem TP-342b, November 1977; submitted to J. Atmos. Sci.

16. Gomberg, R.I. and Stewart, R.B., "A Computer Simulation of the Afterburning Processes Occurring Within Solid Rocket Motor Plumes in the Troposphere," NASA TN D-8303, October 1976.

17. Mikatarian, R.R. and Pergament, H.S.,"AeroChem Axisymmetric Mixing with Nonequilibrium Chemistry Computer Program," AeroChem TP-200, AFRPL-TR-69-167, NTIS AD 856 017, June 1969.

18. Gomberg, R.I. and Wilmoth, R.G., "Effects of Entrained Water and Strong Turbulence on Afterburning Within Solid Rocket Motor Plumes," NASA TP-1111, 1978.

19. Briggs, G.A., "Some Recent Analyses of Plume Rise Observations," presented at the Second International Clean Air Congress, Washington, DC, December 6-11, 1970, Paper ME-8E.

20. Dumbauld, R.K., Bjorklund, J.R., and Bowers, J.F., "NASA/MSFC Multilayer Diffusion Models and Computer Program for Operational Prediction of Toxic Fuel Hazards," NASA CR-129006, 1973.

21. Tyldesley, J.B. and Wallington, C.E., "The Effect of Wind Shear and Vertical Diffusion on Horizontal Dispersion," Quart. J. Roy Meteor. Soc. 91, 158-174 (1965).

22. Record, F.A., Swanson, R.N., Cramer, H.E., and Dumbauld, R.K.,"Analysis of Lower Atmospheric Data for Diffusion Studies," NASA CR-61327, April 1970.

23. Susko, M. and Stephens, J.B., "Baseline Meteorological Soundings for Parametric Environmental Investigations at Kennedy Space Center and Vandenberg Air Force Base," NASA TM X-64986, February 1976.

24. Cramer, H.E., DeSanta, G.M., Dumbauld, R.K., Morganstern, P. and Swanson, R.N., "Meteorological Prediction Techniques and Data System," Final Report, Contract No. DA-42-007-CML-552, Army Dugway Proving Ground, 1964.

25. Hart, W.S., "Dynamics of Large Buoyant Clouds Generated by Rocket Launches," Trans. ASME, J. Basic Eng., 53-60, March 1972.

26. Briggs, G.A., "Discussion: Chimney Plumes in Neutral and Stable Surroundings," Atmos. Env. 6, 511-512 (1972).

27. Potter, A.E., "Shuttle Tropospheric Effects Program," presented at NASA Atmospheric Effects Working Group Meeting, Vandenberg Air Force Base, 27-28 October 1976.

28. Turner, D.B., "A Diffusion Model for an Urban Area," J. Appl. Meteor. 3, 83-91 (1964).

29. Gifford, T.A., "Turbulent Diffusion Typing Scheme: A Review," Nuclear Safety 17, 68-86 (1976).

30. Estoque, M.A., "Numerical Modeling of the Planetary Boundary Layer," Workshop on Micro-meteorology, D.A. Haugen, Ed. (A.M.S., Boston, 1973) pp. 217-270.

31. Blackadar, A.K., Panofsky, H.A., and Fiedler, F., "Investigation of the Turbulent Wind Field below 500 Feet Altitude at the Eastern Test Range, Florida," NASA CR-2438, 1974.

32. Kolmogoroff, A.N., "The Local Structure of Turbulence in Incompressible Viscous Fluid for Very Large Reynolds Number," C.R. (Dok.) Acad. Sci. USSR 30, 301 (1941).

33. Walton, J.J., "Scale-Dependent Diffusion," J. Appl. Meteorol. 12, 547 (1973).

34. Riley, J.J. and Corrsin, S., "The Relation of Turbulent Diffusivities to Lagrangian Velocity Statistics for the Simplest Shear Flow," J. Geophys. Res. 79, 1768-1771 (1974).

35. Corrsin, S., "Remarks on Turbulent Heat Transfer," Proceedings of the Iowa Thermodynamics Symposium (University of Iowa, Iowa City, 1953) pp. 5-30.

36. Fichtl, G.H. and McVehil, G.E., "Longitudinal and Lateral Spectra of Turbulence in the Atmosperic Boundary Layer at the Kennedy Space Center," J. Appl. Meteor. 9, 51-63 (1970).

37. Stephens, J.B., Adelfang, S.I., and Goldford, A.I., "Compendium of Meteorological Data for the Helios A Launch in December 1974," NASA TM X-73337, August 1976.

38. Stephens, J.B., Adelgang, S.I., and Goldford, A.I., "Compendium of Meteorological Data for the Viking A Launch in August 1975," NASA TM X- 73339, August 1976.

39. Blackadar, A.K., Dutton, J.A., Panofsky, H.A., and Chaplin, A., "Investigation of the Turbulent Wind Field below 150 Meters Altitude at the Eastern Test Range," NASA CR-1410, 1969.

40. Kaimal, J.E. et al, "Turbulence Structure in the Convective Boundary Layer," J. Atmos. Sci. 33, 2152-2169 (1976).

41. Paulson, C.A., "The Mathematical Representation of Wind Speed and Temperature Profiles in the Unstable Atmospheric Surface Layer," J. Applied Meteor. 9, 857-861 (1970).

42. Panofsky, H.A., "The Atmospheric Boundary Layer below 150 Meters," Ann. Rev. Fluid Mech. 6, 147-177 (1974).

43. Yaglom, A.M., "Data on Turbulence Characteristics in the Atmospheric Surface Layer," Izv. Atmos. Ocean Phys. 10, 566-586 (1974).

44. Wyngaard, J.C., Cote, O.R. and Izumi, Y., "Local Free Convection, Similarity, and the Budgets of Shear Stress and Heat Flux," J. Atmos. Sci. 28, 1171-1182 (1971).

45. Deardorff, J.W., "Three-Dimensional Numerical Study of Turbulence in an Entraining Mixed Layer," Bound. Layer Meteor. 7, 199-226 (1974).

46. Merry, M. and Panofsky, H.A., "Statistics of Vertical Motion over Land and Water," Quart. J. Roy. Meteor. Soc. 102, 255-263 (1976).

47. Tabata, S., "A Simple but Accurate Formula for the Saturation Vapor Pressure over Liquid Water," J. Appl. Meteor 12, 1410-1411 (1973).

48. Cotton, W.R., Pielke, R.A., and Gannon, P.T., "Numerical Experiments on the Influence of the Mesoscale Circulation on the Cumulus Scale," J. Atmos Sci. 33, 252-261 (1976).

49. Zeman, O. and Tennekes, H., "A Self-Contained Model for the Pressure Terms in the Turbulent Stress Equations of the Neutral Atmospheric Boundary Layer," J. Atmos. Sci. 32, 1808-1813 (1975).

50. Sherman, C.A., "A Mass-Consistent Model for Wind Fields Over Complex Terrain," Preprint UCRL 76171, Rev. 2, December 1976.

51. Gregory, G.L., Hudgins, C.H. and Emerson, B.R., Jr., "Evaluation of a Chemiluminescent Hydrogen Chloride and a NDIR Carbon Monoxide Detector for Environmental Monitoring," presented at 1974 JANNAF Propulsion Meeting, October 22-24, 1974.

52. Fuchs, N.A., The Mechanics of Aerosols, (Macmillan, New York, 1964), Chap. 7.

53. Ibid, Chap. 2..

54. Kritz, M.A.,"Formation Mechanism of the Stratospheric Aerosol," Ph. D. Thesis, Yale University, 1975.

55. Varsi, G., "Particulate Measurements," Proceedings of the Space Shuttle Environmental Assessment Workshop on Stratospheric Effects, (NASA TM X-58198, January 1977), p. E-1 - E-12.

56. Dawborn, R. and Kinslow, M., "Studies of the Exhaust Products of Solid Propellant Motors, " Arnold Air Force Station, Tullahoma, TN, AEDC-TR-76-49, September 1976.(Available as NASA CR-149674.)

57. Kreautle, K.J., "Applications of Particle Size Analysis in Combustion Research," presented at AIAA/SAE 13th Joint Propulsion Conference, Orlando, FL, July 11-13, 1977, AIAA 77-978.

58. Champagne, F.H., Harris, V.G., and Corrsin, S., "Experiments on Nearly Homogeneous Turbulent Shear Flow," J. Fluid Mech. 41, 81-139 (1970).

59. Cramer, H.E., "Turbulent Transfer Processes for Quasi-Homogeneous Flows Within the Atmospheric Surface Layer," Phys. Fluids 10, Suppl. S240-S246 (1967).

60. Klebanoff, P.S., "Characteristics of Turbulence in a Boundary Layer with Zero Pressure Gradient," NACA Report No. 1247, 1955.

61. Wyngaard, J.C., Cote, O.R., and Rao, K.S., "Modeling the Atmospheric Boundary Layer," Advances in Geophysics 18A, 193-212 (1974).

62. So, R.M.S. and Mellor, G.L., "An Experimental Investigation of Turbulent Boundary Layers Along Curved Surfaces," NASA CR-1940, 1972.

63. Comte-Bellot, G., "Ecoulement Turbulent entre Deux Parois Paralleles," Publ. Sci. Tech. Ministere l'Air, Service de Documentation Scientifique et Technique de l'Armament, Paris, No. 419, 1965.

64. Hinze, J.O., Turbulence (McGraw-Hill, New York, 1959) pp. 522-523.

65. Stull, R.B., "Mixed-Layer Depth Model Based on Turbulent Energetics," J. Atmos. Sci. 33, 1268-1278 (1976).

TABLE I

POST-AFTERBURNING PLUME COMPOSITION

	Al_2O_3	N_2	HCl	H_2O	CO_2	Fe_2O_3
Mass Frac. Y_i	0.1214	0.4882	0.0867	0.1344	0.1677	0.0016

TABLE II

COMPARISON OF AFTERBURNING COMPOSITION OF MAJOR SPECIES

	Complete burning (g)	Titan III[a] 0.9 km[b] (g)	Shuttle[a] 0.7 km[b] (g)
HCl	21.6	18.7	19.0
CO_2	41.8	41.4	41.4
H_2O	33.5	29.0	28.7

[a]Value at 1 km downstream of the nozzle exit plane.

[b]Altitude of the rocket motor; determines the ambient undisturbed atmospheric condition and the speed of the rocket.

TABLE III

THE RANGE OF MULTILAYER DIFFUSION MODEL PARAMETER VARIATIONS IN STEWART AND GROSE STUDY

Lateral diffusion exponent, α	0.5 to 1.5
Vertical diffusion exponent, β	0.5 to 1.5
Source strength in each layer, Q_K, ppm-m^2	10^3 to 2×10^7
Source-strength distribution in each layer, Q_K, ppm-m^2	Uniform; Gaussian; step function
Mixing-layer division (layer grid spacing), K	7 layers to 28 layers
Stabilized cloud geometry	Right circular cones; right circular cylinders: both with equal volumes, with and without equal mass loadings
Specific energy release from rocket motor, h_s, cal/gm	690 to 2980
Meteorology	Low-level sea-breeze regime; fall fair-weather regime at Kennedy Space Center
Mixing-layer depth, Z_i, meters	300 to 750

TABLE IV

STANDARD DEVIATIONS OF WIND AZIMUTH ANGLE σ_{A_o} AND ELEVATION ANGLE σ_{E_o} AT REFERENCE HEIGHT 4 m ABOVE GROUND

	10 December 1974 (Towers 110, 313)		20 August 1975 (Towers 110, 308, 311, 313)	
Source	σ_{A_o}	σ_{E_o}	σ_{A_o}	σ_{E_o}
i.1	2	2	10	10
i.2	8	4	11	7
i.3	8	5	11	8
i.4	8	8	23	23

TABLE V

PEAK OF MAXIMUM CONCENTRATION (ppm) AT GROUND FROM MDM BY VARYING THE STANDARD DEVIATION OF THE INITIAL POLLUTANT DISTRIBUTION IN DECEMBER LAUNCH CASE[a]

σ_{x_o} \ σ_{y_o}	+ 0%	+ 20%	+ 50%
+ 0%	0.902	0.870	0.827
+ 20%	0.820	0.798	0.764
+ 50%	0.724	0.706	0.678

[a]The $\sigma_{A_o} = \sigma_{E_o} = 8$ (degree) was used in the calculations.

TABLE VI

BRIEF DESCRIPTION OF SELECTED

DIFFUSION MODELS

Models (Sponsor/User)	Modeling Technique	Turbulence Schemes
ADPIC (ERDA/LLL)	Semi-Trajectory Particle Diffusion Model	Similarity Method for[a] Diagonal Eddy Diffusivity
DISF (NASA/AEROCHEM)	Analytical Model for Uniform Shear Flow	Lagrangian Method Eddy Diffusivity Tensor
MDM (NASA/AEROCHEM)	Gaussian Plume Model	Cramer's Constants[b] Ignoring X-Diffusion
METS (VAFB/SAI)	Gaussian Plume Model	Turner-Pasquill[b] Ignoring X-Diffusion
TREATS (ERDA/NUS)	Gaussian Distribution in Each Horizontal Plane	Moment Method for σ_x, σ_y P-G or Blackadar Type for σ_z

[a]Can be changed for any specified diagonal eddy diffusivity.

[b]Alongwind dispersion σ_x is based on Tyldesley and Wallington's work.

TABLE VII

RATIO OF TURBULENCE PARAMETERS

σ_u	σ_v	σ_w	u_*	Reference	Description
1.68	1.28	1.19	1	Champagne et al[58]	Homogeneous shear flows in a wind tunnel
2.0	1.7	1.25	1	Cramer[59]	Atmospheric surface layer
1.89	1.32	0.97	1	Klebanoff[60]	Wind tunnel boundary layer on a smooth surface
2.0	1.4	1.27	1	Wyngaard et al[61]	Atmospheric surface layer, modified data
1.82	1.3	1.12	1	So and Mellor[62]	Surface layer in wind tunnel smooth wall
2.4	1.43	1.03	1	Comte-Bellot[63]	Turbulent flow between parallel plates
2.2	1.7	0.9	1	Hinze[64]	Turbulent pipe flow
2.5	1.7	1.25	1	Yaglom[43]	Atmospheric surface layer
2.5	2.2		1	Blackadar et al[31]	Atmospheric boundary layer at KSC

TABLE VIII

COMPARISON OF HCl CONCENTRATION AMONG MODELS AND OBSERVATIONS AT MEASUREMENT LOCATION P-10 FOR TITAN III LAUNCH OF AUGUST 20, 1975

	P-10 Measurement	ADPIC[a]	DISF	METS[b]	MDM	TREATS[a]
Maximum instantaneous concentration ppm	1.4×10^{-2}	0.02×10^{-2}	1.7×10^{-2}	---	$54. \times 10^{-2}$	0.68×10^{-2}
Integrated concentration (dosage) ppm-sec	7	≥ 8	39	> 18	241	7

[a]Value obtained after justification of coordinate system for comparison (see text).

[b]Value guessed from available data.

TABLE IX

COMPARISONS OF THE DILUTION RATIOS OF THE UPPER LEVEL CONCENTRATIONS FOR MODEL PREDICTIONS AND AIRBORNE MEASUREMENT FOR 10 DECEMBER 1974

Time	ADPIC	DISF	MDM	TREATS	Measurement
Earlier	0.81	0.94	< 0.11	0.60	---
Later	0.83	0.89	0.51	0.49	0.60 to 0.82

TABLE X

COMPARISON OF HCl CONCENTRATION AMONG MODELS AND OBSERVATIONS AT MONITORING SITES P-2, P-3, P-4 FOR DECEMBER CASE

					MDM				
		Measurement	ADPIC[a]	DISF	b	c	d	METS[e]	TREATS
P-2	Maximum instantaneous concentration	0.35	0.03	0.07	0.12	1.14	0.50	----	0.11
	Integrated concentration	19.5	≥ 6	15	27	240	62	25	58
P-3	Maximum instantaneous concentration	0.022	0.01	0.013	0.14	0.55	0.52	----	0.03
	Integrated concentration	6.2	≥ 6	5	45	183	83	< 0.7	7.5
P-4	Maximum instantaneous concentration	0.50	0.075	0.11	0.28	1.26	0.33	----	0.21
	Integrated concentration	15.2	≥ 45	15	33	145	28	< 40	56

[a]The integrated concentration was based on the first 55 min integration.

[b]Vertically varied σ_{A_o}.

[c]$\sigma_{A_o} = 8°$.

[d]$\sigma_{A_o} = 4°$.

[e]Value was guessed from limited results.

TABLE XI

COMPARISON OF HCl CONCENTRATION USING OBSERVED CLOUD AS INPUT AT MONITORING SITE P-10 FOR TITAN III LAUNCH OF AUGUST 20, 1975

	Measurement	DISF[a]	DISF[b]	MDM	
				Model 3	Model 4
Maximum instantaneous concentration ppm	1.4×10^{-2}	1.5×10^{-2}	0.27×10^{-2}	$63. \times 10^{-2}$	$63. \times 10^{-2}$
Integrated concentration (dosage) ppm-sec	7	33	5.5	117	114

[a]After adjustment.

[b]Before adjustment.

TABLE XII

COMPARISON OF NUMERICAL AND ANALYTICAL SOLUTIONS TO THE COAGULATION RATE EQUATIONS

	time (sec)	N_{total} (ml^{-1})	$d_{N,90}$ (μm)	$d_{N,50}$ (μm)	$d_{N,10}$ (μm)	$d_{\bar{m}}$ (μm)
Analytical Solution	0	1.00×10^6	6.44	9.43	13.9	10.0
	1.25×10^5	2.60×10^4	16.4	29.9	44.6	33.8
	1.7×10^6	1.96×10^3	37.9	70.8	105.5	80.0
Numerical Solutions						
$\alpha = 2$, $\tau = 0.01$	1.25×10^5	2.59×10^4	15.5	29.0	44.5	33.8
$\alpha = 2$, $\tau = 0.1$	1.25×10^5	2.56×10^4	16.0	29.6	44.4	33.6
	1.7×10^6	2.00×10^3	35.5	67.0	103.0	79.5
$\alpha = 10$, $\tau = 0.1$	1.25×10^5	2.56×10^4	13.0	25.1	39.0	33.6
	1.7×10^6	2.04×10^3	26.5	45.8	89.0	78.7

TABLE XIII

VALUES FOR THE COAGULATION KERNEL, K^c_{ij}

(10^{-10} ml particle^{-1} sec^{-1})

Particle[a] diam (μm)	0.010	0.026	0.089	0.30	1.0	3.4
0.10	19.5	43.4	219.2	940.0	3351.0	11390.0
0.026	43.4	24.3	49.3	155.5	515.0	1725.0
0.089	219.2	49.3	16.1	22.6	60.0	189.9
0.30	940.0	155.5	22.6	9.06	12.7	39.2
1.0	3351.0	515.0	60.0	12.7	6.91	35.4
3.4	11390.0	1725.0	189.9	39.2	35.4	6.28

[a]Particles have unit density.

TABLE XIV

INITIAL ALUMINA AND DEBRIS PARTICLE DISTRIBUTIONS

Case	Total Particles (ml^{-1})	Distribution, particles ml^{-1} μm^{-1}	$d_{N,50}$ (μm)	d_m (μm)
Alumina				
Dawborn	5.6×10^7	$2.7 \times 10^9 [d^2 \exp(-10.5\, d^{1/2}) + 1 \times 10^4\, d^3 \exp(-41.25d)]$, $d \geq 0.02$ μm	0.088	0.16
Kreaulte	4.8×10^5	$6.4 \times 10^5 [d^3 \exp(-3.0\, d) + 1.04 \times 10^8\, d^4 \exp(-25.39 d^{1/2})]$, $d \geq 0.02$ μm	0.16	0.77
Varsi	8.8×10^7	$1.10 \times 10^7 \times \begin{cases} d^{-1.25} & 0.02\ \mu m \leq d \leq 0.06\ \mu m \\ 3.6 \times 10^{-2}\, d^{-3.2} & 0.06\ \mu m \leq d \leq 0.10\ \mu m \\ 1.58 \times 10^{-3}\, d^{-4.8} & 0.10\ \mu m \leq d \leq 10\ \mu m \end{cases}$	0.066	0.12
Debris				
With Dawborn (1000 × alumina)	8.6×10^7	$1.05 \times 10^{6}\, d^{-3.27}$ $\quad 0.1\ \mu m \leq d \leq 1000\ \mu m$	0.14	1.36
With Kreautle (100 × alumina)	3.6×10^7	$3.0 \times 10^5\, d^{-3.47}$ $\quad 0.1\ \mu m \leq d \leq 1000\ \mu m$	0.13	0.84
With Kreautle (1000 × alumina)	4.9×10^7	$6.8 \times 10^5\, d^{-3.20}$ $\quad 0.1\ \mu m \leq d \leq 1000\ \mu m$	0.14	1.64
Varsi	1.6×10^8	$1.6 \times 10^6\, d^{-3.35}$ $\quad 0.1\ \mu m \leq d \leq 1000\ \mu m$	0.13	1.11

TABLE XV

ALUMINA LOADINGS BELOW THE CENTER OF THE GROUND CLOUD

Distribution	Loading, g m^{-2}
Dawborn, debris 1000 × alumina	3.0
Kreautle, debris 100 × alumina	0.9
Kreautle, debris 1000 × alumina	4.5
Varsi, debris 1000 × alumina	1.4

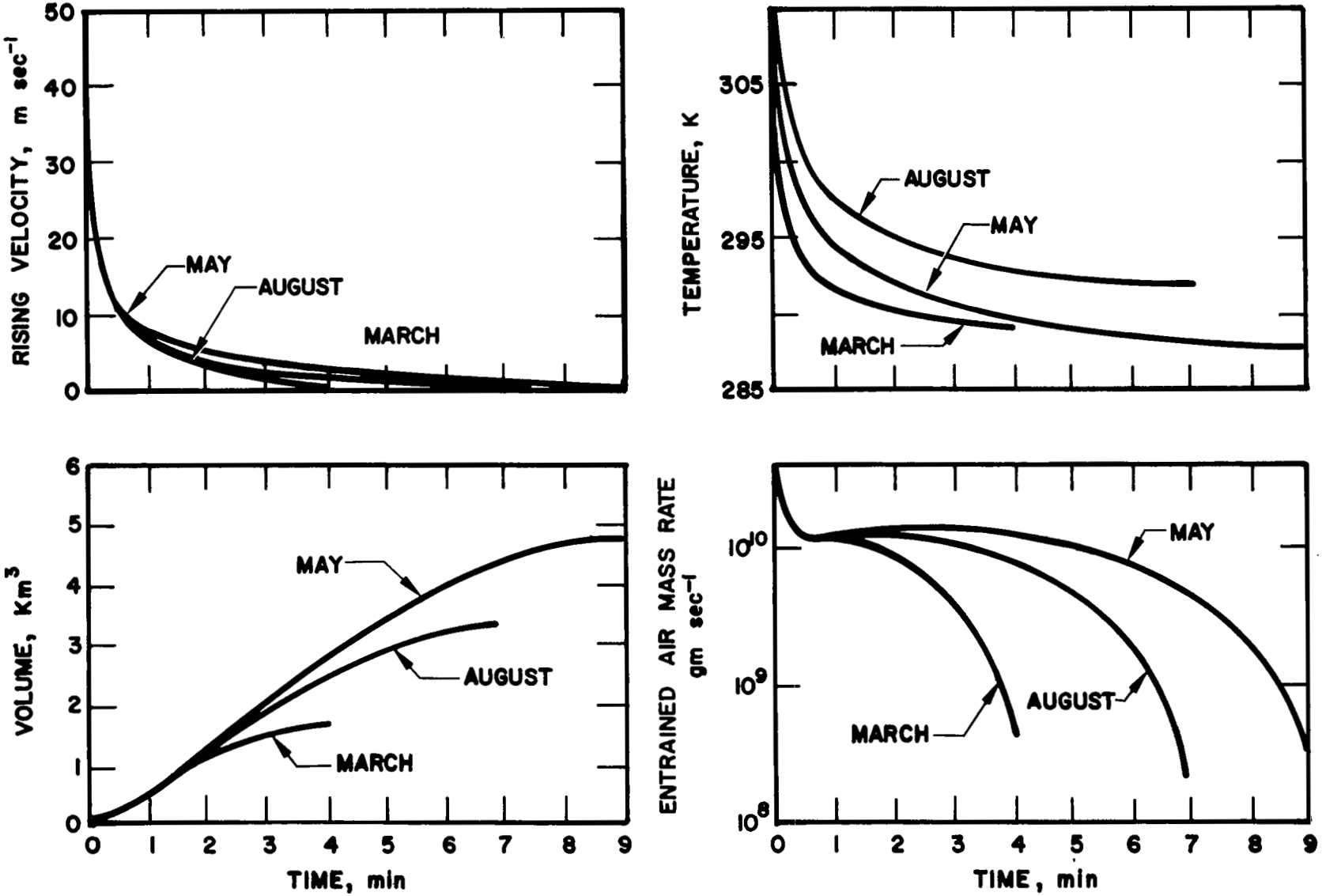

FIGURE 1 PHYSICAL PROPERTIES DURING CLOUD RISE

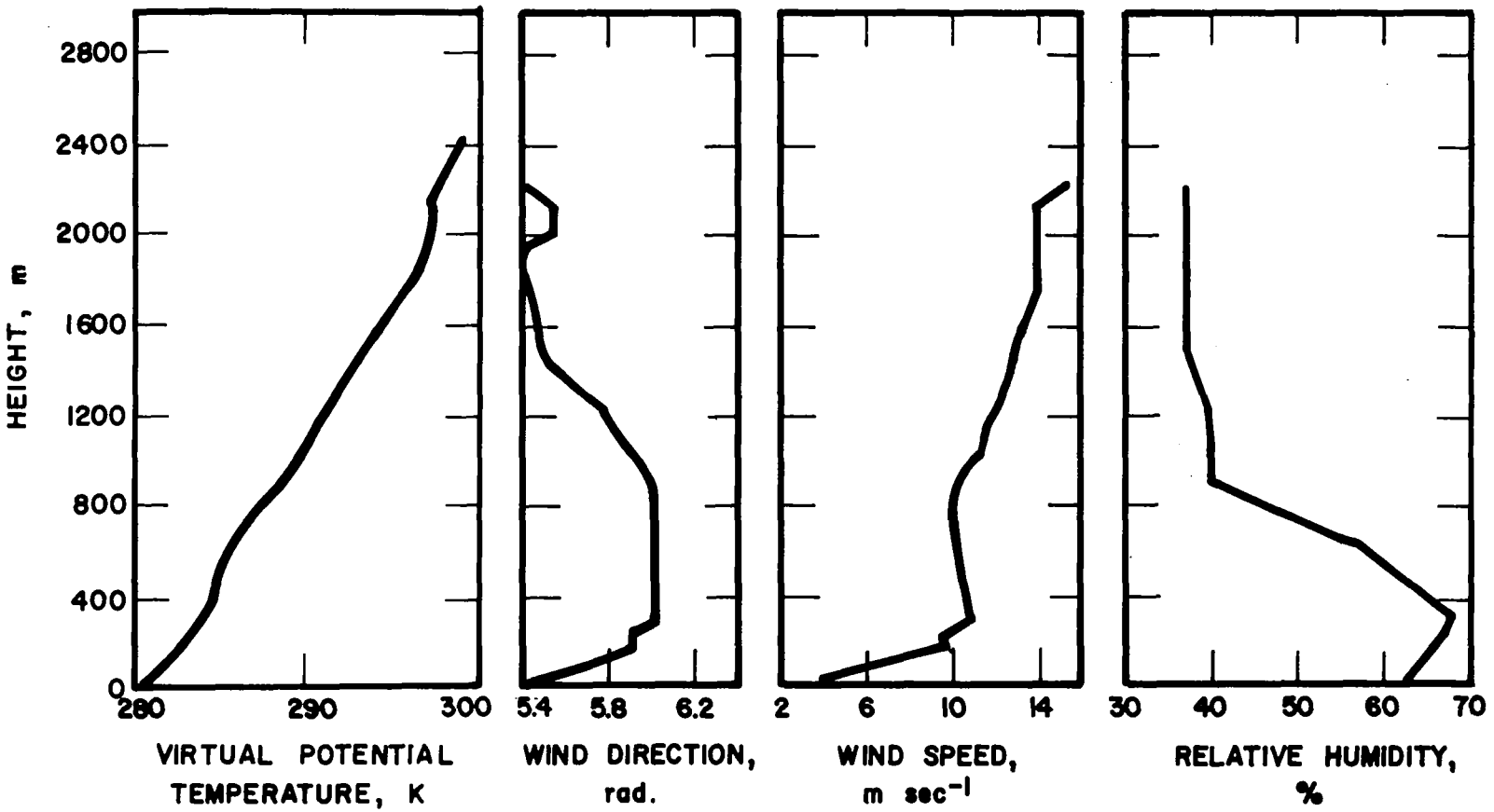

FIGURE 2 VERTICAL PROFILES OF TEMPERATURE, WIND SPEED, WIND DIRECTION, AND RELATIVE HUMIDITY AT KENNEDY SPACE CENTER FROM RAWINSONDE SONDING MEASUREMENT FOR 10 DECEMBER 1974, 02:31 EDT

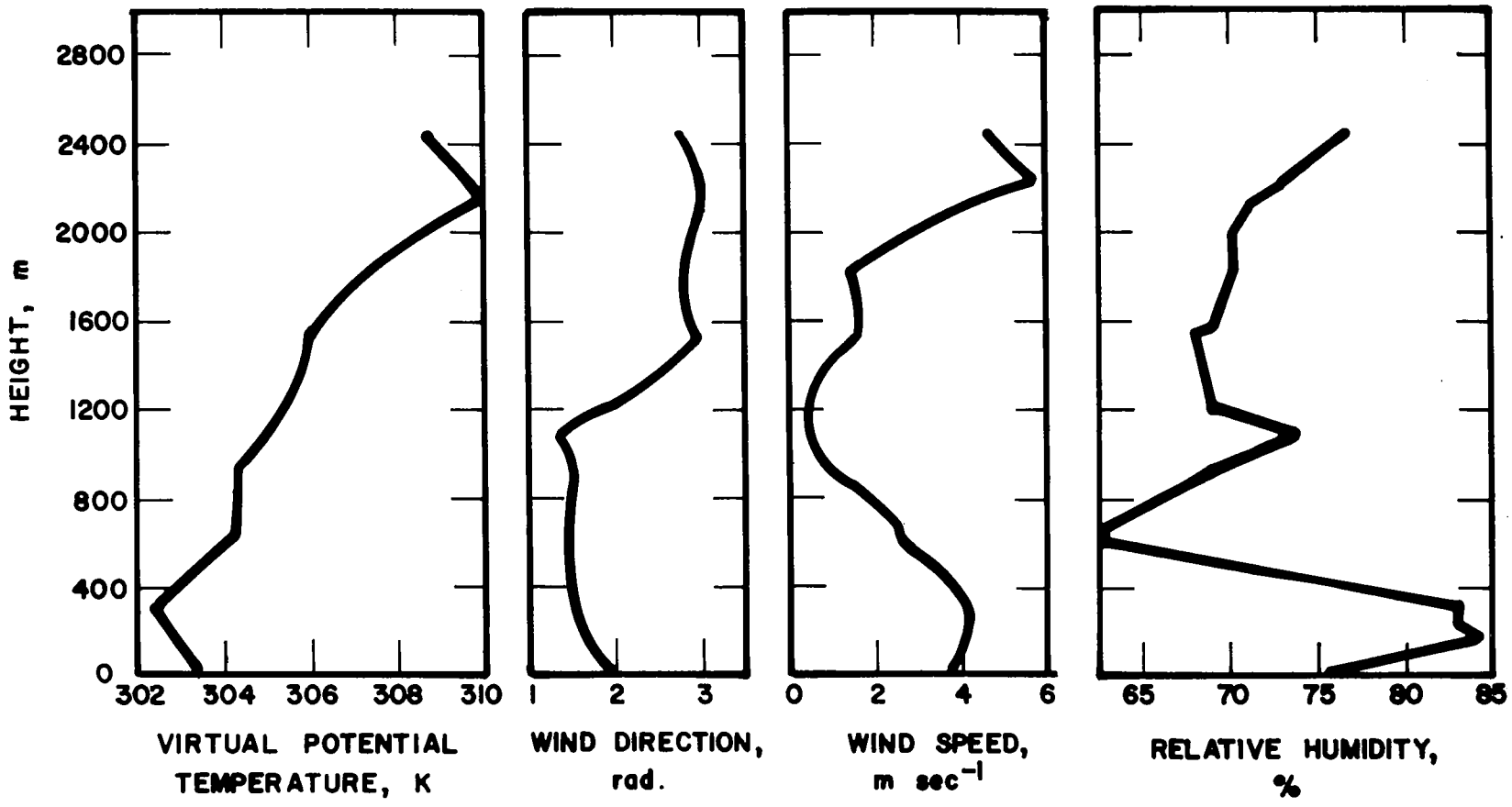

FIGURE 3 VERTICAL PROFILES OF TEMPERATURE, WIND SPEED, WIND DIRECTION, AND RELATIVE HUMIDITY AT KENNEDY SPACE CENTER FROM RAWINSONDE SONDING MEASUREMENT FOR 20 AUGUST 1975, 16:46 EDT

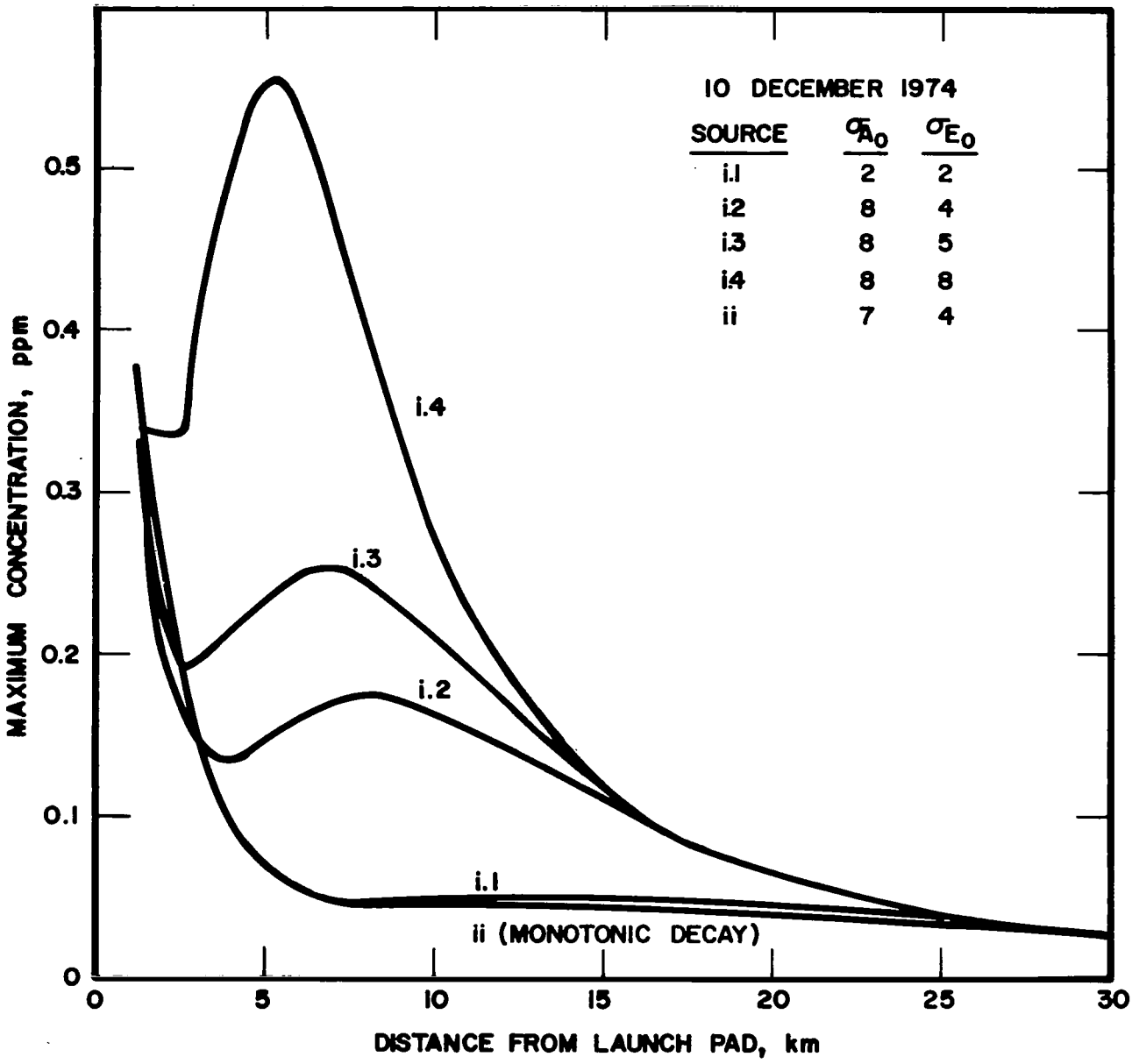

FIGURE 4 MAXIMUM GROUND LEVEL CONCENTRATION PREDICTED BY MDM MODEL 4

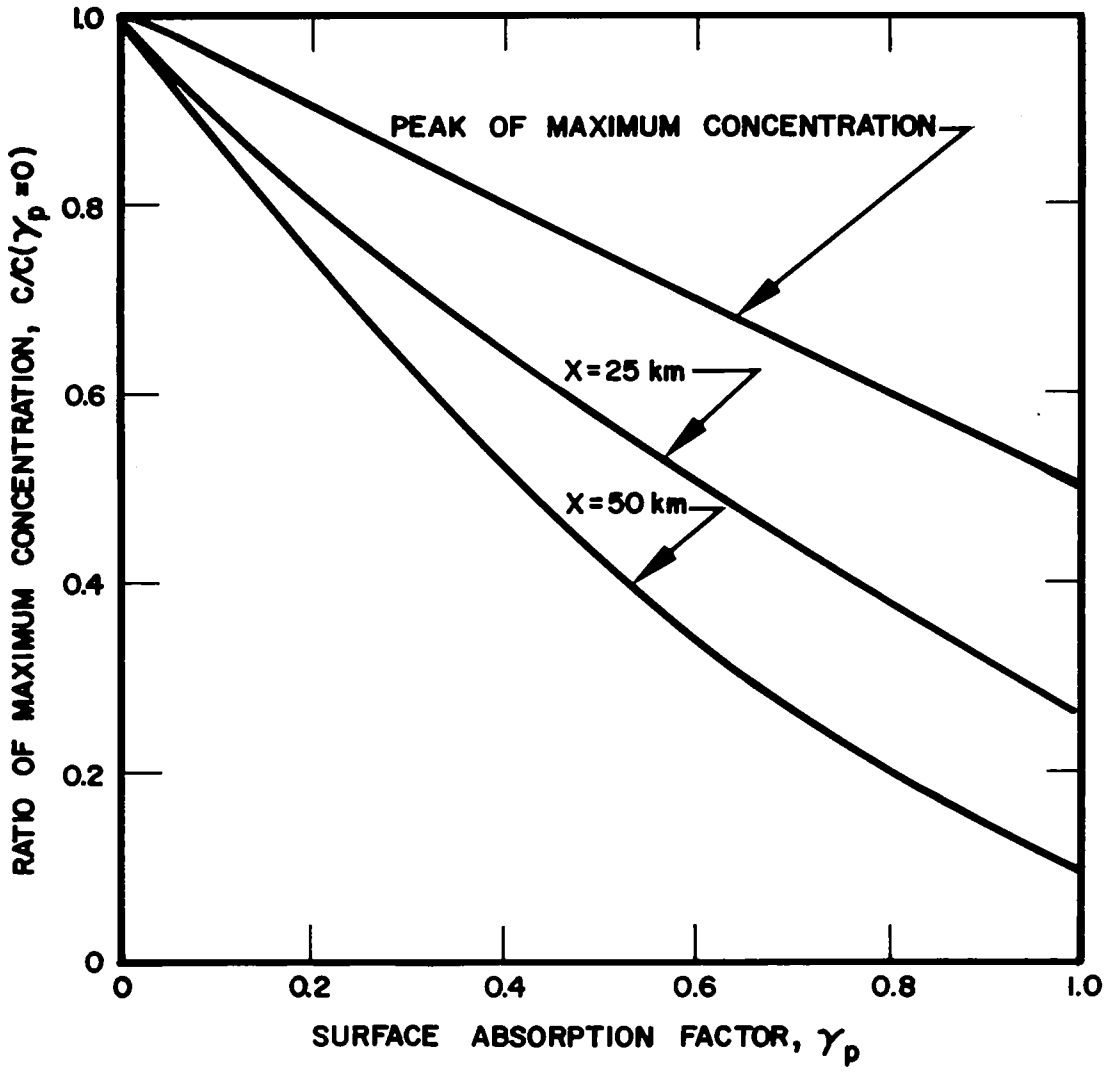

FIGURE 5 RATIO OF GROUND LEVEL MEAN CONCENTRATION PREDICTED FROM MDM MODEL 4 BY VARYING THE SURFACE ABSORPTION FACTOR γ_p FOR THE 10 DECEMBER 1974 AND 20 AUGUST 1975 CASES

γ_p = 0 for total reflection; γ_p = 1 for total absorption

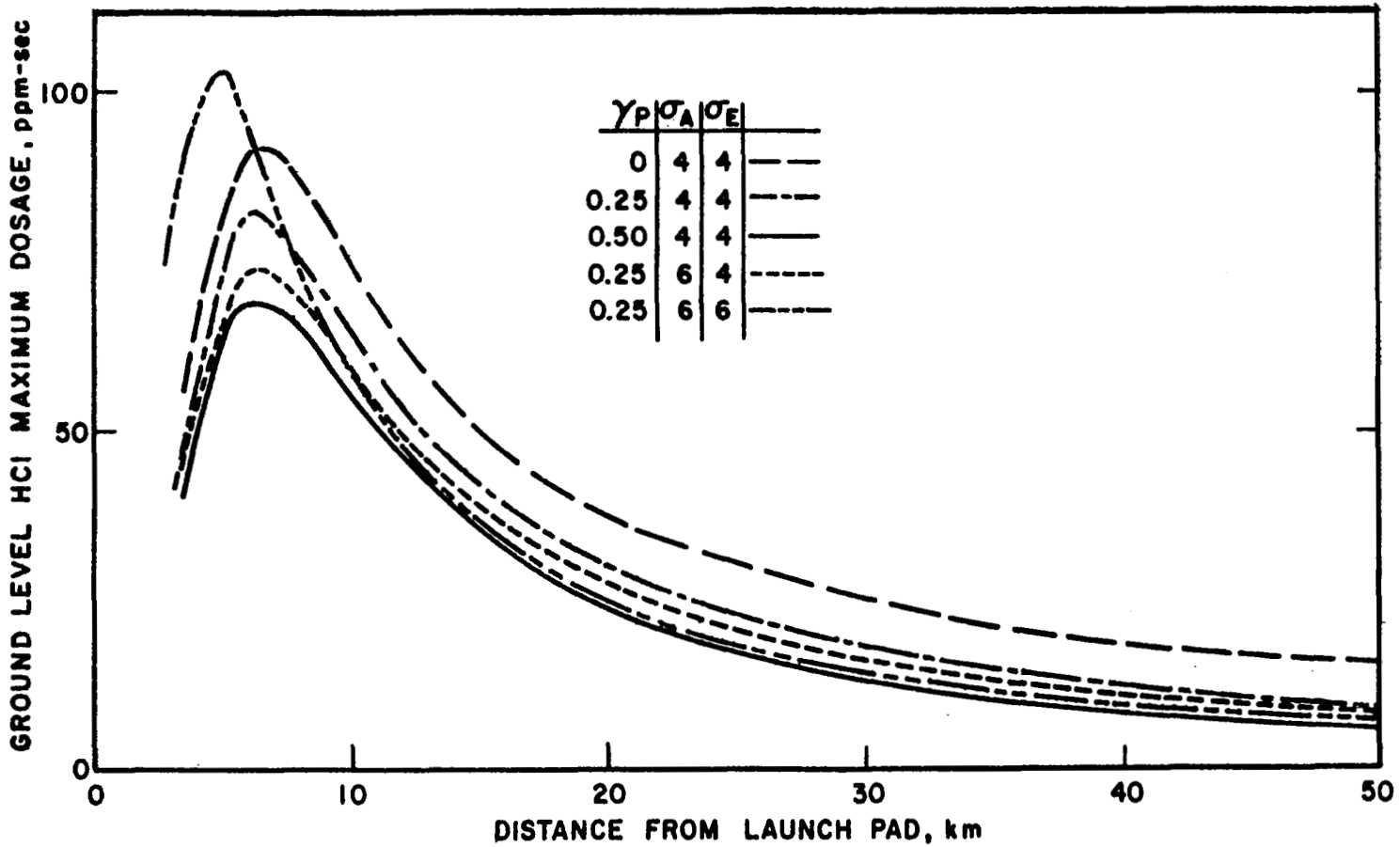

FIGURE 6 VARIATIONS OF PREDICTED GROUND LEVEL HCl MAXIMUM DOSAGE DUE TO VARIATIONS OF SURFACE ABSORPTION FACTOR γ_p AND DIFFUSION PARAMETERS σ_A AND σ_E FOR THE 10 DECEMBER 1974 LAUNCH

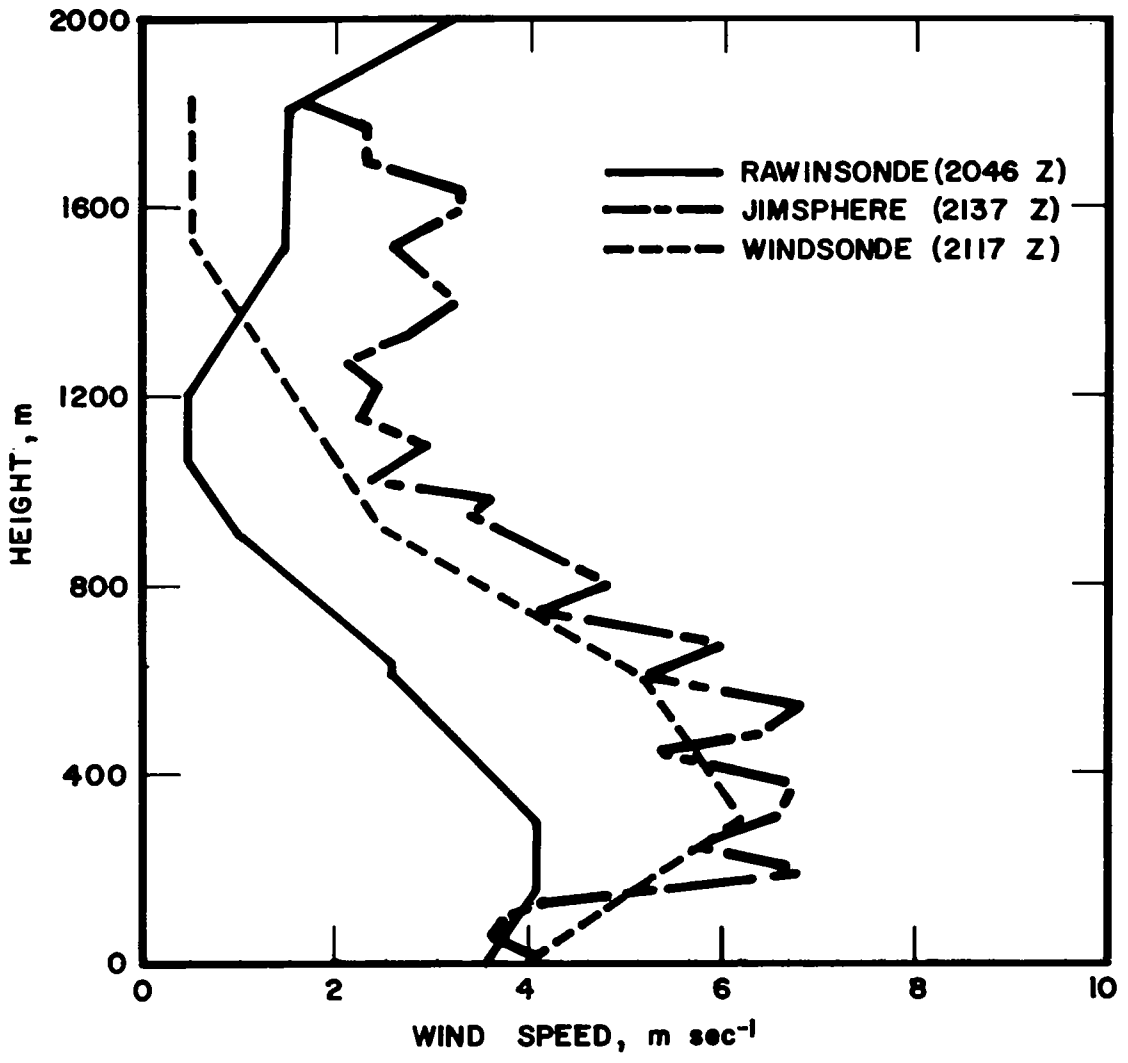

FIGURE 7 WIND SPEED MEASUREMENTS FROM RAWINSONDE, JIMSPHERE, AND WINDSONDE FOR THE 20 AUGUST 1975 CASE AT NEAR LAUNCH TIME

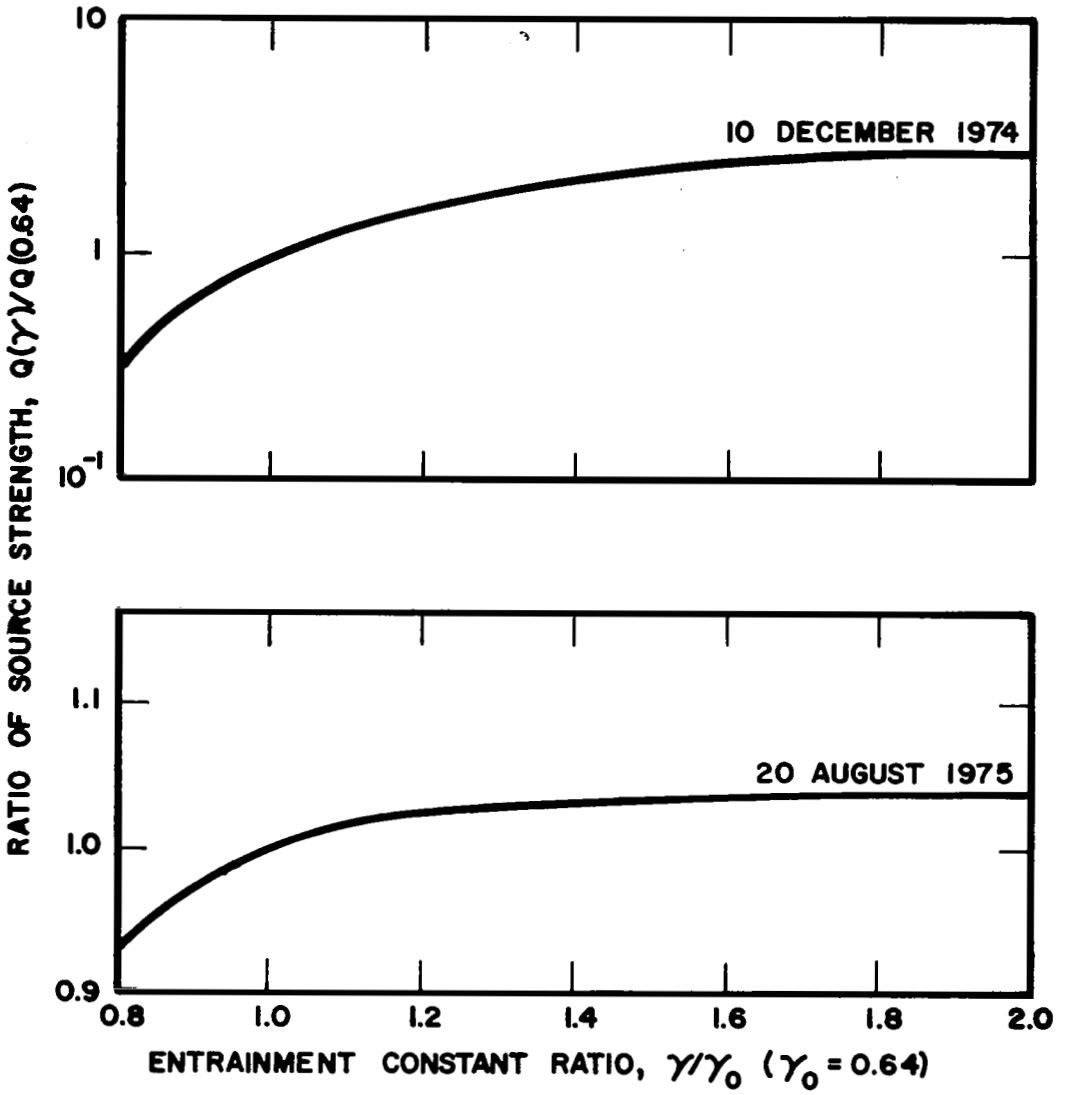

FIGURE 8 VARIATIONS OF PREDICTED SOURCE STRENGTH IN CLOUD USING DIFFERENT ENTRAINMENT CONSTANTS γ FOR THE 10 DECEMBER 1974 AND 20 AUGUST 1975 CASES

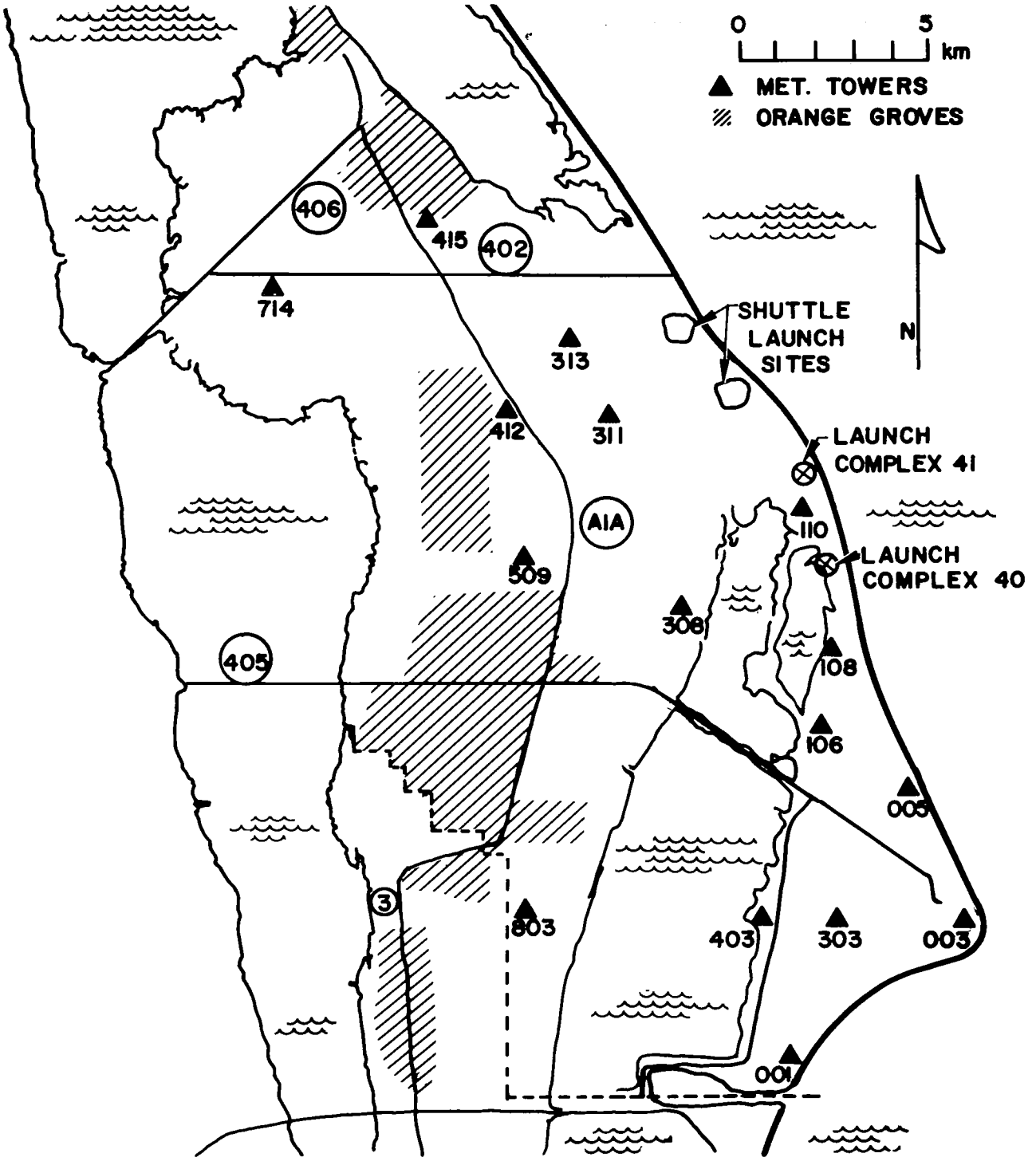

FIGURE 9 MAP OF KSC AREA

Tower heights are 16.5 m except tower
110 (62 m) and tower 313 (150 m)

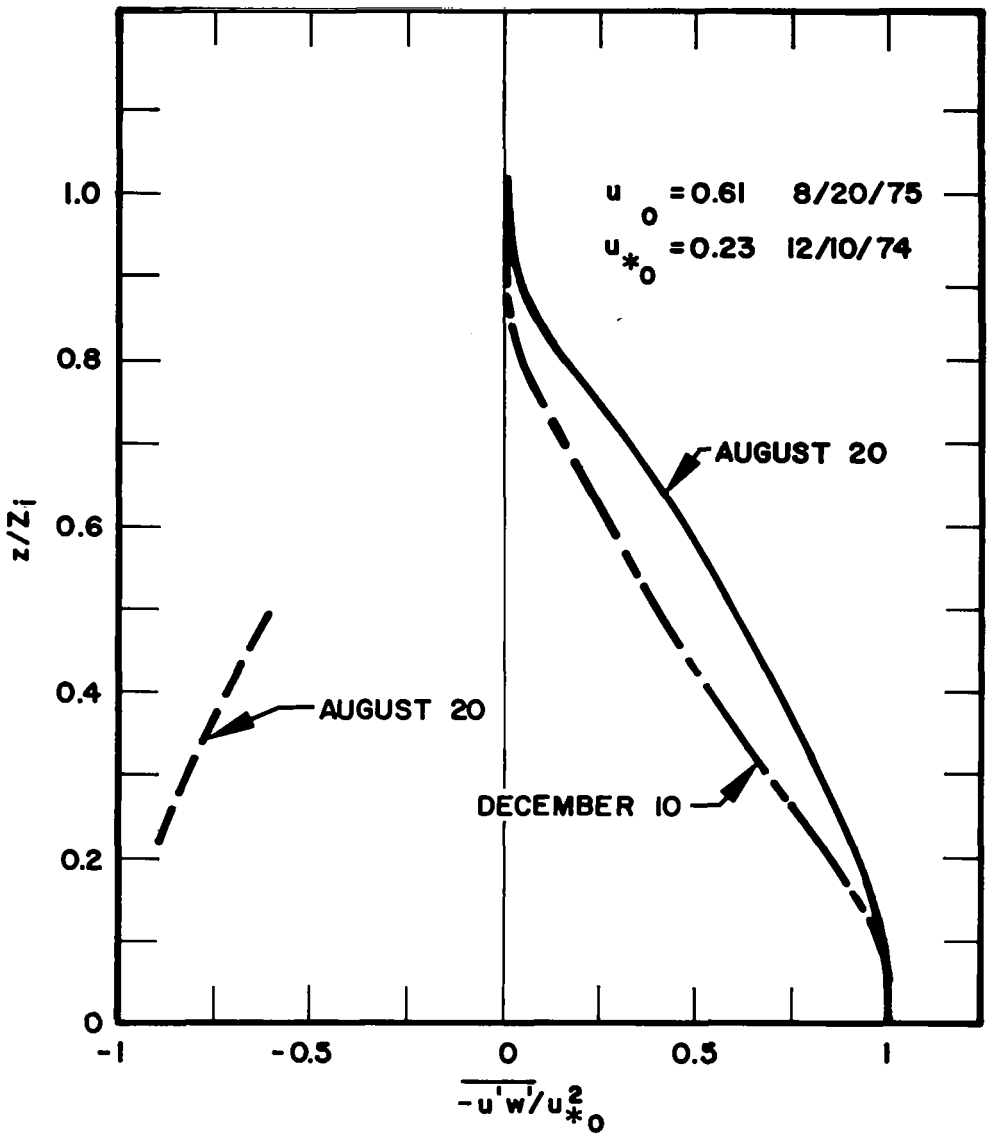

FIGURE 10 MODELED REYNOLDS STRESS IN THE PBL FOR THE 10 DECEMBER 1974 AND 20 AUGUST 1975 CASES

Dashed line is the actual input between 0.2 and 0.5 z/Z_i for the DISF calculation for the August case

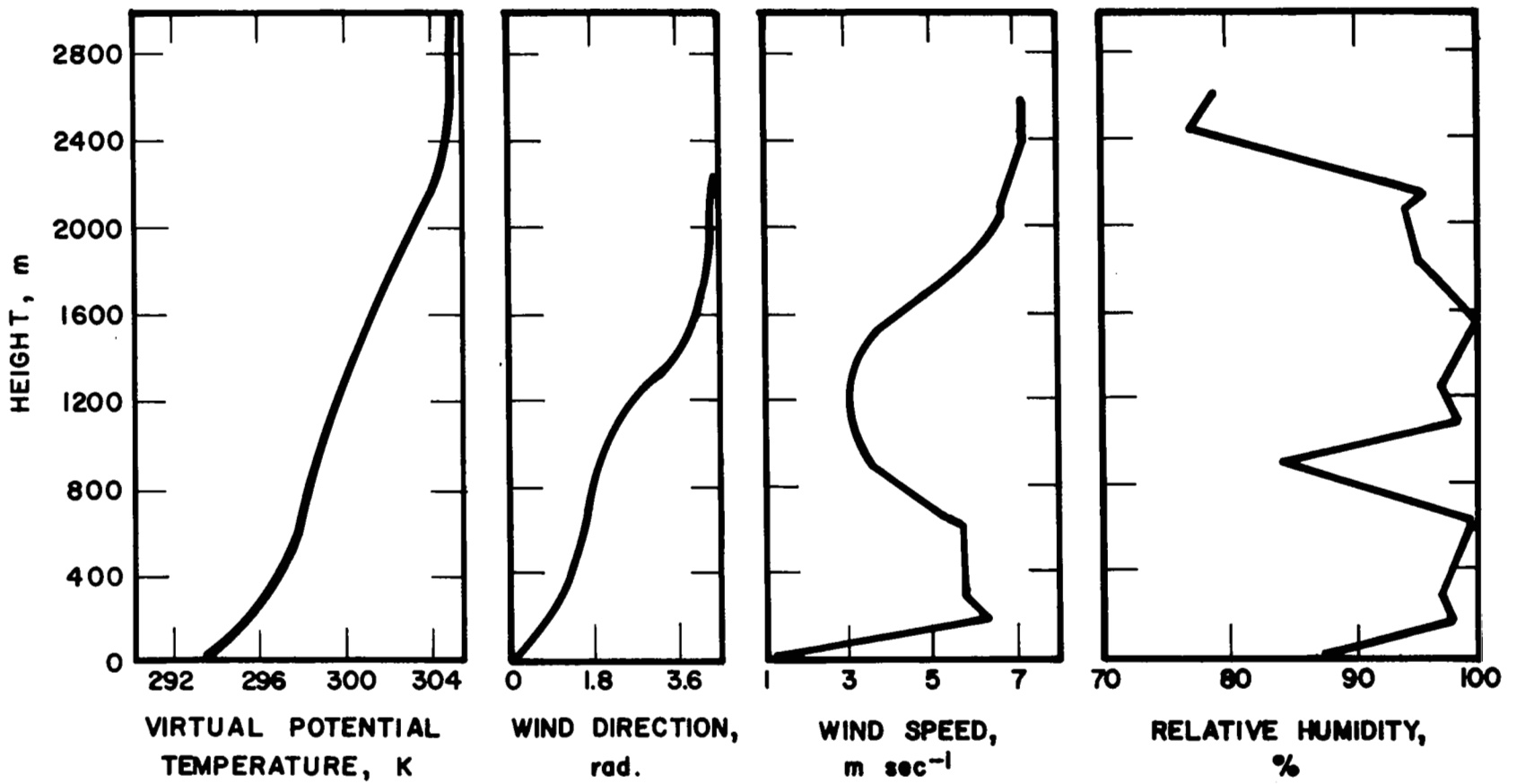

FIGURE 11 VERTICAL PROFILES OF TEMPERATURE, WIND SPEED, WIND DIRECTION, AND RELATIVE HUMIDITY AT KENNEDY SPACE CENTER FROM RAWINSONDE SONDING MEASUREMENT FOR 14 MARCH 1976, 20:27 EDT

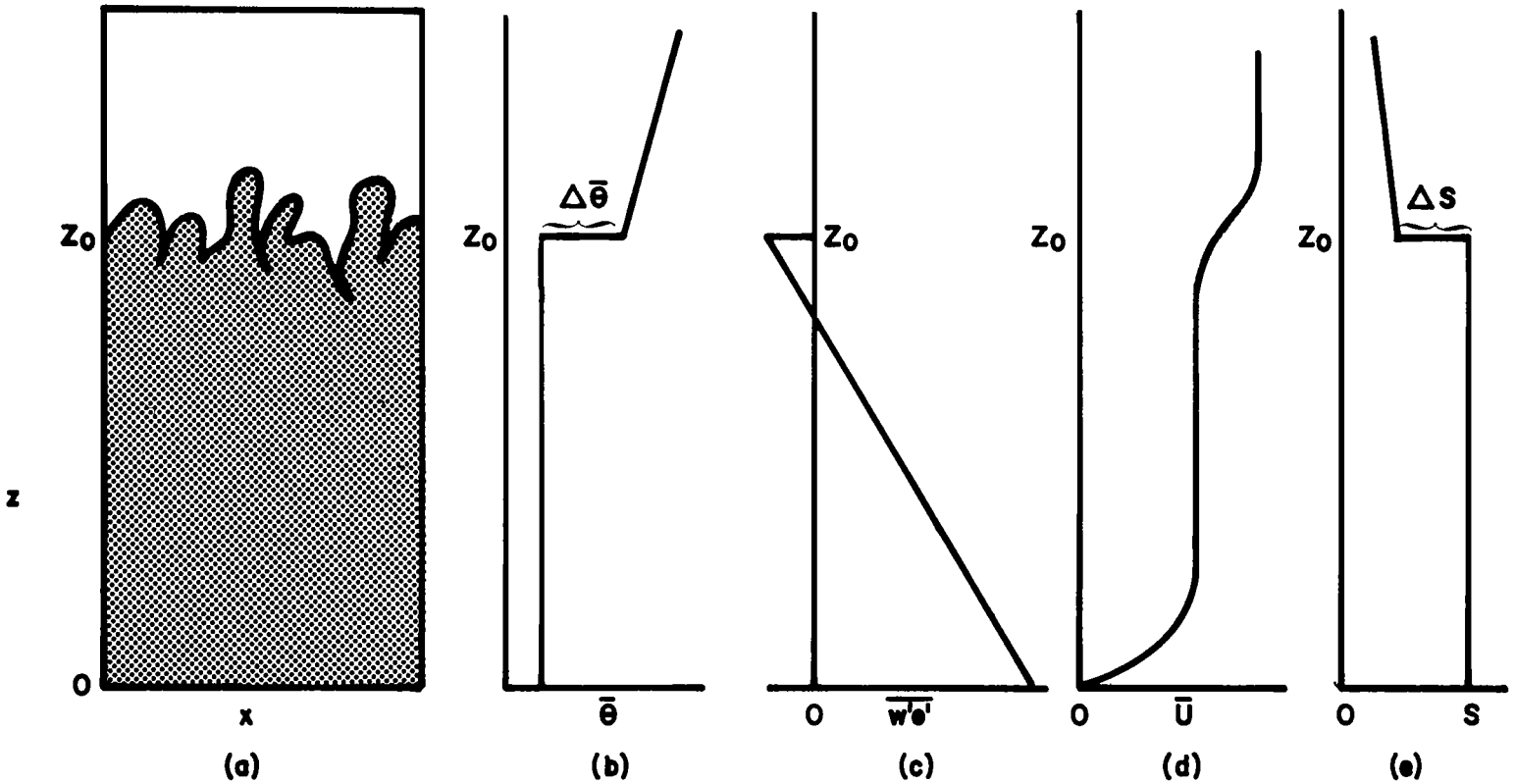

FIGURE 12 IDEALIZED CHARACTERISTICS OF A WELL-MIXED PBL

(a) Vertical cross section; (b) virtual potential temperature profile; (c) heat flux profile; (d) mean wind profile; (e) profile of a scalar such as humidity. (Adapted from Stull[65])

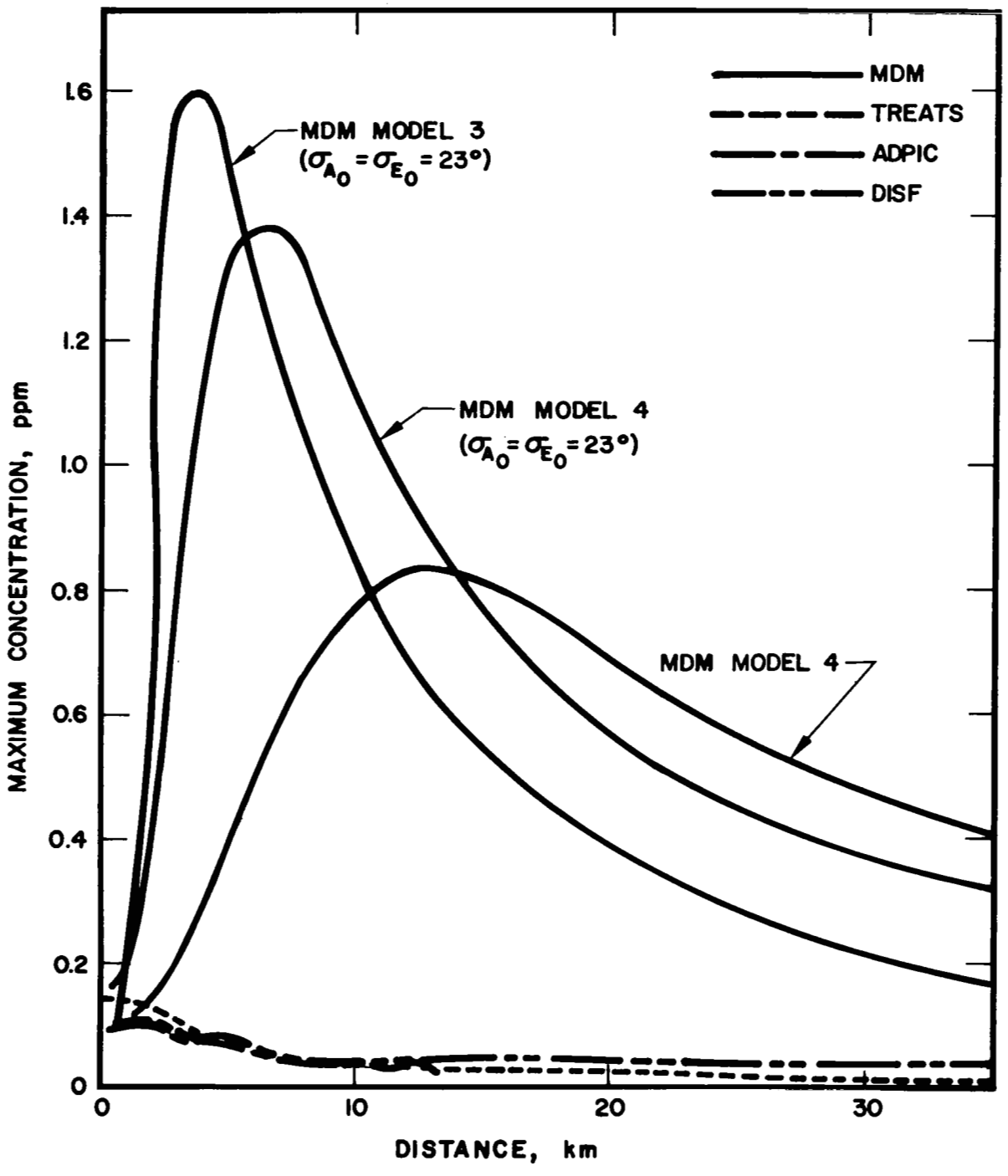

FIGURE 13 COMPARISONS OF MAXIMUM GROUND LEVEL CONCENTRATION PREDICTIONS FOR THE 20 AUGUST 1975 CASE

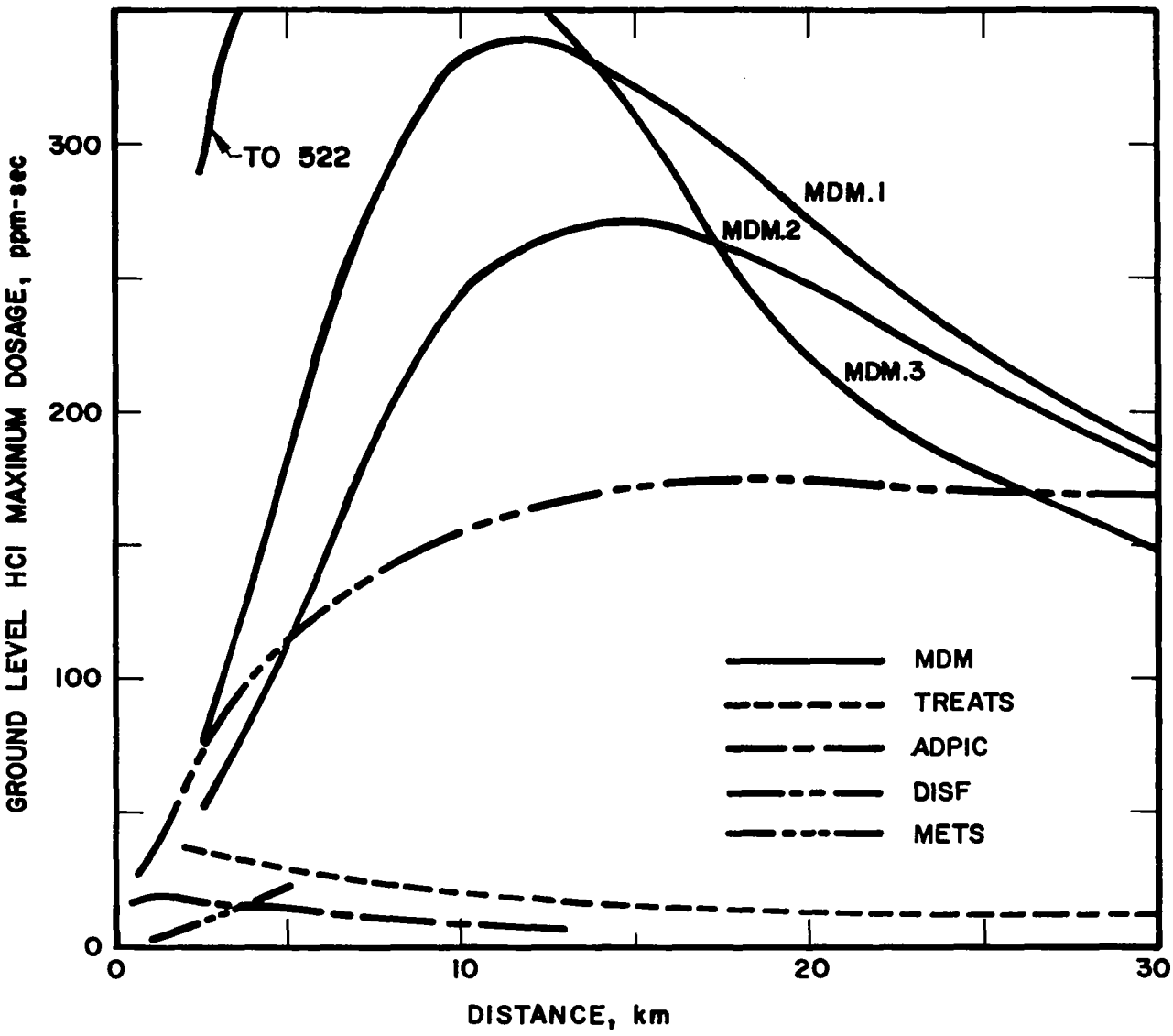

FIGURE 14 COMPARISONS OF GROUND LEVEL HCl MAXIMUM DOSAGE PREDICTIONS FOR THE 20 AUGUST 1975 CASE

MDM.1 refers to results using measured σ_{A_o};
MDM.2 to σ_{A_o} from theoretical interpolation;
MDM.3 to σ_{A_o} given in Ref. 23

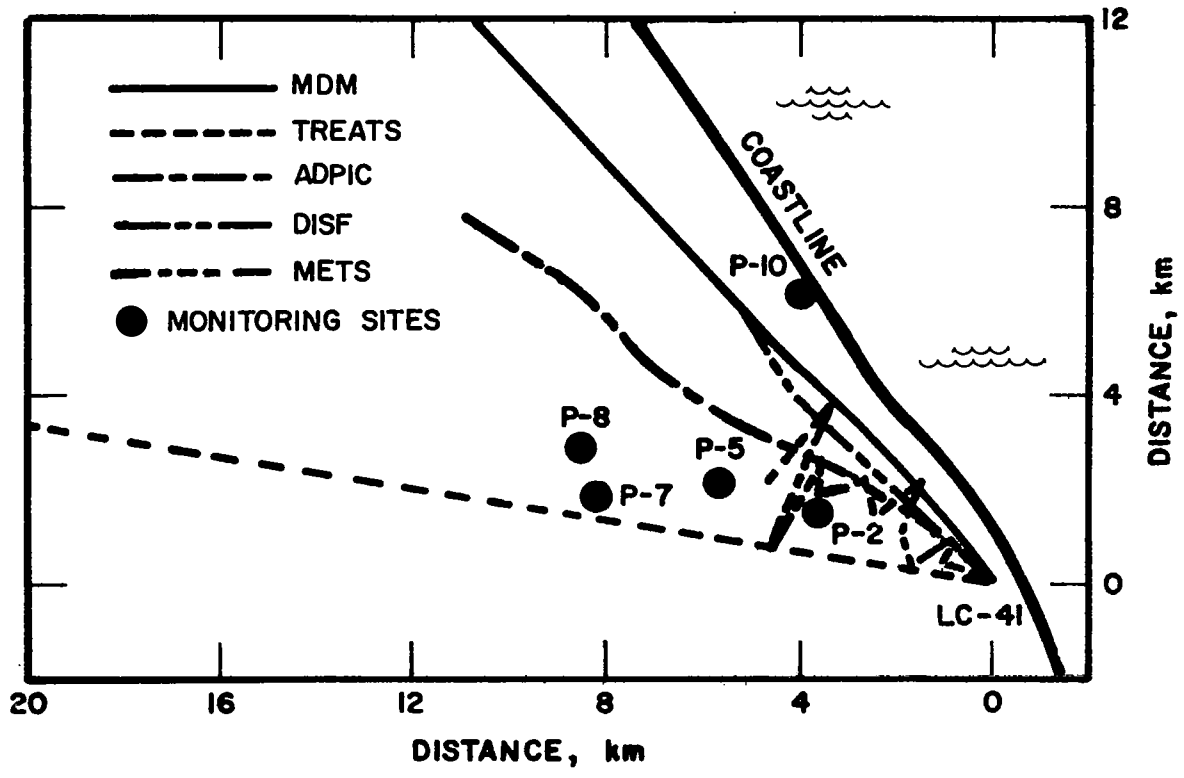

FIGURE 15 PREDICTED PATHS OF MAXIMUM GROUND CONCENTRATION FOR THE 20 AUGUST 1975 CASE

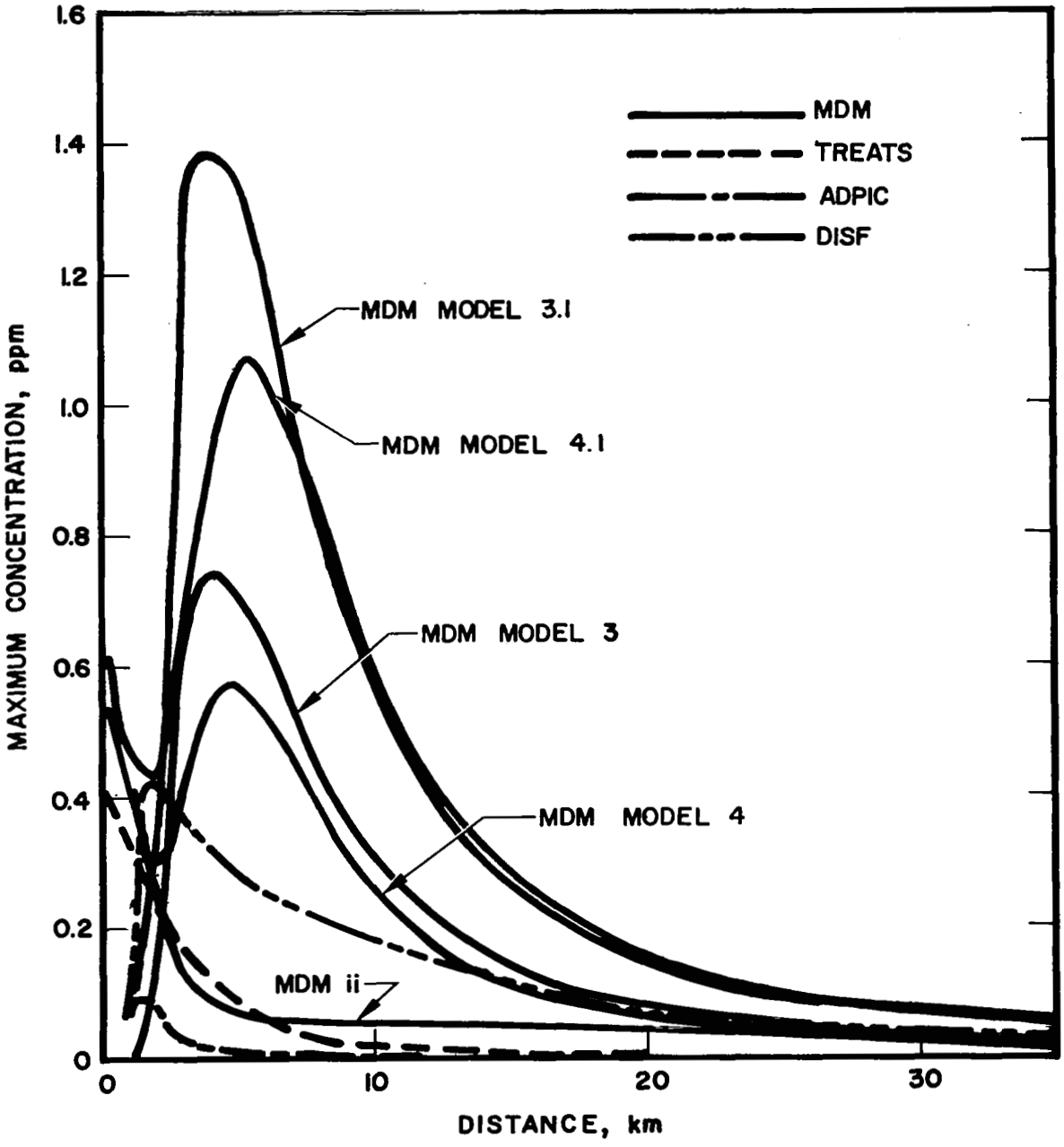

FIGURE 16 COMPARISONS OF MAXIMUM GROUND LEVEL CONCENTRATION PREDICTIONS FOR THE 10 DECEMBER 1974 CASE

MDM Model 3.1 and MDM Model 4.1 calculated using input from SAI preprocessor version. MDM ii calculated using monotonically decaying σ_A and σ_E.

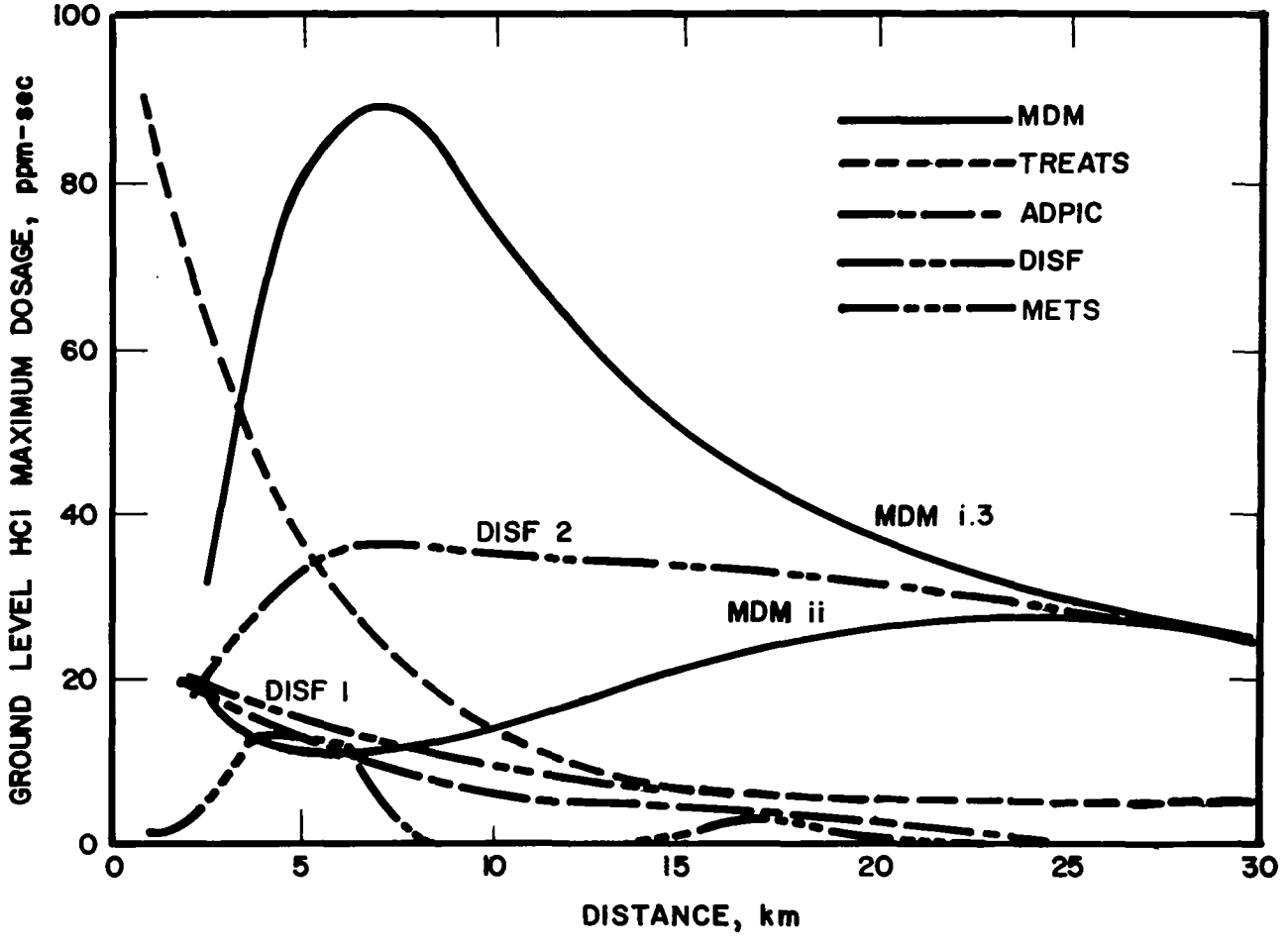

FIGURE 17 COMPARISONS OF GROUND LEVEL HCl MAXIMUM DOSAGE PREDICTIONS FOR THE 10 DECEMBER 1974 CASE

MDM i.3 calculated using $\sigma_{A_o} = 8$, $\sigma_{E_o} = 5$. MDM ii calculated using monotonically decaying σ_A and σ_E. DISF 1 and DISF 2 calculated including and ignoring variations in wind direction, respectively.

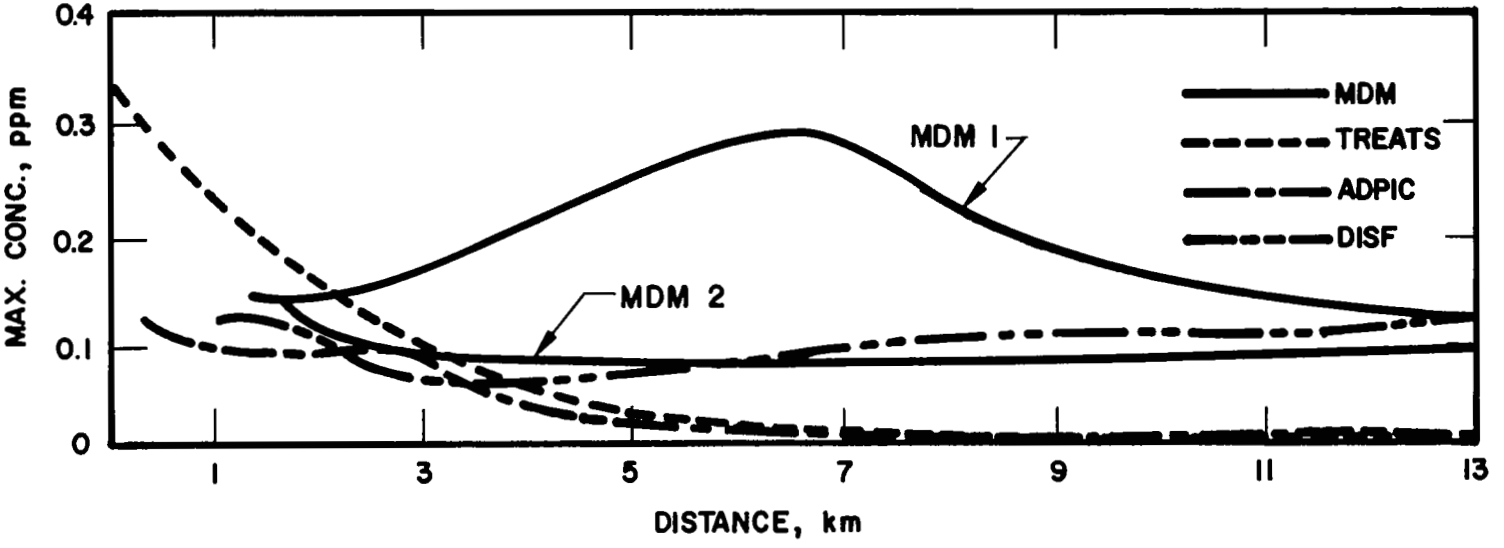

FIGURE 18 COMPARISONS OF MAXIMUM GROUND LEVEL CONCENTRATION PREDICTIONS FOR THE 14 MARCH 1976 CASE

MDM 1 calculated using interpolated σ_{A_o}.

MDM 2 calculated using measured σ_{A_o}.

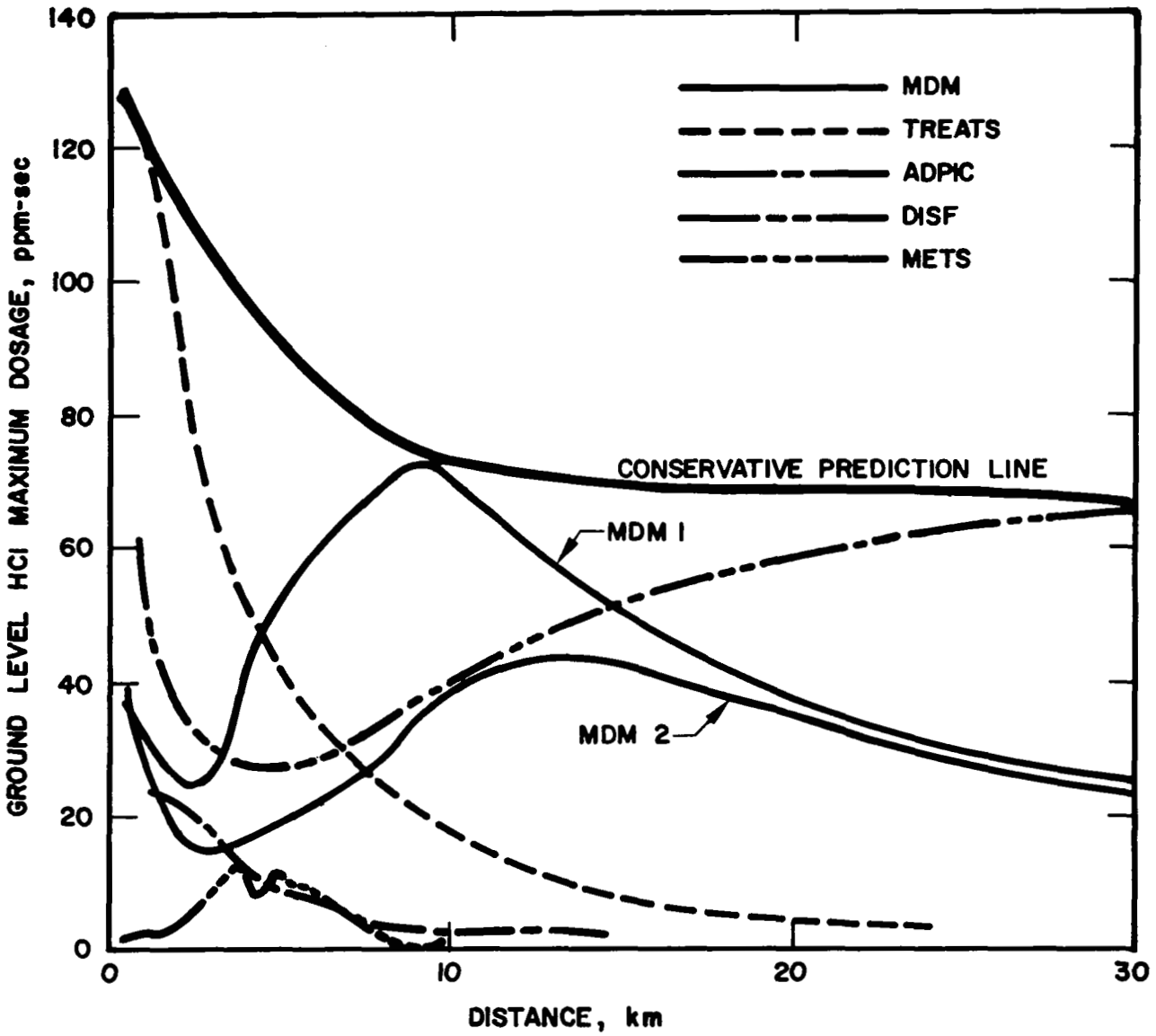

FIGURE 19 . COMPARISONS OF GROUND LEVEL HCl MAXIMUM DOSAGE PREDICTIONS FOR THE 14 MARCH 1976 CASE

MDM 1 calculated using interpolated σ_{A_o}.

MDM 2 calculated using measured σ_{A_o}.

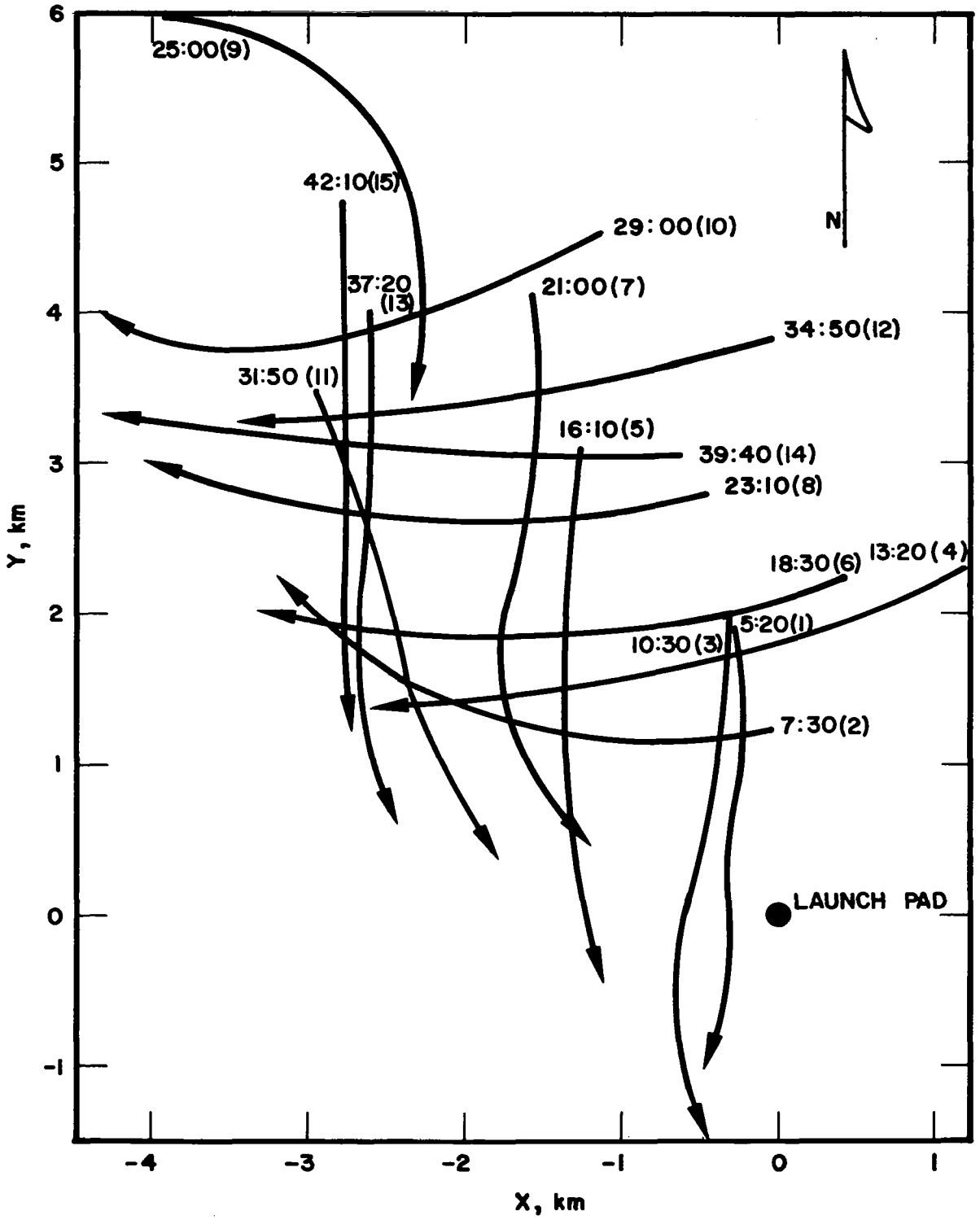

FIGURE 20 PROJECTION OF FLIGHT PATHS ON 20 AUGUST 1975

Each line represents one minute. Numbers in parentheses represent aircraft pass numbers.

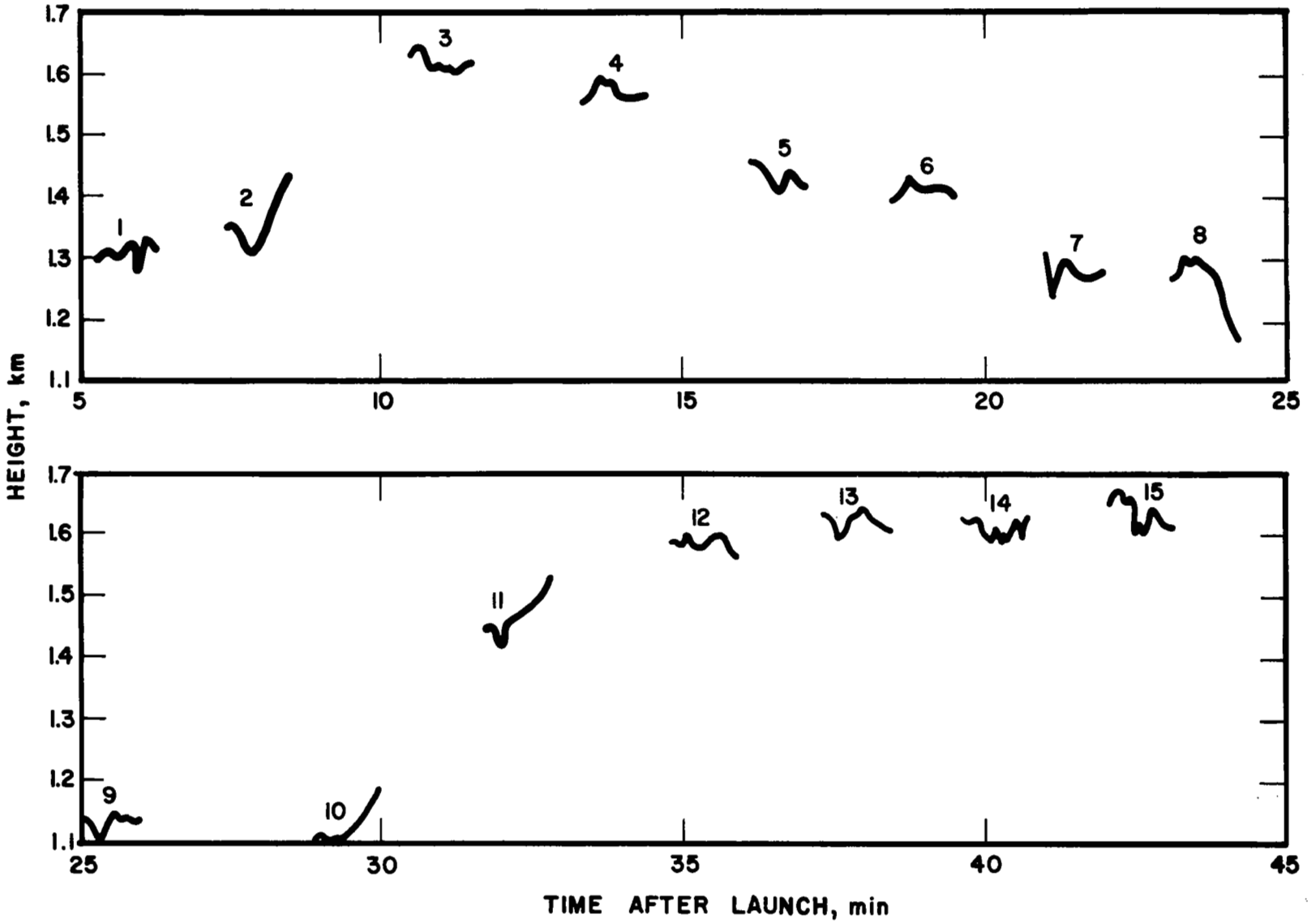

FIGURE 21 AIRCRAFT ALTITUDE ON 20 AUGUST 1975 FOR CLOUD PASSES 1 THROUGH 15

Each pass of one minute duration. Numbers represent aircraft pass numbers.

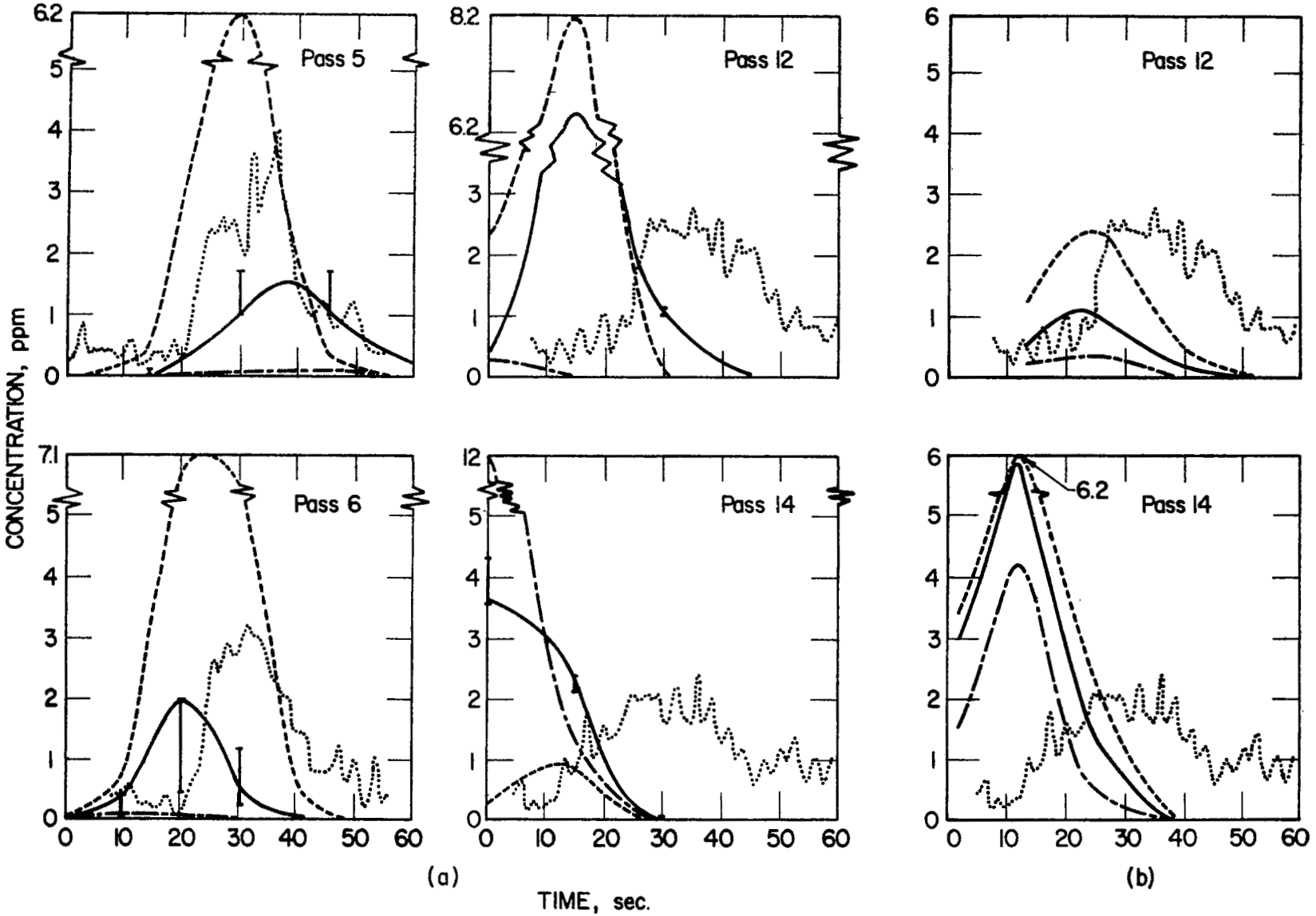

FIGURE 22 COMPARISONS OF AIRBORNE SAMPLING DATA WITH (a) THE TREATS RESULTS AND (b) THE ADPIC RESULTS FOR THE 20 AUGUST 1975 CASE

Key: ——— Model ----- Upwind relocation
····· Measured data —·— Downwind relocation

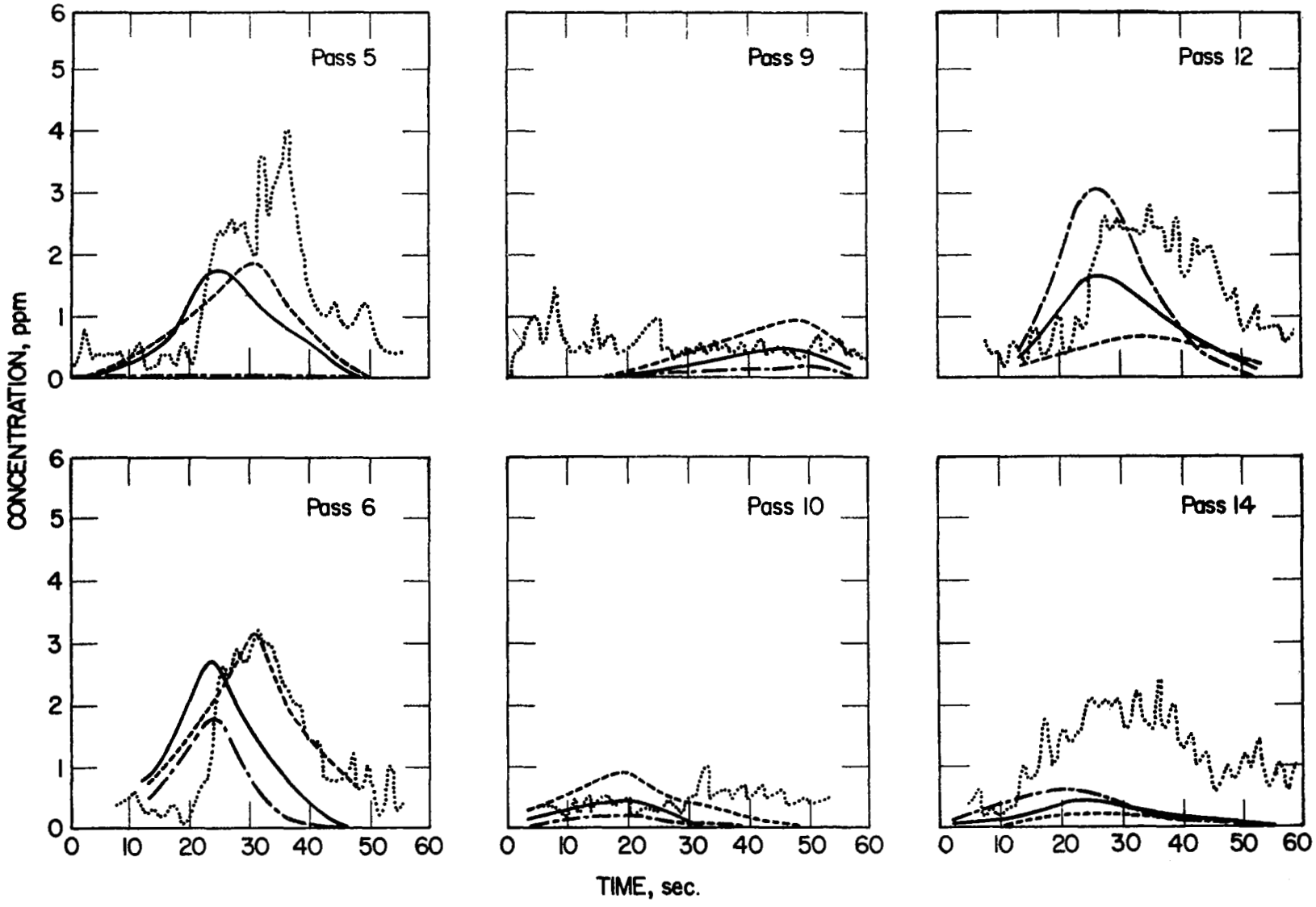

FIGURE 23 COMPARISONS OF AIRBORNE SAMPLING DATA WITH RESULTS PREDICTED FROM DISF FOR THE 20 AUGUST 1975 CASE

Key: ——— Model
····· Measured data
----- Upwind relocation
—·—· Downwind relocation

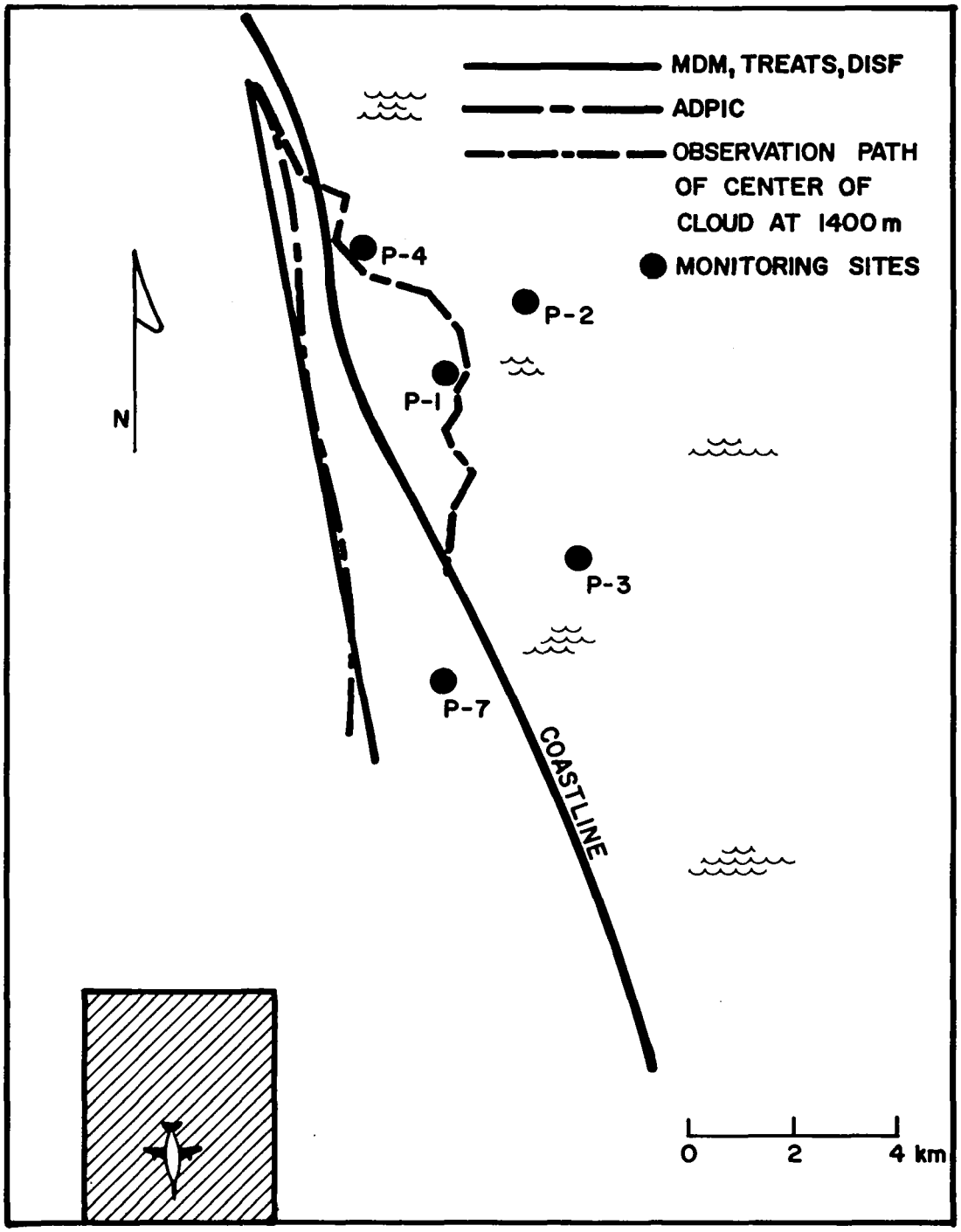

FIGURE 24 PREDICTED PATHS OF MAXIMUM CONCENTRATION AT 600 m ALTITUDE IN THE 10 DECEMBER 1974 CASE

Shaded area represents region where airborne samples were taken.

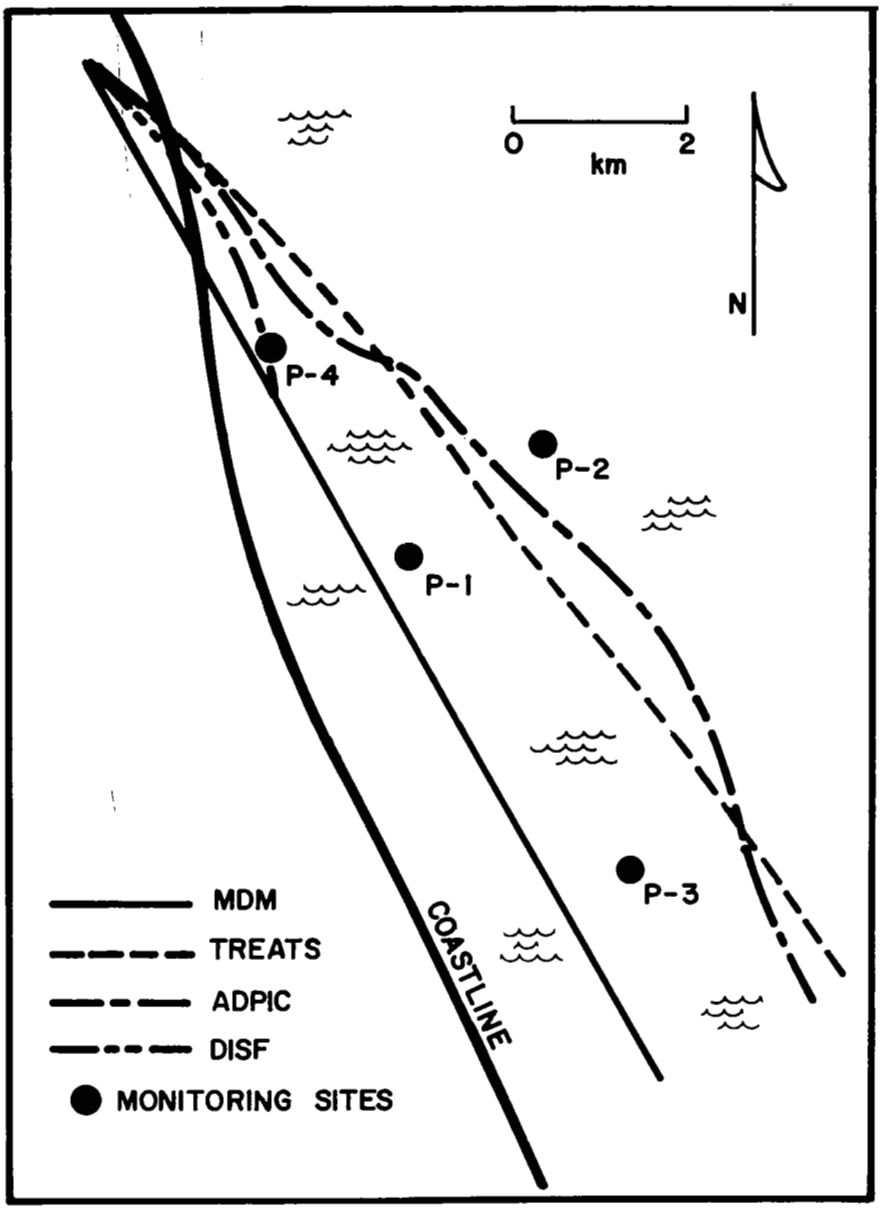

FIGURE 25 PREDICTED PATHS OF MAXIMUM GROUND LEVEL CONCENTRATION FOR THE 10 DECEMBER 1974 CASE

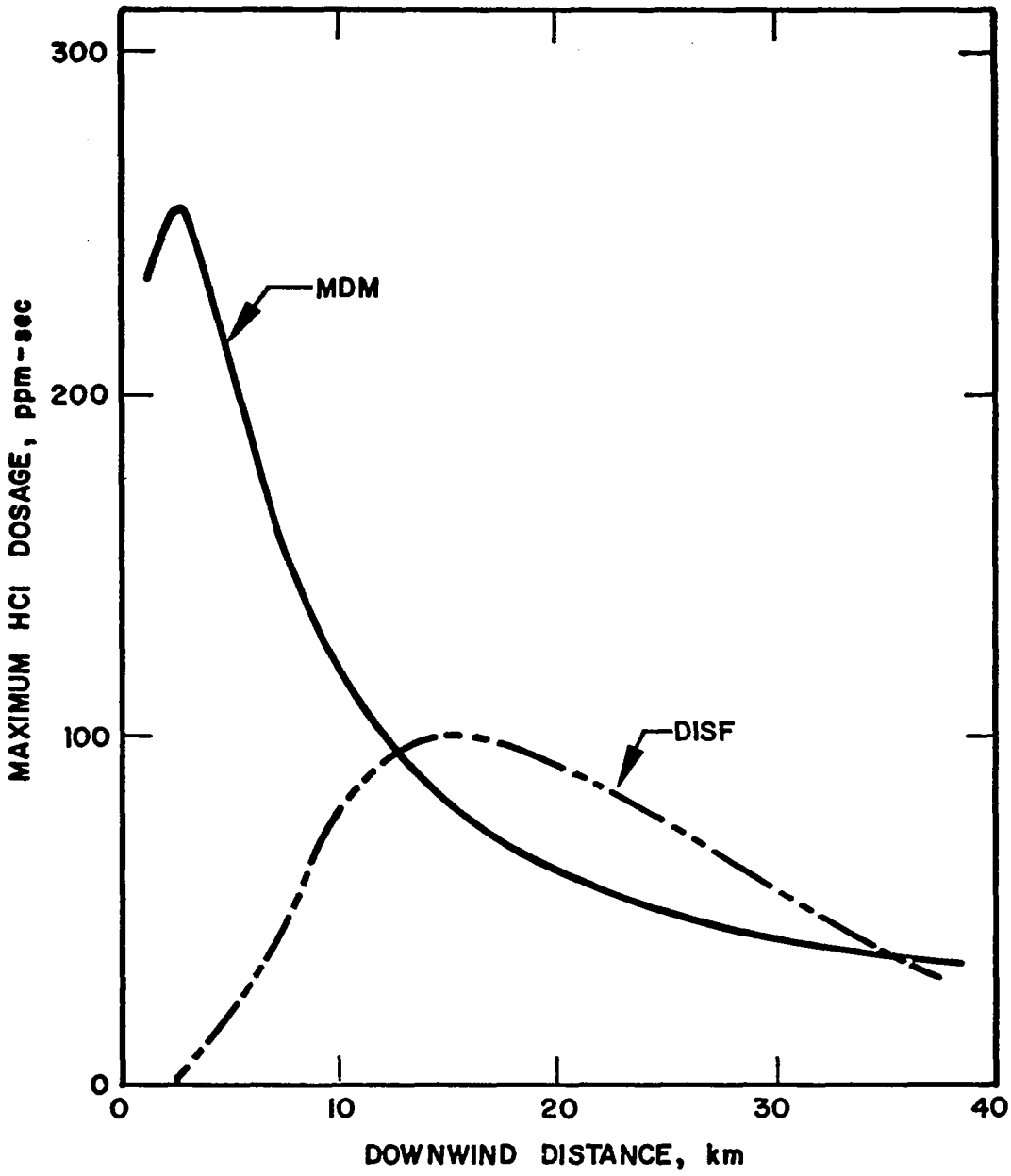

FIGURE 26 COMPARISONS OF GROUND LEVEL HCl MAXIMUM DOSAGE PREDICTIONS FOR THE 20 AUGUST 1975 CASE USING OBSERVED CLOUD AS INPUT

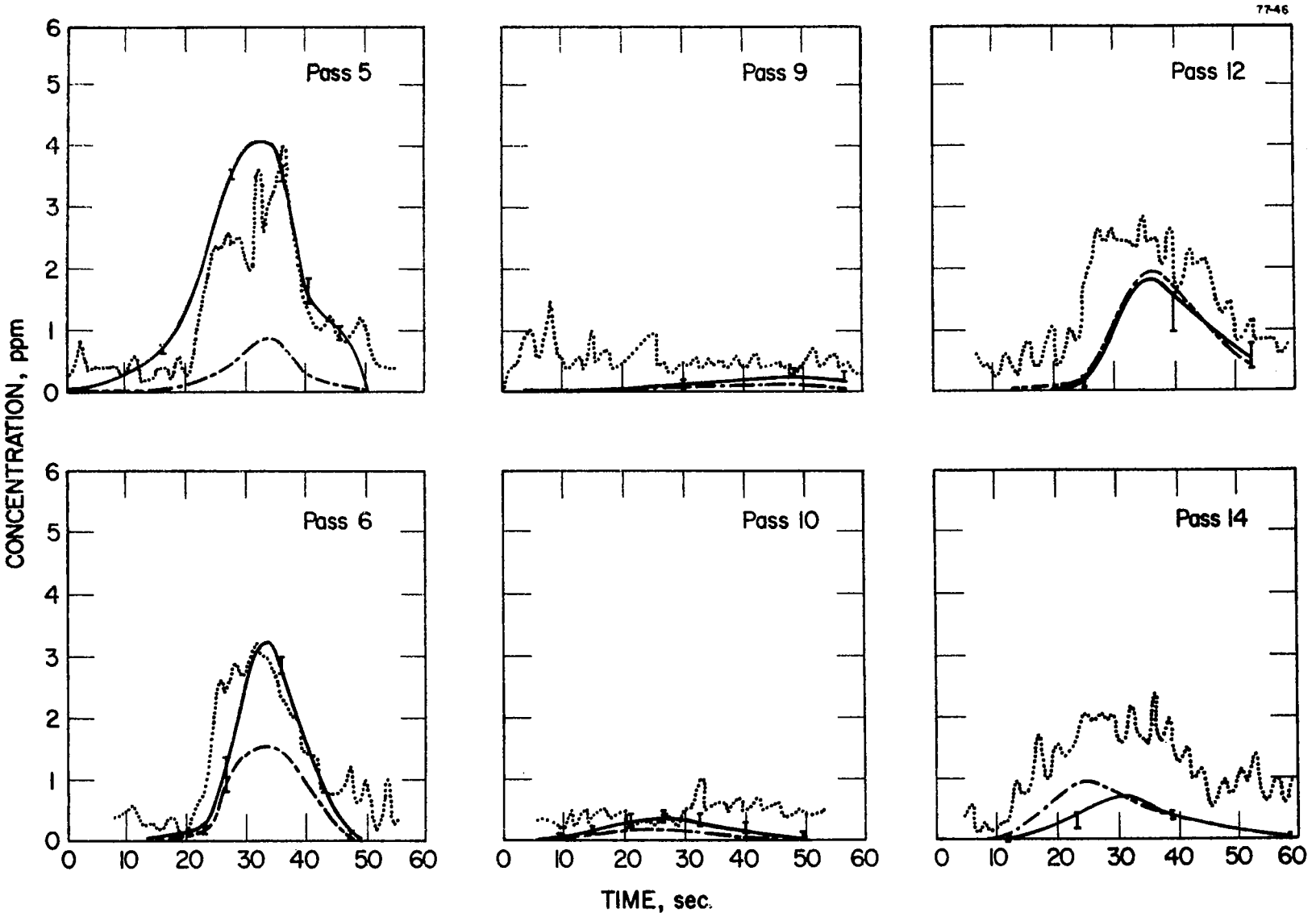

FIGURE 27 COMPARISONS OF AIRBORNE SAMPLING DATA WITH RESULTS PREDICTED FROM DISF USING OBSERVED CLOUD AS INPUT FOR THE 20 AUGUST 1975 CASE

Key: ——— Model
····· Measured data
— — — Downwind relocation

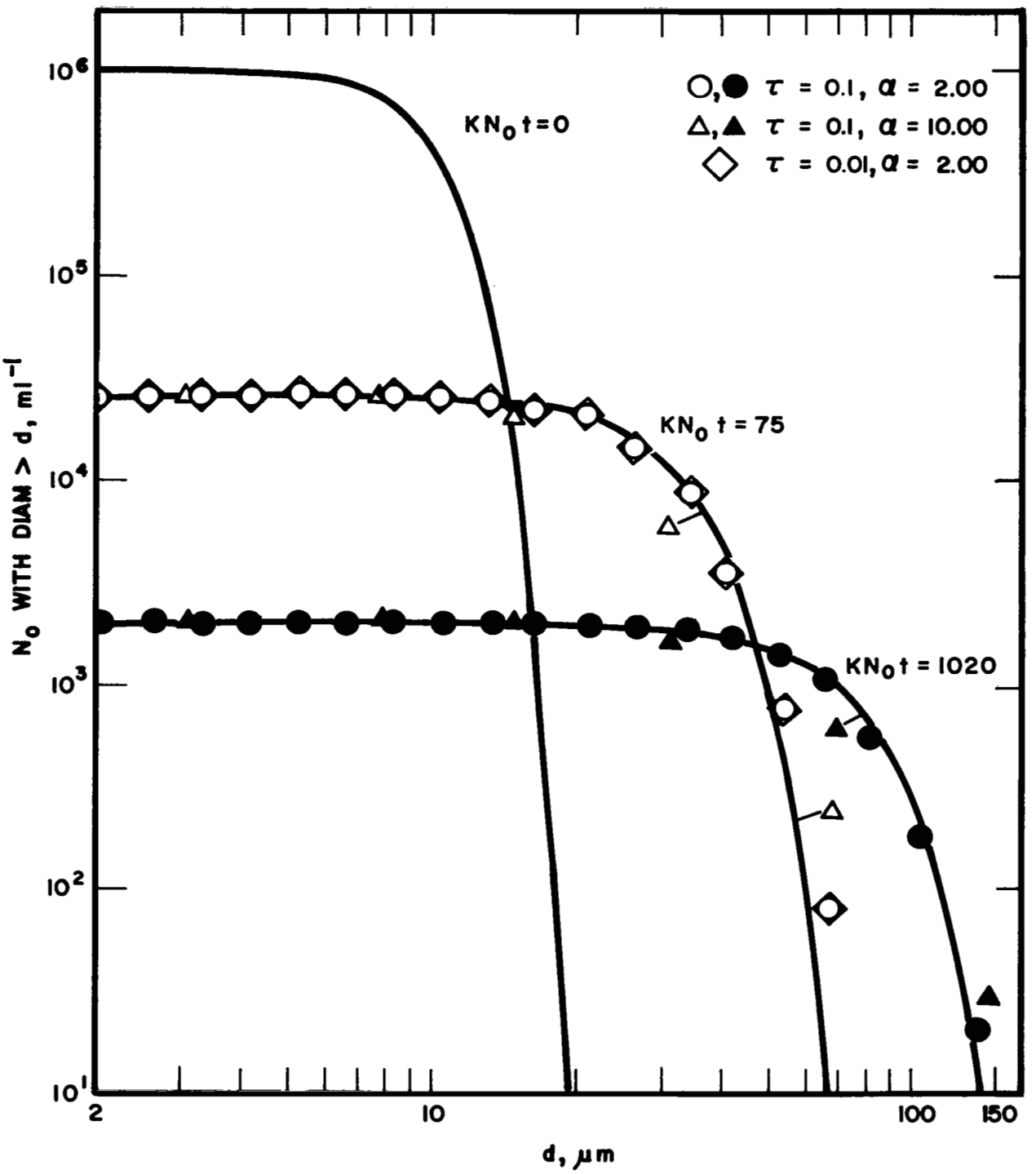

FIGURE 28 COMPARISON OF COMPUTED AND ANALYTICAL SOLUTIONS TO THE COAGULATION EQUATION (EQ. (90))

Curves are analytical solutions (Eq. (93)).
α = mass class size; τ = time step.

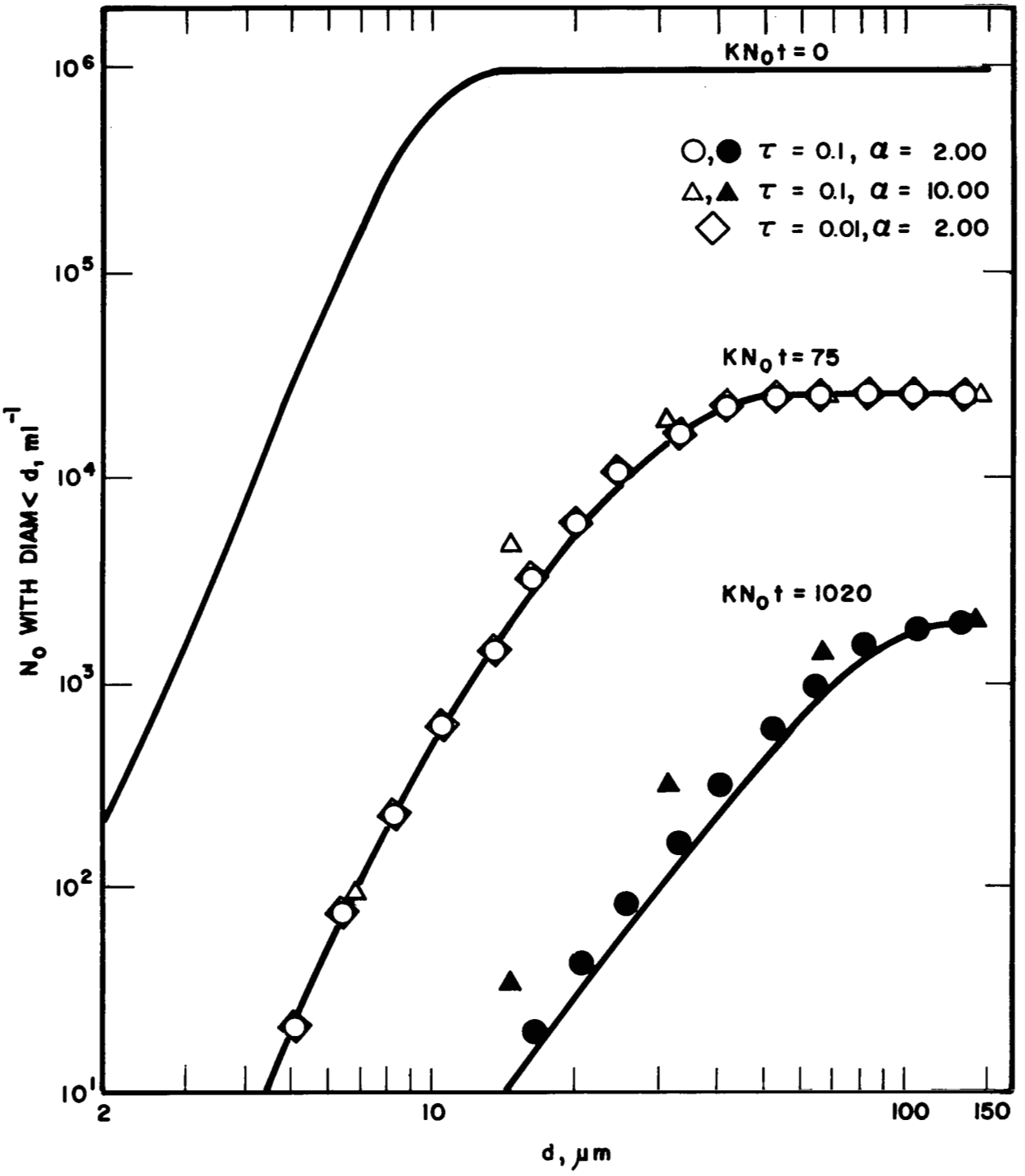

FIGURE 29 COMPARISON OF COMPUTED AND ANALYTICAL SOLUTIONS TO THE COAGULATION EQUATION (EQ. (90))

Curves are analytical solutions (Eq. (94)).
α = mass class size; τ = time step.

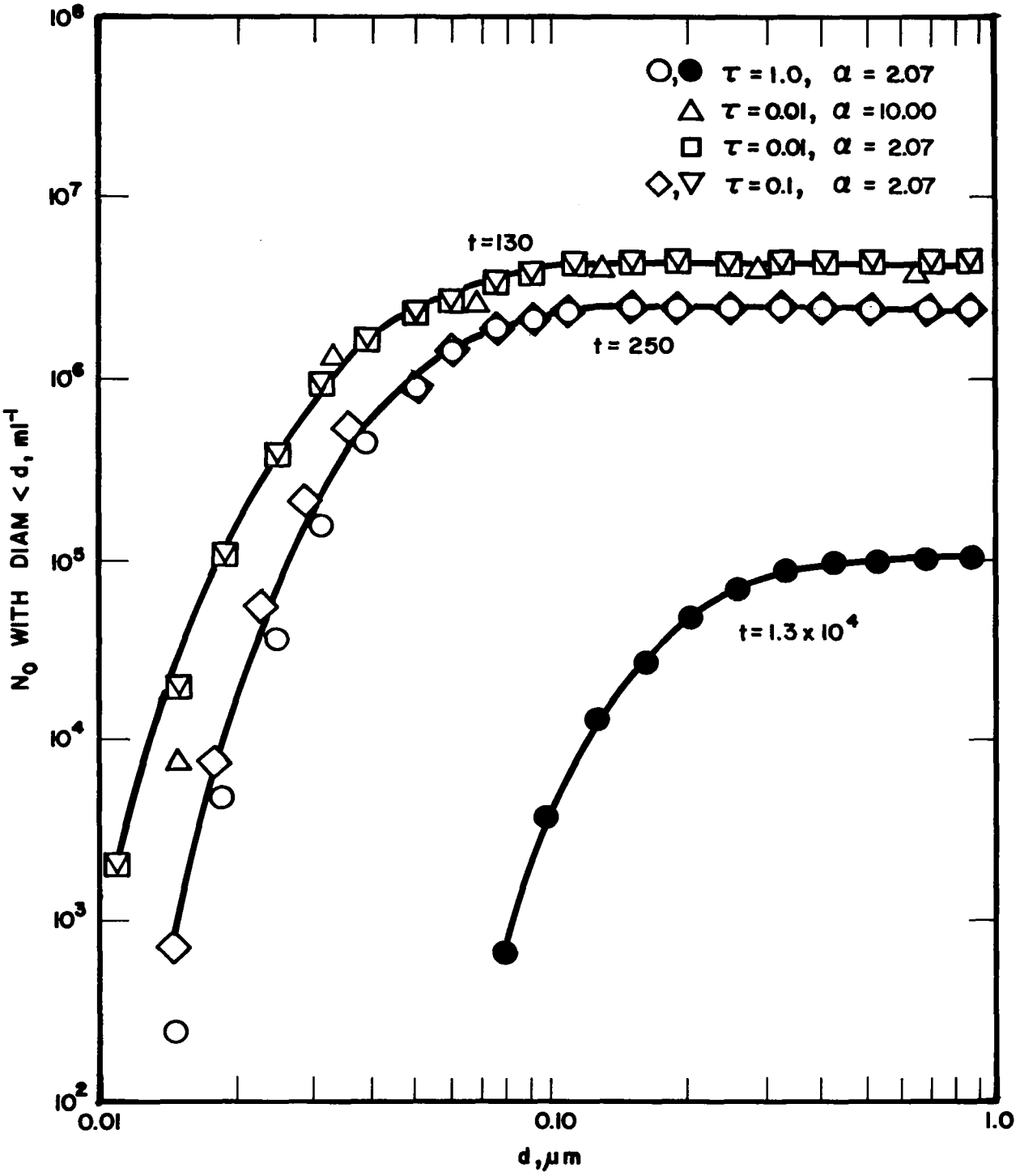

FIGURE 30 EVOLUTION OF A COAGULATING AEROSOL WITH INITIAL DISTRIBUTION $N'(d) \propto d^{-3}$

Curves are drawn through points calculated with the smallest time step and mass class sizes at each time.
α = mass class size; τ = time step.

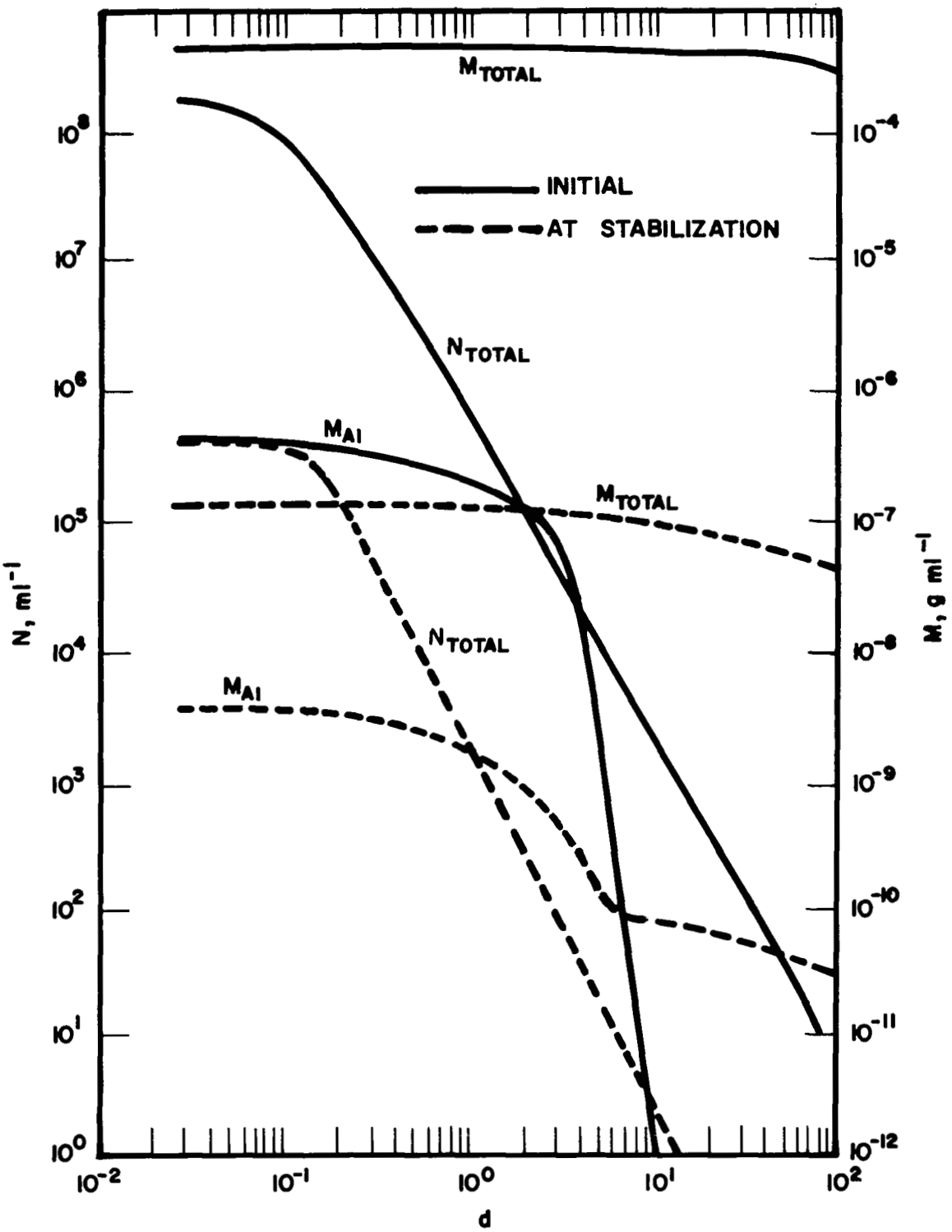

FIGURE 31 PARTICLE SIZE AND MASS DISTRIBUTIONS
FOR THE 20 MAY 1975 CASE
Dawborn's Alumina Distribution with Debris Having
1000 Times the Mass of Alumina

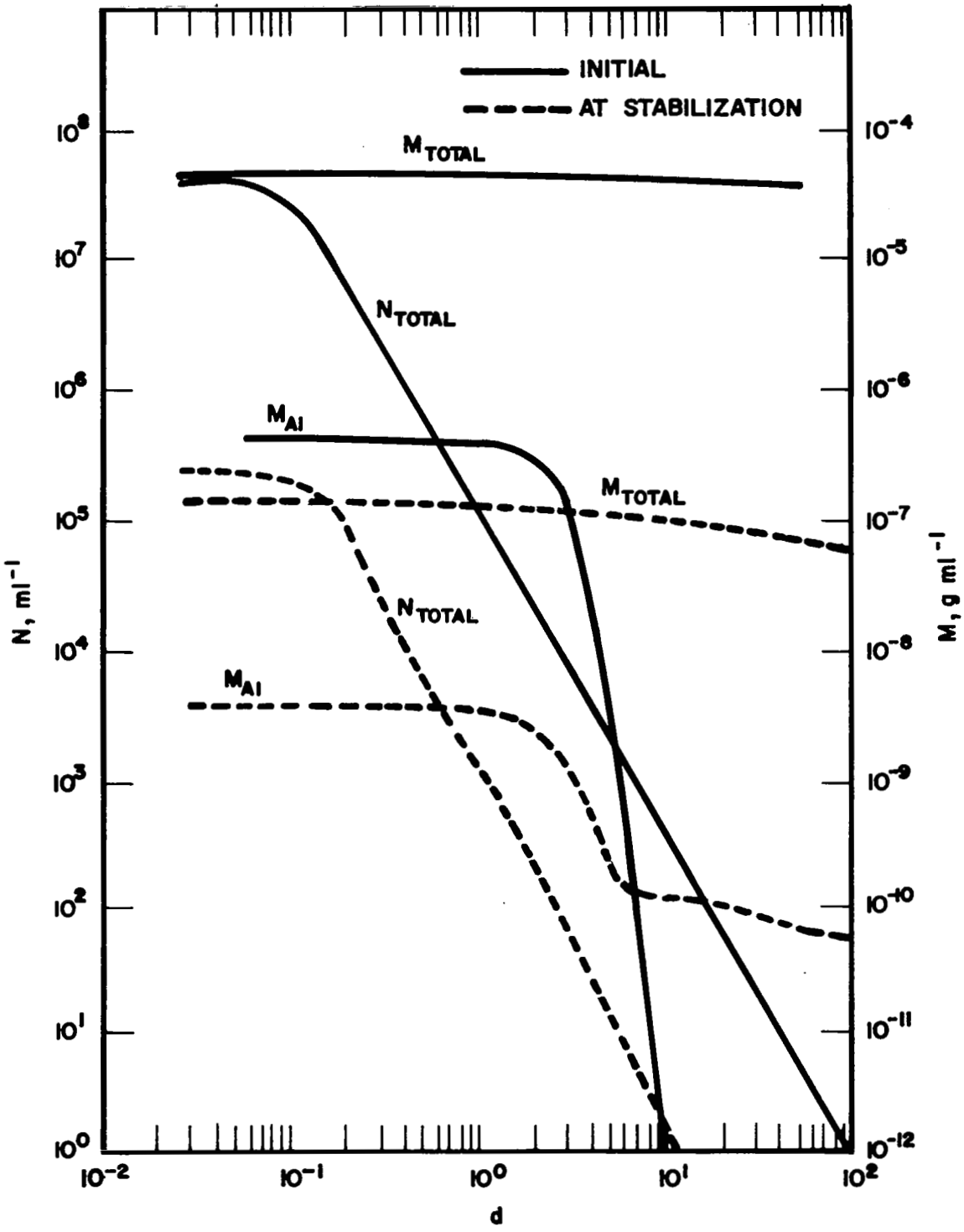

FIGURE 32 PARTICLE SIZE AND MASS DISTRIBUTIONS FOR THE 20 MAY 1975 CASE
Kreautle's Alumina Distribution with Debris Having 100 Times the Mass of Alumina

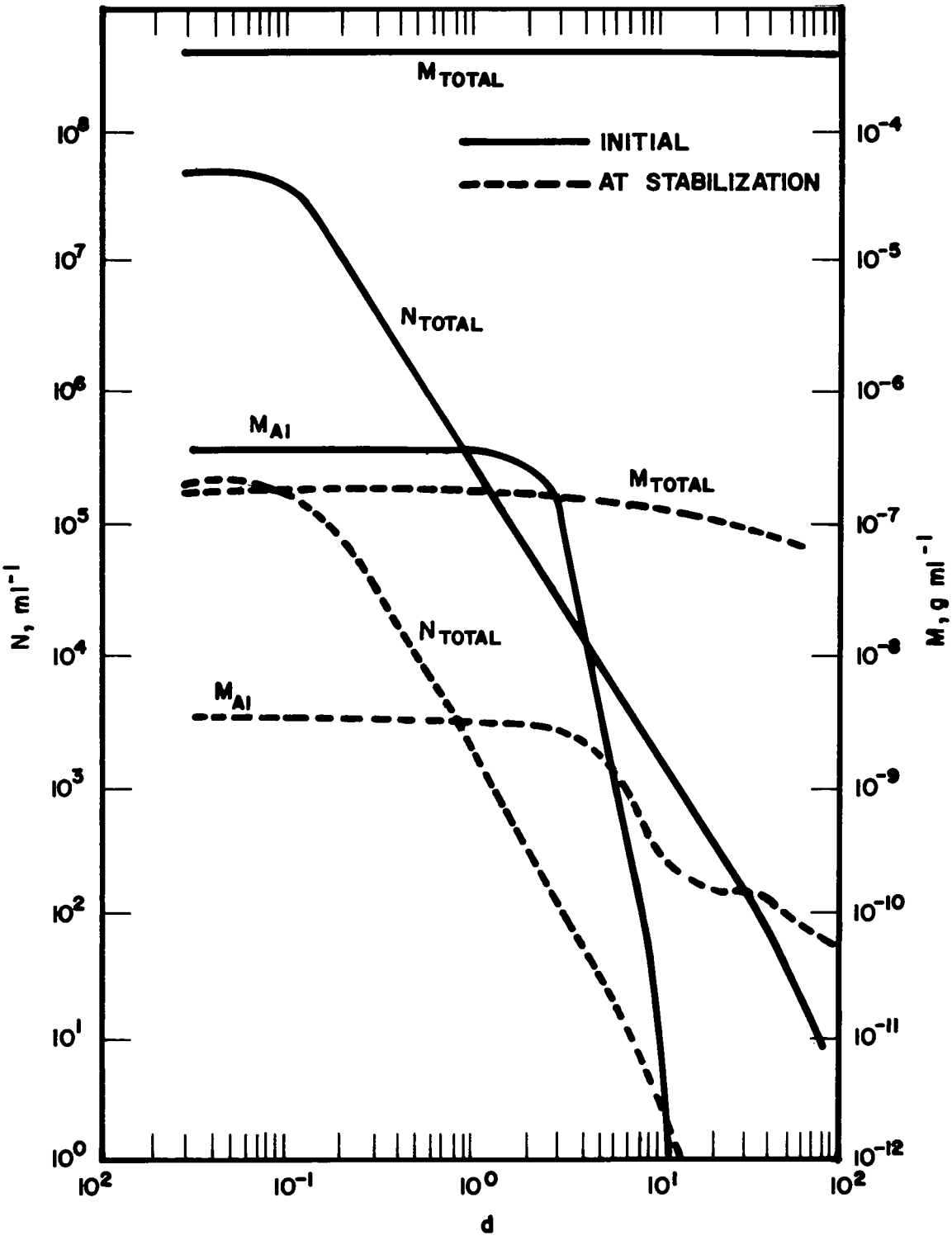

FIGURE 33 PARTICLE SIZE AND MASS DISTRIBUTIONS
FOR THE 20 MAY 1975 CASE
Kreautle's Alumina Distribution with Debris
Having 1000 Times the Mass of Alumina

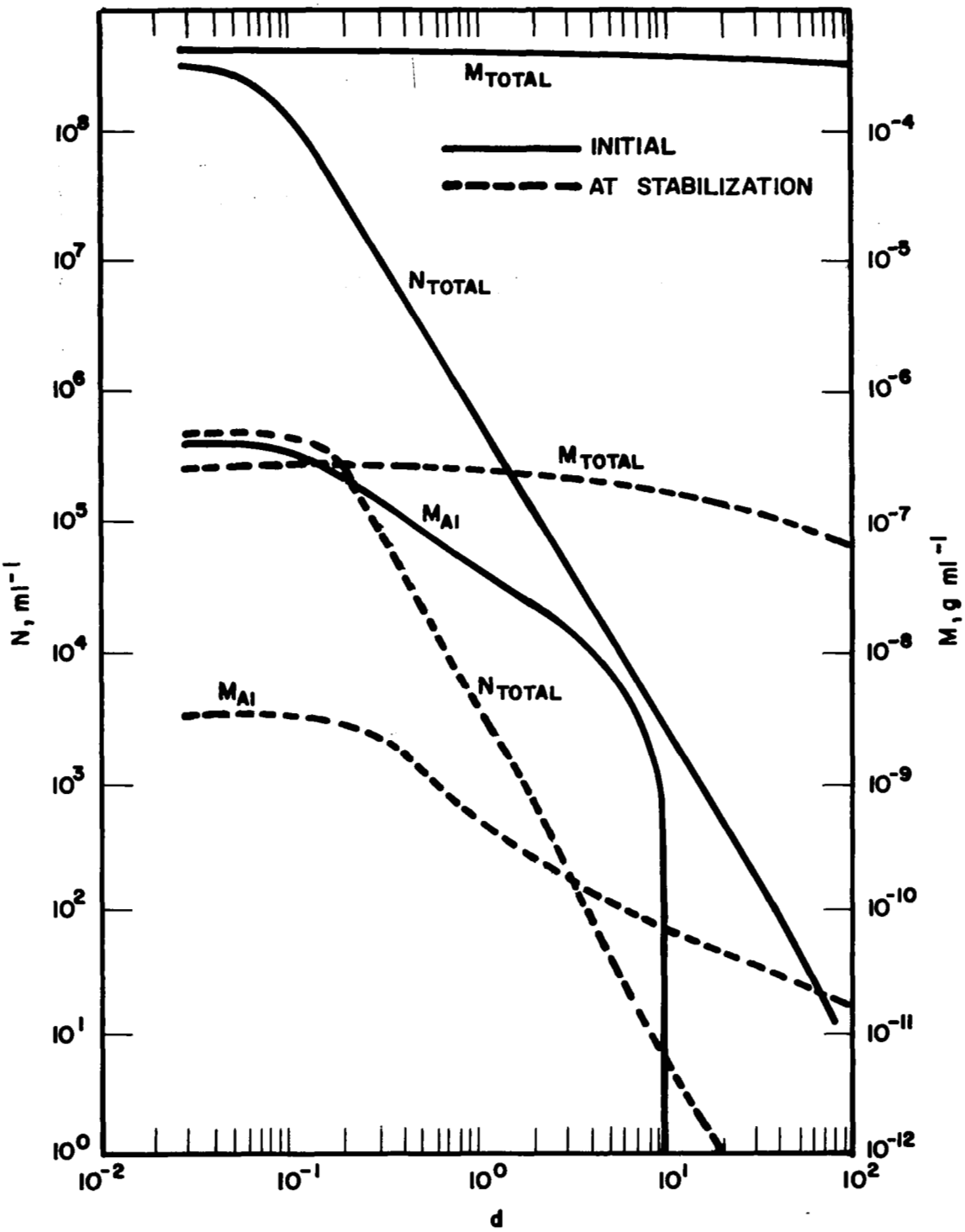

FIGURE 34 PARTICLE SIZE AND MASS DISTRIBUTIONS
FOR THE 20 MAY 1975 CASE
Varsi's Alumina Distribution with Debris
Having 1000 Times the Mass of Alumina

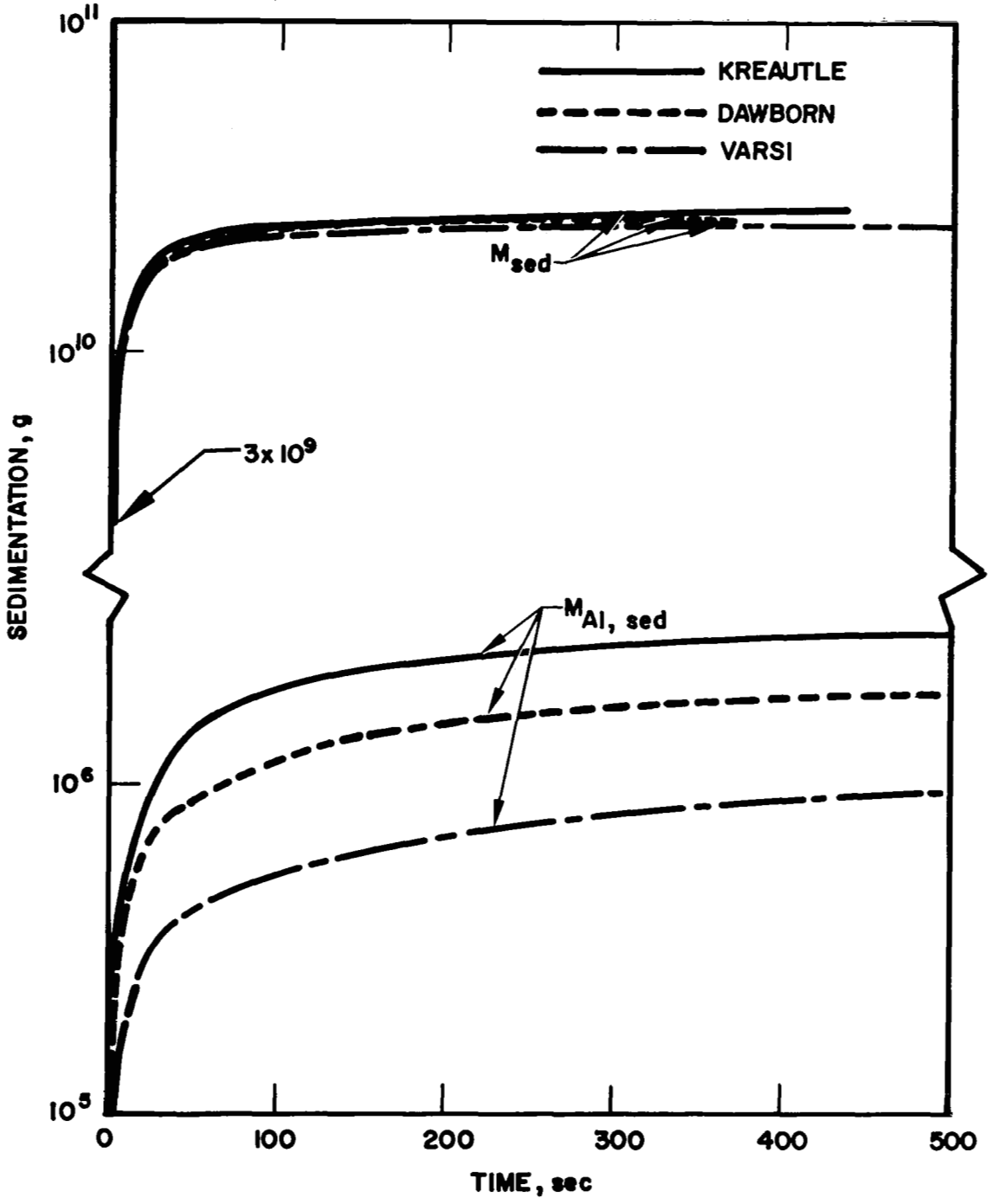

FIGURE 35 MASSES OF ALUMINA AND DEBRIS LOST FROM GROUND CLOUD DURING CLOUD RISE PERIOD

Mass Ratio of Debris to Alumina = 1000

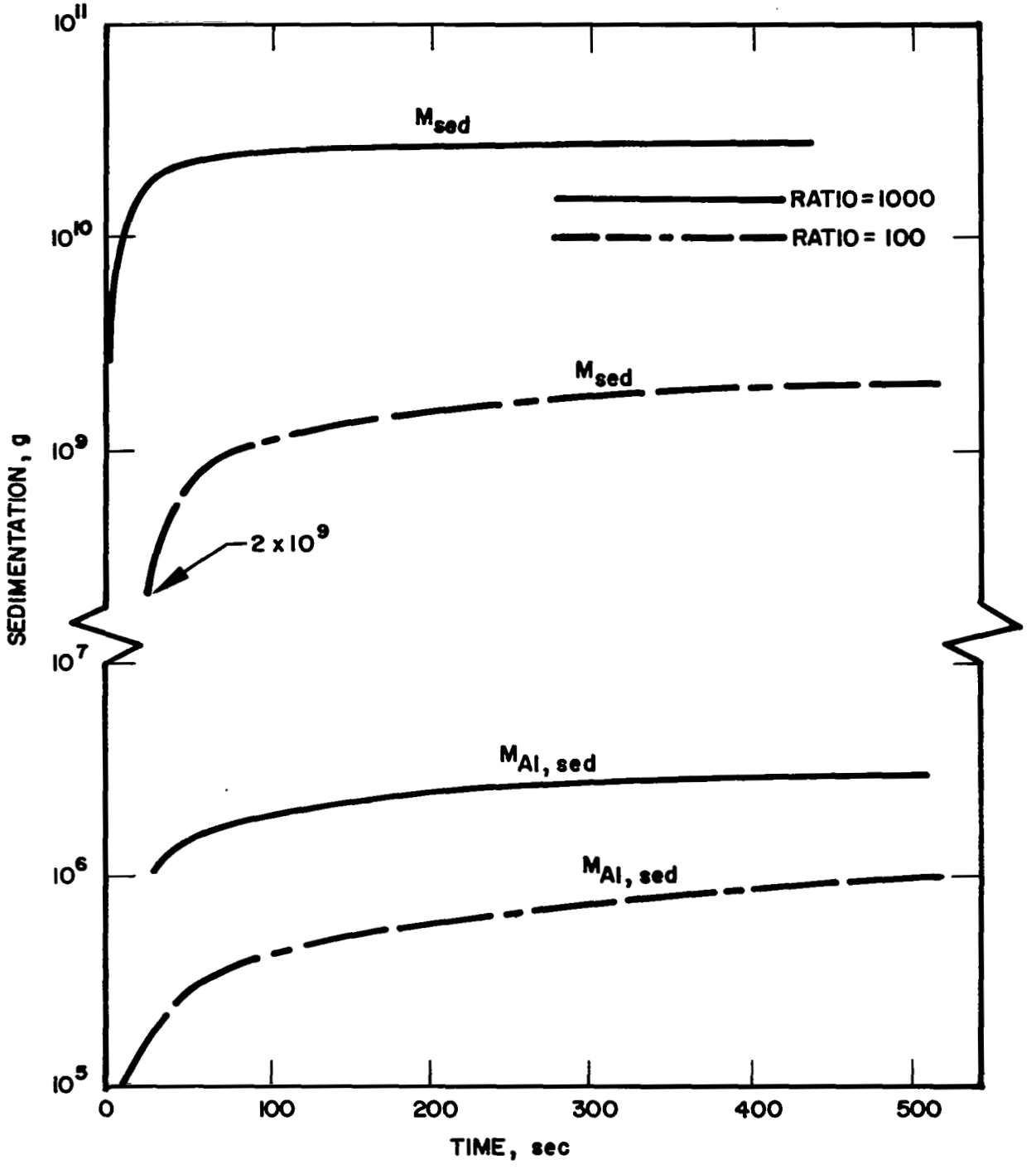

FIGURE 36 MASSES OF ALUMINA AND DEBRIS LOST FROM GROUND CLOUD DURING CLOUD RISE PERIOD CALCULATED USING KREAUTLE'S ALUMINA DISTRIBUTION

1. Report No.	2. Government Accession No.	3. Recipient's Catalog No.
NASA CR-2978		

4. Title and Subtitle	5. Report Date
ROCKET EXHAUST GROUND CLOUD/ATMOSPHERIC INTERACTIONS	July 1978
	6. Performing Organization Code

7. Author(s)	8. Performing Organization Report No.
BaoChuan Hwang and Robert K. Gould	AeroChem TP-362
	10. Work Unit No.

9. Performing Organization Name and Address	11. Contract or Grant No.
AeroChem Research Laboratories, Inc. P.O. Box 12 Princeton, NJ 08540	NAS1-14504
	13. Type of Report and Period Covered
12. Sponsoring Agency Name and Address	Contractor Report
National Aeronautics and Space Administration Washington, DC 20546	14. Sponsoring Agency Code

15. Supplementary Notes

Langley Technical Monitor: Joseph J. Mathis, Jr.

Final Report

16. Abstract

An attempt to identify and minimize the uncertainties and potential inaccuracies of the NASA Multilayer Diffusion Model (MDM) is performed using data from selected Titan III launches. The study is based on detailed parametric calculations using the MDM code and a comparative study of several other diffusion models, the NASA measurements, and the MDM. The results are discussed and evaluated. In addition, the physical/chemical processes taking place during the rocket cloud rise are analyzed. The exhaust properties and the deluge water effects are evaluated. A time-dependent model for two aerosol coagulations is developed and documented. Calculations using this model for dry deposition during cloud rise are made. A simple model for calculating physical properties such as temperature and air mass entrainment during cloud rise is also developed and incorporated with the aerosol model.

17. Key Words (Suggested by Author(s))		18. Distribution Statement
Diffusion Models	Dry Deposition	Unclassified - Unlimited
Atmospheric Turbulence	Computer Codes	
Rocket Cloud		
Cloud Rise		
Aerosol Coagulation		Subject Category 45

19. Security Classif. (of this report)	20. Security Classif. (of this page)	21. No. of Pages	22. Price*
Unclassified	Unclassified	187	$9.00

* For sale by the National Technical Information Service, Springfield, Virginia 22161

NASA-Langley, 1978